UNIVERSITY
OF TRENTO - Italy
Department of Materials Engineering
and Industrial Technologies

Doctoral School in Materials Engineering – XXII cycle

Nanocomposite coatings produced by electrodeposition from additive-free bath: the potential of the ultrasonic vibrations

Caterina Zanella

January 2010

Abstract

The main objectives of this Ph.D. research work are the development of enhanced nickel matrix nanocomposite coatings and the optimization of the codeposition parameters. Two different nanopowder, i.e. silicon carbide and alumina, were added to a Watts type galvanic bath in order to produce the nanocomposites coatings and ultrasonic vibrations have been considered as an alternative to pitting control agents in order to produce pore-free layers. The powders and the stability of their suspensions have been studied by DLS and ζ-potential measurements.

After the study of the relationship between process parameters and embedded ceramic particle amount, the optimized deposition condition have been evaluated and used for the production of the sample for the final properties characterization and to test the use of the ultrasounds.

Unique, functional properties of composite coatings are derived not only from the presence of the particles dispersed in the bulk of the metallic matrix but also on the matrix microstructural changes induced by the interaction between particles and electrocrystallization. Therefore the microstructure of all type of coatings have been analyze by SEM on the top-view and on the

cross-section, the agglomeration of the powder have been observed by LOM in case of Ni/Al_2O_3 and by TEM in case of Ni/SiC. It has been demonstrated that the codeposition of the SiC particles induces an important microstructural refinement while the Al_2O_3 powder is strongly agglomerated and only under ultrasonic vibrations can be dispersed and change the field oriented columnar structure into un-oriented fine grains.

Ultrasounds revealed to have positive effect not only in avoiding the porosity but also dispersing the ceramic powder and increasing the codeposition rate. This allowed to produce protective and very refined coatings.

All these interactions between ultrasounds, nanopowder and electrocrystallization lead to improved mechanical properties and the enhancement is proportional both to powder content and dispersion degree. Moreover a well dispersed powder induce, an improvement also in the corrosion protection leading to the formation of a more stable and resistant passive oxide.

Concluding, Ni/Al_2O_3 nanopowder codeposition leads to hardening effect, but does not affect the corrosion resistance because the particles agglomeration is not completely avoided even if deposited under ultrasonic vibrations. The SiC particles, on the contrary, can be better dispersed thus leading to improved both mechanical and protective properties.

Acknowledgements

I would like to thank Prof. P.L. Bonora, my advisor during the Ph.D. course.
I gratefully acknowledge Mr. Luca Benedetti for his absolutely essential advise in the experimental set-up.

I would like to thank the assistance provided by Dr. L. Maines and Dr. G. Ischia from Microscopy Lab. for the TEM analyses and Dr. M. D'Incau for the XRD analyses and interpretation. Many thanks to Prof A. Bund and Dr. D. Thiemig from the Technical University of Dresden for the hospitality and cooperation in the ζ-potential and DLS measurements and to Prof Fedrizzi and Ing A. Lanzutti from University of Udine for the GDOES measurements.

I would like to acknowledge my colleagues in the Corrosion Control Laboratory, M. Fedel, E. Scrinzi and V. Telch for many stimulating and useful technical discussions.

I would also like to thank Dr. M. Lekka, C. Valbusa and F. Bonapace for the cooperation in the wider project on the electrodeposition of nickel-matrix nanocomposites.

“Mit dem Wissen wächst der Zweifel.”

Johann Wolfgang von Goethe , Sprüche 1819

Summary

Preface

This thesis summarizes the research activity performed during my Ph.D. studies in Materials Engineering. This work performed during the last three years is a part of a wider project on electrodeposition of metal matrix composite coatings developed by the researchers of the Corrosion Control Laboratory of the University of Trento in the last 10 years. The aim of this project is to study the electrodeposited composite coatings by an engineering point of view, that takes into account not only the electrodeposition process, but also the final properties. Moreover the optimization of the industrial process was a constant issue considering that these coatings need to be applied on mechanical devices and should offer enhanced characteristic.

The previous work was based on the codeposition of silicon carbide micro- and nanoparticles in nickel or copper matrix, and was focused on the characterization of the influence of particles size on the final properties of the coatings. The main results confirmed that microparticles are easier codeposited and a high ceramic content metal coatings could be produced, while nanocomposites contain a ceramic amount lower than 1%. Nevertheless important improvements in mechanical hardening and corrosion resistance could be achieved by the nanocomposites. The aim of my Ph.D research was

therefore the development and the optimization of the codeposition process in order to obtain nanocomposites richer in nanoparticles and to evaluate the improvement of the mechanical and corrosion protection due to the codeposition. Moreover alumina nanoparticles have been considered beside silicon carbide ones for the codeposition. Ultrasonic vibrations have been considered as new process parameter to improve the dispersion of the powder and to substitute pitting control agents for the production of defect-free coatings.

Chapter 2 and 4 report the characterization of the powder, their suspension and the optimization of process parameter in order to improve the particles codeposition rate. Ultrasonic vibrations have been considered as new process parameter to improve the dispersion of the powder and to substitute pitting control agents for the production of defect-free coatings.

In order to study both the effect of the codeposition process on the composites structure and the influence of the application of the ultrasounds during the electrodeposition process, the deposits are analyzed in chapter 5 as for the microstructural changes and composite structure. Moreover a complete characterization of the performances of the deposits have been carried out. In chapter 6 the mechanical properties of the coating are discussed and chapter 7 presents the electrochemical characterization. In this way the coating have been studied deeply and all the aspect have been considered.

The final aim was the development of protection systems with improved both mechanical and corrosion protection properties and it was achieved with the Ni/SiC system.

1. Review and theoretical remarks

Electrodeposition or electroplating is the process by which an applied current or potential is used to deposit a film of metal or alloy by the reduction of metallic ions onto a conductive substrate. Electroplating process is a widely used industrial procedure and is applied in order to produce films that provide corrosion resistance, wear resistance and could change thermal, magnetic and optical characteristics of the surfaces. The interest in electrolytic and electroless composite coatings has increased substantially during the last decades due to the improved properties and the relatively low cost of these coatings[1]. The electrocodeposition describes the embedding of a solid phase, usually particles, in an electrodeposited metal matrix from a dispersion of those particles in the plating bath leading to the formation of a composite, and therefore to surface coatings with improved or sometimes completely new properties[2]. The final properties of the composite coatings depend on the combination of both particles and metal matrix, and ideally combine the best of the two worlds. Several metals have been studied for this application but,

[1] G.Di Bari, Metal Finishing, (2002), 35

[2] J.R. Roos et al, JOM November 1990, pp. 60-63

nickel and copper are the most studied metal matrixes[3] since they are the widest industrially applied coatings. The codeposition of ceramic particles such as Al_2O_3[4,5], SiC[6,7], CeO_2[8,9], SiO_2[10,11], TiO_2[12,13], WC[14,15] leads to the hardening of the metal layer and to the improvement of wear and abrasion resistance, while PTFE[16],[17] or MoS_2[18] could be added in order to reduce the friction.

The unique, functional properties of composite coatings are derived not only from the presence of the particles but also from the matrix microstructural changes induced by the interaction between the particles and the electrocrystallization process[19] leading to a change in the matrix microstructure[20].

---

[3] A.Hovestad, L.J.J. Jansenn, J.Appl. Electroche. 25 (1995) 519

[4] M.E. Bahrololoom, R.Sani, Surf. Coat. Tech., 192, (2005), 154

[5] A. B. Vidrine, E.J.Podlaha, J.Apll.Electrochem, 31, (2001) 461

[6] K.H. Hou, M.D.Ger, L.M. Wang, S.T. Ke, War 253, (2002) 994

[7] L. Orlovskaja, N.Periene, M.Krtinaitiene, S.Surviliene, Surf.Coat. Tech., 111, (1999), 234

[8] S.T. Aruna, C.N.Bindu, V.Ezhil Selvi, V.K. Grips, K.S.Rajam, Surf. Coat. Tech., 200, (2006), 6871

[9] N.S. Qu, D.Zhu, K.C. Chan, Scripta Materialia, 54, (2006), 1421

[10] R. P.Socha, P.Nowak, , K.Laajalehto, J.Vayrynen, Colloids Surf. A, 235, (2004) 45

[11] J. Fransaer, J.P.Celis, Galavanotechnik, 92, (2001), 1544

[12] J. Li, J. Jiang, H.He, Y.Sun, J. Mat.Sci.Lett., 21, (2002), 939

[13] J. Li Y.Sun, X.Sun, J.Qiao, Surf. Coat. Tech., 192, (2005), 331

[14] M. Stroumbouli, P.Gyftou, E.A. Plavlatou, N.Spyrellis, Surf. Coat. Tech., 195, (2005), 325

[15] B. Jugovic, J.Stevanovic, M.Maksimovic, J.Appl.Electrochm., 34, (2004), 175

[16] G.N.K. Ramesh, S.Mohan, Plat.Surf.Finish., 4, (1995) 86

[17] B.L osiewiez, A. Stepien, D. Gierlotka, A. Budniok, Thin Solid Film, 349, (1999), 43

[18] Y.-C. Cang, Y.Y. Chang, C.-I. Lin, Electrocim. Acta, 43, (1998) 315

[19] P. Nowak, R.P.Socha, M.KAisheva, J.Fransaer, J.-P. Celis, J. Appl. Electrochem., 30, (2000) 429

[20] A.F. Zimmerman, D.G. Clark, K.T.Aust, U. Erb, Mater. Lett., 52, (2002), 85

Electrodeposition of composite coatings – Theoretical remarks

Several theoretical models have been proposed to describe the codeposition phenomenon. However the mechanism is not fully understood and the mathematical model to predict the amount of codeposited particles are verified only for few systems and in controlled conditions and the equation can not take into account all the variables of the process and therefore have been developed for particular experimental conditions. Moreover these models have been developed from the investigation on the micro-sized particles and could not simply be applied to nano-sized systems since in the nano-range all the forces act in completely different way. Nevertheless the physical description of the process can be considered valid for nanoparticles as well and could help to understand the interaction between particles, electrolyte, electrodes and process parameter as pH, temperature and current conditions.

A first model of the electrolyte codeposition was made by Guglielmi[21] and was based on a two-step codeposition mechanism. Guglielmi assumed that the particles are first reversibly loosely adsorbed on the cathode surface and then embedded in the metal layer. The adsorbtion of metals ions on the particles surface forming an ionic cloud was subsequently considered[22] taking therefore into account the ζ-potential and electrophoretic forces. This model has been adopted for many years but the amount of embedded particles was meant to

[21] N. Guglielmi, J. Electrochem. Soc., 119, (1972), 1009

[22] J. Foster, A.M.J.Kariapper, Trans. Inst. Met. Finish., 54, (1973), 27

be dependent only on the particles concentration and on the current density. To overcome the shortcoming in the Guglielmi's model Celis et al.[23] first and Fransaer et al.[24] then developed a model that took into account also the hydrodynamic effect and the particles characteristics. The basic assumption of this model is that all particles are surrounded by a cloud of adsorbed species, mainly metal ions, and can be incorporated into the metal matrix only if an efficient part of these chemical species is reduced at the same time with the metal ions on the cathode. Moreover, the model considers that the current efficiency is 100% and the particles spherical and is based on the important influence of the electrolyte stirring. The model consists in five consecutive steps as schematically described inFig.1.1:

- Formation of ionic clouds on the particles;
- Convection towards the cathode surface;
- Diffusion through a hydrodynamic boundary layer;
- Diffusion through a concentration boundary layer;
- Adsorption at the cathode where particles are entrapped within the metal deposit by the reduction of the ionic cloud.

[23] J.P. Celis, J.R. Roos, C. Buelens, J. Electrochem. Soc., 13, (1987), 1402

[24] J. Fransear, J.P. Celis, J.R. Roos, J. Electrochem. Soc., 139, (1992), 413

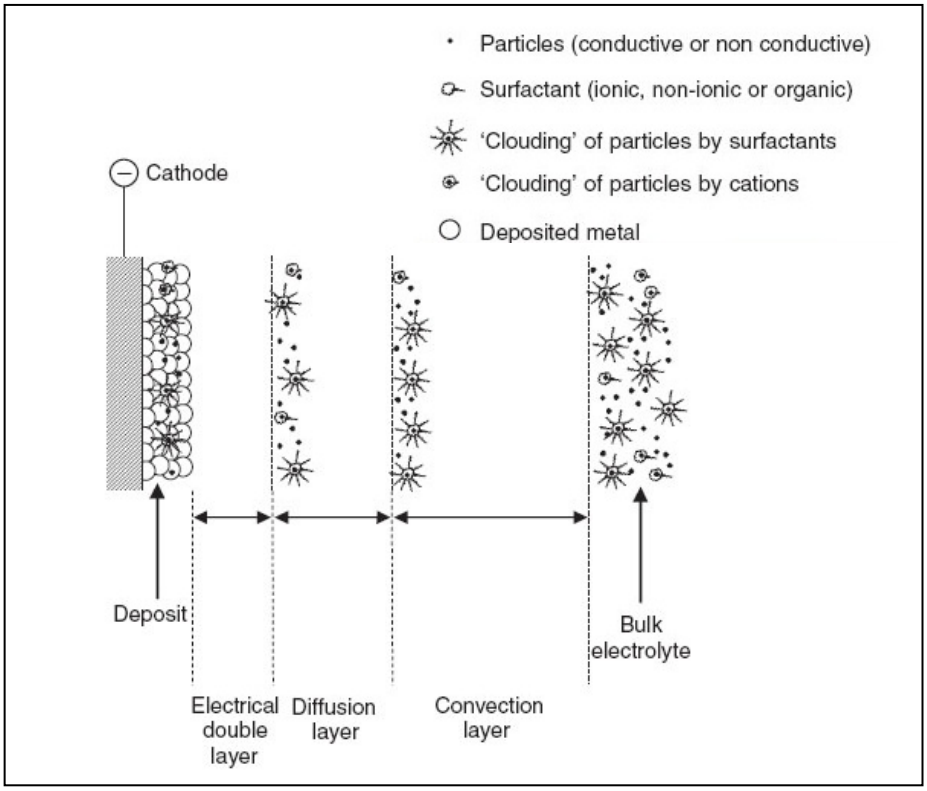

Fig 1.1 Mechanism of particles codeposition [23]

Other models which have been formulated afterwards did not succeed to provide a general approach to the codeposition of inert particles into metallic coatings even if much more factors have been taken into consideration. However, the flexibility and the reliability of each model to describe the behaviour of a wide range of metallic coatings and particle types still requires validation. Often the mathematical relationship is strictly related to the experimental set-up and in all model available so far the effect of the particles codeposition on the deposit electrocrystallization have not been considered.

Moreover when the particles have nano dimensions all the forces act differently on the system and Brownian motion becomes more important. These model have therefore not been validated for the nanocomposites.

One the other hand, the properties of the metal matrix composite coatings have been widely studied. A lot of publications are available regarding different types of micro-composite coatings using different kind and sizes of particles as well as different kind of metal or alloy matrix, while the most part of the studies on the nanocomposite coatings are limited to the codeposition optimization and the mechanism understanding and no systematic research have been carried out on the relationship between nanoparticles codeposition and both mechanical and protective protection.

Electrodeposition of nickel composite coatings– a review

Due to the wide use of nickel as a protective coating, nickel composite coatings containing especially ceramic particles have been discussed frequently in the literature [25,26,27]. A large number of ceramic powder have been incorporated into nickel to improve the hardness and the wear resistance and most of the studies focused on the embedding silicon carbides[28,29, 30] or alumina[31,32,33,34].

[25] P.R. Webb ,N.L. Robertson, J. Electrochem. Soc., 141, (1994), 669

[26] C. Dedeloudis, M.K. Kaisheva, N. Muleshkov, T. Muleshkov, P. Nowak, J. Fransaer, J.P. Celis, Plat. Surf. Finish., 86, (1999), 57

[27] D. Gierlotka, E. Rowinski, A. Budnik, E. Lagiewka, J. Appl. Electrochem., 27, (1997), 1349

[28] S.k. Kim, H.J. Yoo, Surf. Coat. Tech., 108, (1998), 564

[29] L. Orlvskaja, N. Perìiene, M. Krtinaitiene, G. Bikulcius, Surf. Coat. Tech., 105, (1998), 8

The first paper on the electrodeposition of metal matrix composite coatings studied the copper-graphite system for self-lubricating surfaces in car engines[35], but only in the 1960s[36] started the development of hardened films.

The first electroplating baths containing particles appeared in the industrial scale for the production of Ni/SiC and Co/Cr_2O_3 coatings used for car engines, aircrafts construction and printed circuits. Specifically the Ni/SiC deposits have been used as internal coating of the aluminium cylinders of car engines[37].

The wear properties of Ni/SiC as well as Ni/Al_2O_3 composite coatings have been studied by many research groups as these coatings could be a good candidate to substitute the hard chromium coatings[38,39,40].

Sautter[41] found that the codeposited content of Al_2O_3 particles in nickel matrix increases by increasing of the particles content in the galvanic bath with a decreasing rate and reaches a plateau that depends on the bath, temperature and current condition. This behaviour was confirmed by other studies for a

[30] A.F. Zimmerman, G. Palumbo, K.T. Aust, U. Erb, Mater. Sci. Eng. A, 390, (2005), 137

[31] K. Barmak, S.W. Banovic, C.M. Petronis, D.F. Susan, A.R., Marder, J. Microsc., 185, (1997), 265

[32] J. Steinbach, H. Ferkel, Scr. Mater., 44 (2001), 1813

[33] A.B. Vidrine, E.J. Podlaha, J. Appl. Electrochem. 31, (2001), 461

[34] D .Simunovich, M. Schlesinger and D.S nyder , J. Electrochem. Soc. 141 (1994)

[35] C.G. Fink, J.D. Pince, Trans. Am. Electrochem. Soc., 54, (1928), 315

[36] R.V. Williams, Electroplat. Met. Finish., 19, (1966), 92

[37] J. Ross, J.P. Celis, J. Fransaer, C. Buelens, JOM, (1990)

[38] P.Gyftou, M. Stroumbouli, E.A. Pavlatou, P. Asimidis, N. Spyrellis, Electrochimica Acta 50 (2005), 4544

[39] I.R. Aslanyan, J.P. Bonino, J.P. Celis, Surface & Coatings Tech. 200 (2006), 2909

[40] A.A. Aal, K.M. Ibrahim, A.A. Hamid, Wear 260 (2006), 1070

[41] F.K. Sautter, J. Electrochem. Soc., 110, (1963), 557

wide range of codeposition systems[42,43,44]. On the other hand the value of codeposited particles varies for different systems.

Different particles sizes, current conditions and different electroplating baths have been studied. The wear resistance of the coatings increases by the addition of micro or submicron particles due to the high amount of incorporated particles and their high intrinsic hardness. On the other hand, the presence of a high amount of relatively big particles could worsen the corrosion properties of the coating due to the presence of voids between the particles and the metal matrix, which are the preferred path of propagation for the corrosive solutions. The researchers started to concentrate on the codeposition of smaller particles that could enhance the mechanical properties without penalizing the corrosion resistance of the coating. Moreover the presence of a smaller hard phase could avoid the formation of an abrasive third body during the wear process. Ding *et al*[45]. in1998 used submicron particle sizes of alpha-alumina (0.11 micron and 0.4 micron) and showed that there is a linear increase in microhardness in both Ni and Cu with particle volume fraction in the deposit. The smaller particles produced a larger hardening effect and the strengthening mechanism was explained by a combination of the Orowan-type strengthening and Hall-Petch effects.

In the last 10 years the interest on the metal matrix composite coatings has been revived due the development of new nanotechnological methods for the production of nano-particles of carbide or oxides.

---

[42] Y.S. Chang, J.Y. Lee, Mater. Chem. Phys., 20, (1998), 309

[43] J.W. Graydon, D.W. Kirk, J. Electrochem. Soc., 137, (1990), 2061

[44] G.N.K. Ramesh Bapu, M. M. Yusuf, Mat. Chem Phys., 36, (1993), 134

[45]X.M. Ding, N. Merk, B. Ilschner, J. Mater. Sci., 33, (1998), 803

Generally the volume fraction of codeposited particles is limited for nanoparticles and usually it is inversely proportional to their size[46]. For example, Shaou et al. studied the rate of incorporation of two different sizes of Al_2O_3 nanoparticles (50 nm and 300 nm) into a nickel deposit. Using similar operating parameters (1000 rpm, 20 mA cm^{-2}), it was found that the percentage volume fraction of the 300 nm Al_2O_3 in the nickel deposit was much higher compared to the 50 nm Al_2O_3 [47].

The presence of nanosized particles in a metal deposit may induce changes in the crystalline structure of the metallic coating. It has been shown that 20 nm SiC nanoparticles influence the competitive formation of nickel nuclei and crystal growth[48], and that the presence of nanoparticles will perturb the crystalline growth of a metal deposit, resulting in an increased number of defects in the crystal structure, facilitating a nanocrystalline structure[49,50]. The hardening effect is therefore related not only to the presence of the second hard phase but also to the changes induced in the metal.

The amount of embedded nanoparticles depends on the operational parameters such as current density, pH, bath temperature, additives type and concentration, stirring; but the relationship between operating parameters and codeposition amount is not clear and often the results are inconsistent.

Erler et al. demonstrated that alumina nanoparticles content in the deposit

[46] G. Maurin, A. Lavanant, J. Appl. Electrochem., 25, (1995), 1113

[47] I. Shao, P.M. Vereecken, R.C. Cammarata, P.C. Searson, J. Electrochem. Soc., 149, (2002), C610

[48] L. Benea, P.L. Bonora, A. Borello, S. Martelli, Wear, 249, (2002), 995

[49] J. Li, Y. Sun, X. Sun, J. Qiao, Surf. Coat. Technol, 192, (2005), 331.

[50] Y. Zhang, X. Peng, F. Wang, Mater. Lett., 58, (2004), 1134.

increases decreasing the deposition current[51]. On the contrary Bund et al. show that the embedded fraction of nano alumina is not affected by the current density in acidic nickel deposition bath, while it increases by increasing the current in alkaline deposition bath[52].

The results regarding the effect of particles incorporation on the final properties is often contradictory because it depends on a lot of parameters and on both the embedded amount and the dispersion of the particles. The hardening effect caused by the codeposition of nanoparticles has been reported by many authors[53],[54],[55]: the increase in the hardness of nickel nanocomposite film is associated to the presence of the intrinsic hardness of the codeposited ceramic phase, to a dispersion hardening and to the refinement of the microstructure. As a consequence the wear resistance is improved[56]. Garcia et al.[57] demonstrated that the wear resistance of Ni/SiC composites is higher for SiC size of 300 nm than microparticles because larger particles could improve the wear load due to the abrasion performed by the pulled-out particles. Zimmerman[58] demonstrated that not only hardness but also the yield and tensile strengths are improved by codeposition of nanoparticles of SiC.

---

[51] F. Erler, C. Jacobs, H. Romanus, L. Spiess, B. Wielage, T.LAmpke, S. Steinhauser, Electrochimica Acta, 48, (2003), 3063

[52] A. Bund, D. Thiemig, Surf. Coat. Tech., 201, (2007), 7092

[53] E. Pavlatou, M. Stroumbouli, P. Gyftou, N. Spyrellis, J. Appl. Electrochem., 36, (2006), 385

[54] H. Ferkel, B. Muller, W. Riehemann, Mater. Sci. Eng. A, 234, (1997), 474

[55] L.Du, B. Xu, S. Dong, H. Yang, Y. Wu, Surf. Coat. Tech., 192, (2005), 311

[56] K.H. Hou, M. D. Ger, L.M. Wang, S.T. Ke, Wear, 253, (2002), 994

[57] I. Garcia, J. Fransear, J-P. Celis, Surf. Coat. Tech., 148, (2001), 171

[58] A.F. Zimermann, G. Palumbo, K.T. Aust, U. Erb, Mater. Sci. Eng. A, 328, (2002), 137

Regarding the protective properties of the Ni nanocomposite coatings there is no certain result shared by all researchers. According to some groups the incorporation of sub-micron SiC particles in the nickel matrix increases the corrosion resistance of the coatings, mostly due to the microstructural modifications[59,60]. In these cases the codeposition of small particles leads to the formation of nano-crystalline, more compact, pore-free coatings, thus having higher corrosion resistance to both uniform corrosion and pitting corrosion.

According to other studies[61] the codeposition of SiC particles decreases the current density but only due to the fact that the coatings surface is covered by ceramic particles and the free Ni surface in contact with the electrolyte is lower than in the case of pure nickel coatings. Others[62] demonstrated that nanocomposite coatings offer less protection, but this is mainly due to the presence of pores and defects caused by the agglomeration of the powder. Nevertheless is widely believed that the corrosion properties of composite coatings should increase if the grain size decreases. For this reason many different attempts have been done by the use of different types of surfactants in order to avoid the agglomeration of the particles[63,64], or by the use of pulse or triangular current in order to break the columnar structure of Ni deposits, to avoid pores and defects, and create finer and more homogeneous

[59] I.Garcia, A.Conde, G.Langelaan, J.Fransaer, J.P.Celis, Corrosion Science 45 (2003) 1173-1189

[60] V. Medeliené, Surf. & Coat. Tech. 154 (2002), 104-111

[61] C.F. Malfatti, J. Z. Ferreira, C.B. Santos, B.V. Souza, E.P. Fallavena, S.Vaillant, J.P. Bonino, Corrosion Science 47, (2005) 567-580

[62] T. Lampke, A. Leopold, D. Dietrich, G. Alisch, B. Wielage, Surf. Coat. Tech., 201, (2006), 3510

[63] N. Shrera, M. Masuko, T. Saji, Wera 254 (2003), 555-564

[64] M.D. Ger, Materials Chem. & Phys. 87 (2004), 67-74

microstructures[65,66]. These attempts lead to finest deposits but the corrosion properties of these coatings have not been systematically studied.

Conclusively, we can say that the Ni matrix nanocomposite coatings have been studied to a certain extent, but their corrosion properties are still a field of disagreement.

.

[65] F.hu, K.C. Chan, Applied Surface Science 243 (2005) 251-258

[66] E.A. Pavlatou, M. Stroumbouli, P. Gyftou, N. Spyrellis, J. Applied Electrochem. 36 (2006), 385-394

2. Nano-powder characterization

For the production of the nickel matrix composites two different nanopowders have been considered for the codeposition: silicon carbide and alumina. Both of them have a very small diameter <100 nm, but they are very different regarding their surface state. Oxides have usually hydrophilic surfaces, while carbides should present a hydrophobic surface. These two powders have been chosen to study and compare how the different surface characteristic affect the suspension and the codeposition.
In this chapter the main features of the two ceramic powders used for the production of the nickel metal matrix composite coatings are analyzed.

SiC nanopowder

The silicon carbide nano-powder was produced by ENEA Frascati as the result of the laser pyrolisys of acetylene and silanes[67,68]. During the process, the

[67] E. Borsella, S. Botti, C. Cesile, S. Martelli, R. Alexandrescu, R. Giorni, C.A. Nannetti, S. Turtù, G. Zappa, Nanostructured Materials 6 (1995), 341-345

[68] R. Giorgi, S. Turtù, G. Zappa, E. Borsella, S. Botti, M.C. Cecile, S. Martelli, Applied Surface Science 93 (1993), 101-108

reactant gases (C_2H_2 and SiH_4) are heated by the absorption of CO_2 laser radiation and decomposed, causing particles to nucleate and to grow rapidly. The laser radiation is absorbed by gas molecules in a small, well defined reaction zone producing a high temperature and very steep temperature gradients, allowing in this way a precise control of the composition, shape and size distribution of the resulting powder.

Thanks to this procedure, the powder produced has a narrow size distribution with a mean diameter of 20 nm and a regular spherical shape. In order to verify the geometrical properties, the powder was observed by transmission electron microscopy (TEM) after being dispersed in alcohol under ultrasound vibrations.

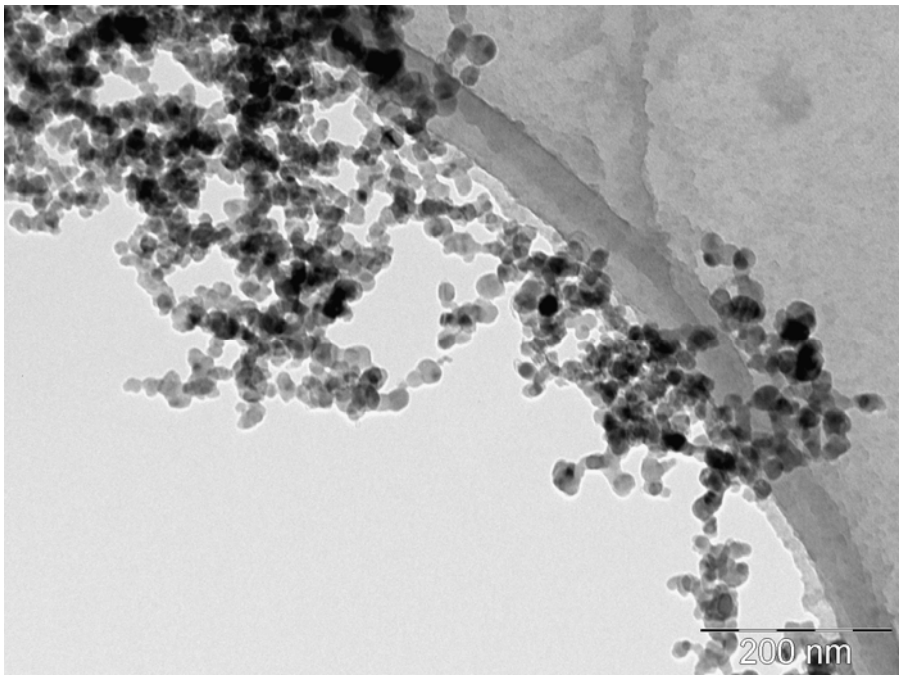

Fig 2.1. TEM micrograph of SiC powder

In the image of Fig 2.1 it is possible to appreciate an agglomerate held by the amorphous carbon film of the sample holder.

At higher magnifications (Fig 2.2) it is possible to observe the single particles and their regular spherical shape. Moreover the particles size distribution appears very narrow and controlled.

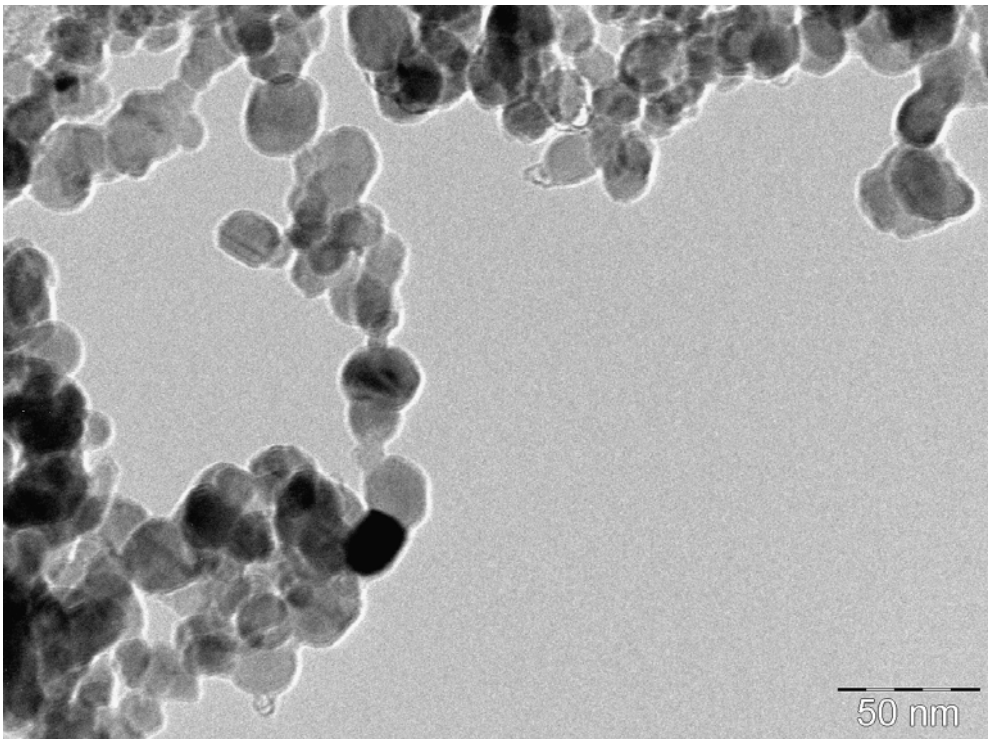

Fig 2.2. TEM micrograph of SiC

The powder was also analyzed by XRD diffraction to investigate the crystal phase, the XRD pattern is reported in Fig 2.3.

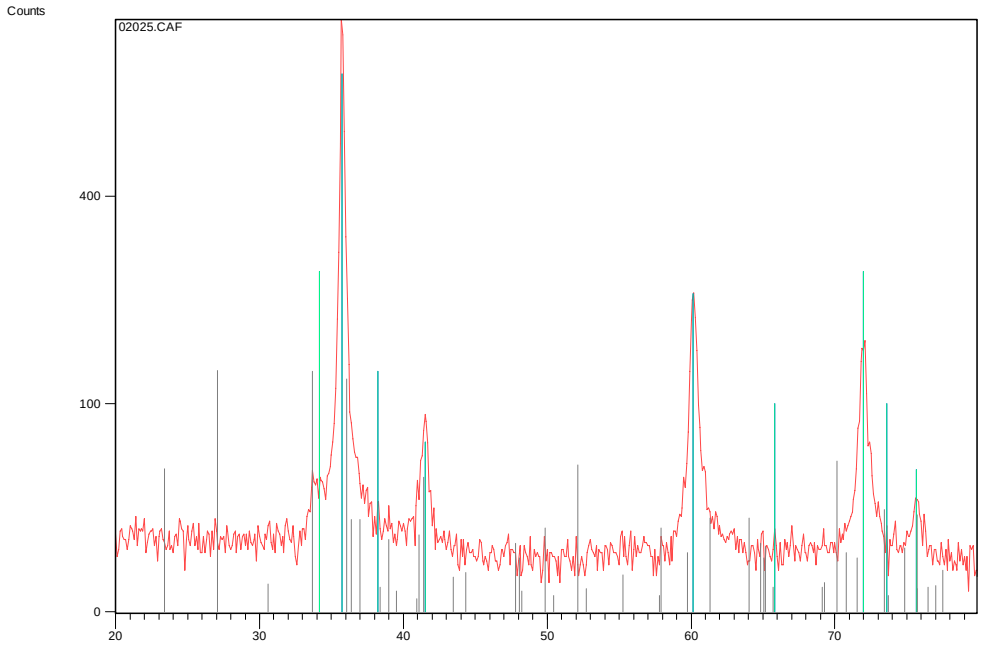

Fig 2.3. XRD spectrum of SiC nanopowder

XRD pattern indicates that the particles are mainly crystallized in the β-SiC phase which has a cubic crystal domain.

In order to evaluate the stability and the agglomeration degree of the as-received powder, ζ-potential and dynamic light scattering measurements were performed.

Most materials exhibit a ζ-potential when immersed in water and its value is influenced by pH, chemical species in solution and ionic strength of the medium[69]. The magnitude of the ζ-potential of the particles is a measure of the particles interaction, and therefore can be used to predict the long-term

[69] The Measurement of Zeta potential Using an Autotitrator: Effect of pH, Application Note by Malvern Instruments, 2005.

stability of a suspension. If the suspended particles have a large negative or positive ζ-potential then they will tend to repel each others and will not aggregate. On the contrary, if the particles have low ζ- potential values, i.e. close to zero, then by no way it is possible to prevent the particles approaching each other and aggregating. The limiting value between stable and unstable suspensions is generally taken at 30 mV or −30 mV [3].

Many surfaces, such as an oxide dispersed in a diluted salt solution, will show a common pattern when the pH is varied: as the pH increases by adding alkali, the surface will become more negative, or at least less positive. Vice versa when acid is added, ionization will cause the loss of hydroxyl ions which will make the surface more positive. In the ζ- potential vs. pH plot, there may be a point where the curve passes through the value zero called the iso-electric point (IEP).

ζ-potential was measured by Zetasizer Nano ZS (Malvern Instruments). The principle of determining ζ- potential is very simple. A controlled electric field is applied via electrodes immersed in a sample suspension and this causes the charged particles to move towards the electrode of opposite polarity because of electrophoresis. The ζ-potential is derived from measuring the mobility distribution of a suspension of charged particles as they are subjected to an electric field. Mobility is defined as the velocity of a particle per electric field unit and is measured by applying an electric field to the suspension of particles and measuring their average velocity. This velocity is measured using the technique of Laser Doppler Anemometry. The frequency shift or phase shift of an incident laser beam caused by these moving particles is measured as the particle mobility, and this mobility is converted to the ζ-

potential by inputting the dispersant viscosity, and the application of the Smoluchowski theory[70].

The charge can arise from ionization of surface groups, chemical bonding or physical adsorption of ions from the liquid medium. Consequently, a charged particle suspended in an electrolyte solution tends to be surrounded by an ionic cloud. Various experimental ζ-potential values of the SiC particles were reported in the literature[71,72,73] and it is reported that the surface charge of the SiC particles can be changed by adding various additives into the solution[74,75]. It was reported that the surface of the SiC can adsorb Ni^{2+} ions that change the polarity of the SiC from negative to positive in an aqueous solution containing Ni^{2+} salts [76].

The Dynamic Light Scattering (DLS) was applied in order to obtain information about the size distribution of the particles dispersed in the solution. By this technique Brownian motion is measured[77] and related to the particles size using the Stokes-Einstein equation[78]: the larger the particles, the slower the Brownian motion will be. The diameter measured by DLS is a value

[70] M. von Smoluchowski, Bull. Int. Acad. Sci. Cracovie, 184 (1903)

[71] X. Zhu, D. Jiang, S. Tan, Mater. Sci. Eng., A Struct. Mater.: Prop. Microstruct. Process. 323 (2002) 232.

[72] S.C. Wang, W.J. Wei, J. Am. Ceram. Soc. 84 (2001) 1411.

[73] M. Hashiba, H. Okamoto, Y. Nurishi, K. Hiramatsu, J. Mater. Sci. 23

[74] L.M. Wang, W.C. Wei, J. Ceram. Soc. Jpn. 103 (1995) 434.

[75] J. Iskra, Ceram. Int. 23 (1997) 337.

[76] S.C. Wang, W.J. Wei, J. Am. Ceram. Soc. 84 (2001) 1411.

[77] Dynamic light scattering: an introduction, Malvern technical notes 2005

[78] R. Xu, Particle Characterization: Light Scattering Methods. Kluwer Academic Publishers, London, 2000.

that refers to how a particle diffuses in a fluid and therefore is the hydrodynamic diameter of a sphere with the same diffusion motion as the particle.

ζ-potential and DLS measurements have been performed in 2 different solutions: a 10^{-3} M KCl aqueous solution and a Watts galvanic bath 50% diluted in deionised water, and in both cases the powder load was 0,2 g/l. The first one is a neutral environment for the ceramic nanopowders and is usually used[79] to determine the agglomeration degree and the suspension behavior of the powder in the as-received state, while the second one is necessary to better understand the behavior of the powder suspended in the real working condition. The dilution was necessary because of the very high ionic strength of the deposition bath, too high for the ζ- potential measurements. In this solution the effect of the presence of Ni ions on the suspension stability was monitored. In literature it has been demonstrated that the variation of the ζ-potential with the bath concentration increases and reaches a near-constant value for a bath dilution of 5-10% [80]. In this solution the pH was always maintained lower than 6.5 in order to prevent nickel hydroxide precipitation.

Fig 2.4 presents the values of the ζ-potential and hydrodynamic diameter of SiC powder suspended in 10^{-3} M KCl as a function of the pH.

[79] A.Bund, D. Thiemig, Surf.Coat. Tech., 201, (2007), 7092

[80] M. Sarret, C. Muller and A. Amell, Journal of Nanoparticle Research (2007) 9:1073–1080

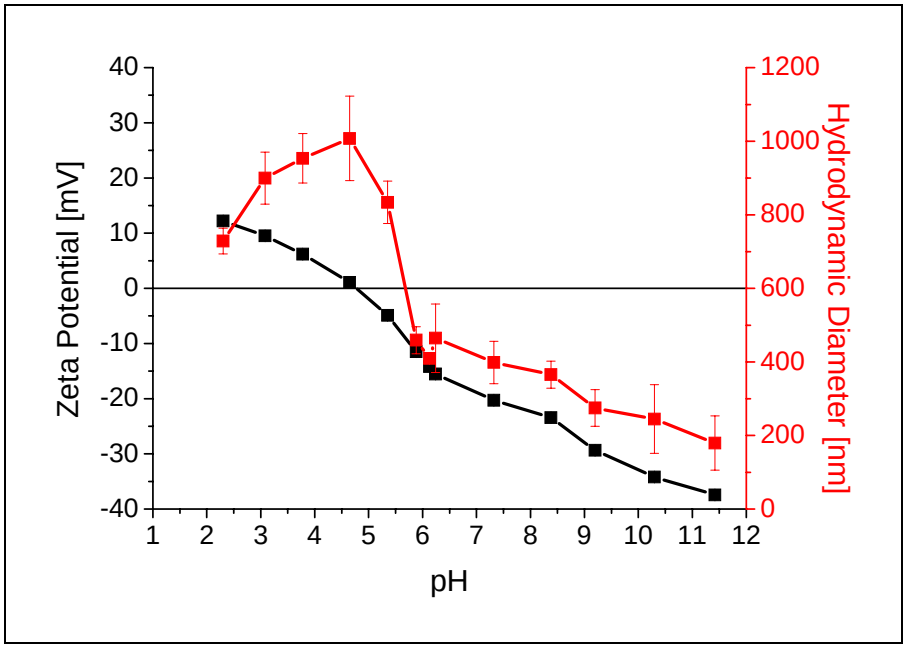

Fig 2.4. ζ- potential and hydrodynamic mean diameter of SiC nanopowder in 10^{-3} M KCl solution as a function of the pH.

The powder presents the isoelectric point at pH 4.5, pH value of the deposition bath. At lower pH the powder is positively charged, but the ζ-potential does not reach the stability threshold value. For higher pH values the powder has a negative surface charge and in alkaline media can form a stable suspension. Consequentially, the powder agglomeration degree increases increasing the pH from 2 to the IEP and then decreases. In the graph of Fig 2.5 the ζ-potential and hydrodynamic diameter are plotted as a function of the pH in diluted Watts bath.

The SiC powder shows the same IEP as in KCL solution (Fig 2.5), but for other pH values the ζ-potential is much lower in absolute value. This means that the ionic species of the bath decrease the stability of the suspension.

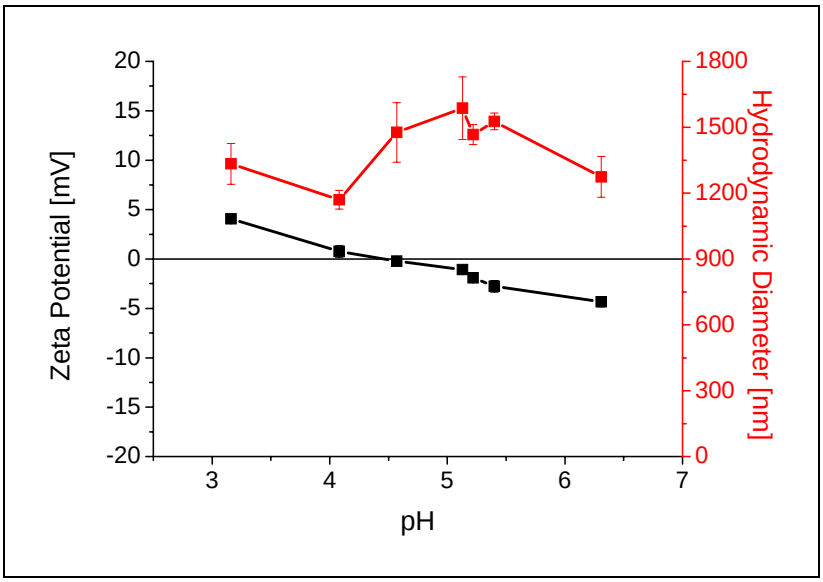

Fig 2.5. ζ- potential and hydrodynamic mean diameter of SiC nanopowder in diluted Watts solution as a function of the pH.

The mean hydrodynamic diameter measured in diluted Watts solution is much higher than in the neutral solution and does not change very much varying the pH. These results confirms that in this solution the powder tends to flocculate.

Al_2O_3 nanopowder

The alumina nanopowder used for the Ni/Al_2O_3 nanocomposites is a commercial nanopowder purchased by Sigma Aldrich® with a mean diameter of 45 nm and a surface area >40 m^2/g (both calculated from BET analysis). In order to verify the geometrical properties, the powder was observed by transmission electron microscopy (TEM) after having been dispersed in alcohol under ultrasonic vibrations.

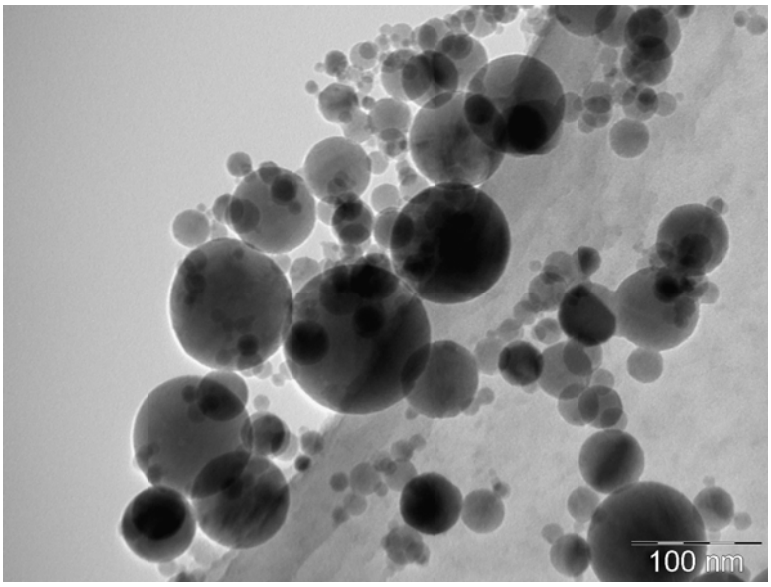

Fig 2.6. TEM micrograph of alumina powder

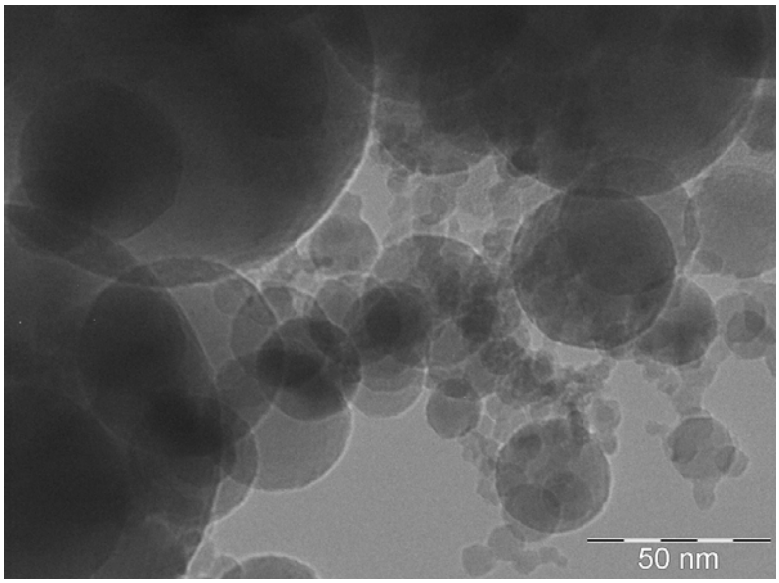

Fig 2.7. TEM micrograph of alumina powder

In Fig 2.6 an agglomerate of alumina particles is visible, held on the border of the amorphous carbon film of the sample-holder. The particles are spherical and very regular the size distribution is quite large: a-side big spheres of about 100 nm there are smaller particles. At higher magnifications, Fig 2.7, also the smallest particles are clearly visible: the particles size varies from 100 nm to 5 nm.

Like silicon carbide, also alumina was characterized by X-rays diffraction to define the crystal structure of the powder.

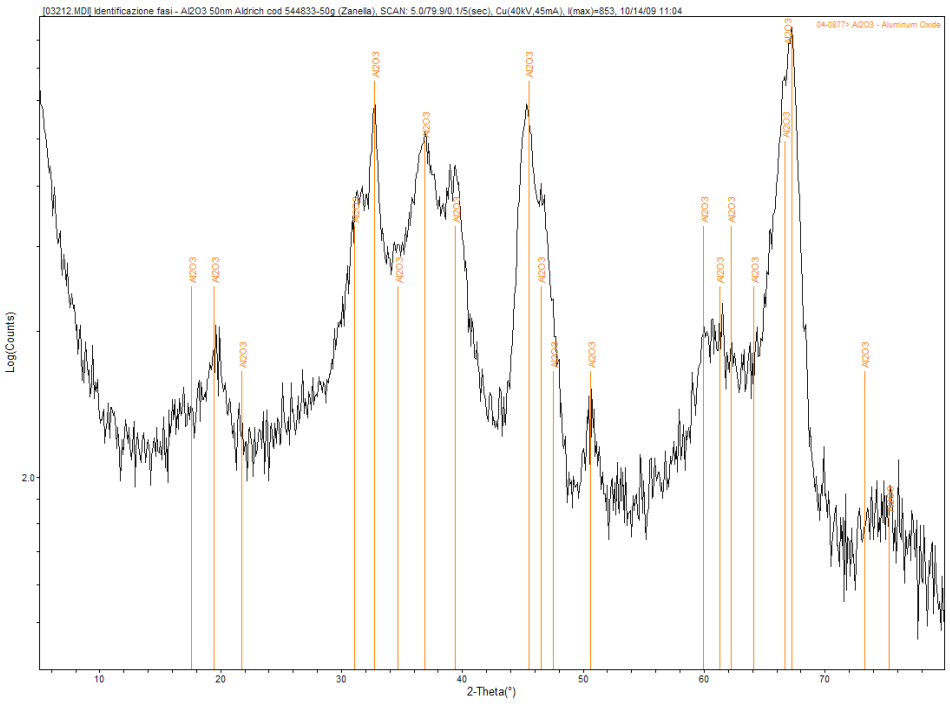

Fig 2.8. XRD pattern of alumina powder

Moreover dynamic light scattering and ζ-potential measurements have been performed to acquire some information about the agglomeration degree of the powder and the stability of the suspension. Also in this case, the measurements have been carried out in 2 different solutions: a 10^{-3} M KCl in aqueous solution and a Watts galvanic bath diluted at 50% in deionised water.

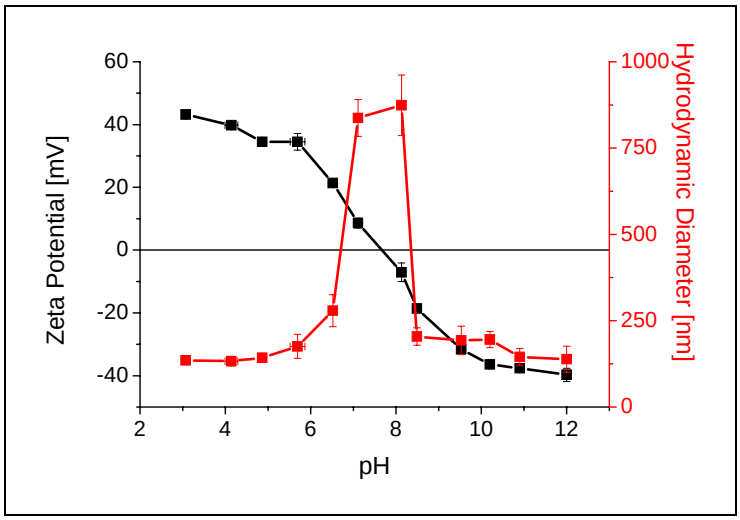

Fig 2.9. ζ- potential and hydrodynamic mean diameter of Al_2O_3 nanopowder in 10^{-3} M KCl solution as a function of the pH.

The Fig 2.9 shows both ζ-potential and hydrodynamic diameter of alumina powder suspended in the neutral solution (10^{-3} KCl) as a function of the pH. The ζ-potential is positive for acidic pH and decreases increasing the pH value, reaching negative values in the alkaline environment. In this solution it is possible to obtain a stable suspension for pH <6 and pH >9. Corresponding to these values the hydrodynamic diameter increases abruptly from 100 nm to almost 1 micron demonstrating that the powder is flocculating and the particles are agglomerated (Fig 2.9). Compared to SiC powder, alumina

presents a higher isoelectric point of about 7.5 and shows higher absolute values of ζ-potential. Moreover the mean diameter is much smaller compared to the SiC powder one. These results show that in the as-received state the alumina powder is more stable compared to SiC. The measurements were repeated in the diluted Watts electrolyte and Fig 2.10 reports the results plot.

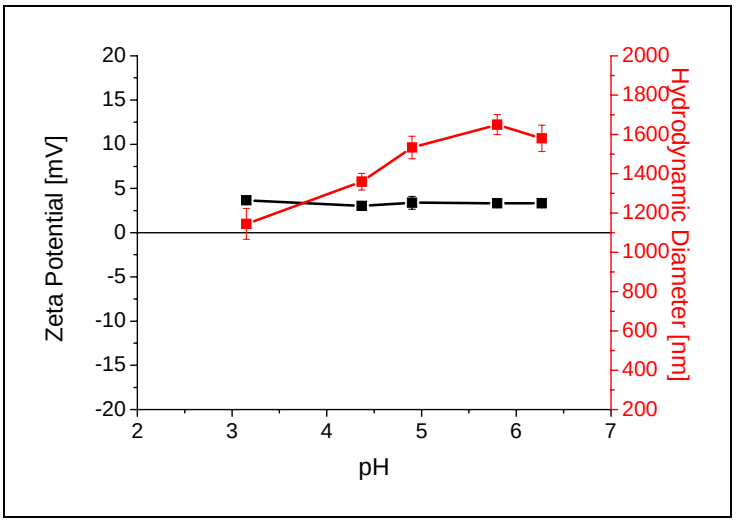

Fig 2.10. ζ- potential and hydrodynamic mean diameter of Al_2O_3 nanopowder in diluted Watts solution as a function of the pH.

Since nickel hydroxide tends to precipitate at pH higher than 6.5, the measurements in the Watts deposition bath were stopped at that value and therefore the isoelectric point of alumina is not visible. In the tested pH range, the powder shows a constant value of ζ- potential of about 5 mV. The mean hydrodynamic diameter measured in Watts solution is much higher than in the neutral solution and tends to increase approaching the IEP. We can conclude that the presence and the high concentration of metal ions decrease the stability of the solution and lead to the powder agglomeration.

Comments

Comparing the suspensions produced with silicon carbide and alumina a big difference is noticed in the neutral KCl solution: alumina is better dispersed in almost all the pH range tested and both ζ-potential and hydrodynamic diameter demonstrate that a stable suspension can be obtained at the working pH of 4.5. Moreover alumina shows a wide range of pH values where the ζ-potential has a positive value. The sign of the ζ-potential is not very important for the stability of the suspension and for the agglomeration degree, but is very important for the codeposition process. The powder should be positively charged in order to be moved toward the cathodic surface by electrophoresis. The silicon carbide powder on the contrary does not have a pH value range where the suspension is stable and the particles positively charged.

On the contrary, the two suspensions in the Watts deposition bath show similar results. The ζ- potential values are so small that no consideration on the long term suspension stability can be done and the mean hydrodynamic diameter is practically the same in the two cases. The only difference to notice is at the working pH range (near 4.5), where the silicon carbide presents the isoelectric point while alumina is slightly positively charged. In the case of SiC suspension, it is not possible to determine the ζ- potential value since the pH near to the cathodic surface can differ from the pH of the bulk solution.

3. Galvanic bath and deposition parameters

Deposition bath

One of the first nickel bath receipts was developed by Oliver P. Watts at the University of Wisconsin in 1916. He formulated a simple salt solution that combined nickel sulphate, nickel chloride and boric acid that nowadays has his name. The advantages of his hot, high-speed formulation led to its industrialization and the fact that the solution can be operated successfully from pH 2 to 5 and at quite high current densities is part of the reason it has survived[81]. Today, the Watts solution is widely used and its impact on the development of modern nickel electroplating cannot be overstated. It is the basis of a majority of the semibright and bright nickel electroplating solutions now in use. The only other solutions to gain commercial acceptance on a reasonably large scale are those based on nickel sulphamate [Cambi and Piontelli, Italian Patent 368,824 (193911)].

[81] George A. DiBari, "Electrodeposition of Nickel" ,in "Modern Electroplating", Fourth Edition, edited by Schlesinger and Paunovic

The electroplating bath used for the deposition of nickel matrix coatings was a Watts type bath, having the following composition:

- 240 g/l of $NiSO_4$
- 45g/l of $NiCl_2$
- 30g/l of H_3BO_4

The necessary amount of Ni ions is given by the $NiSO_4$, while the $NiCl_2$ primarily improves anode corrosion, but also increases conductivity and uniformity of coating thickness distribution. The H_3BO_3 is a buffer and maintains the value of the pH stable between 4.5 and 5[82]. The anode is a pure nickel plate. The soluble anode permits to restore the reduced nickel ions and to maintain a constant Ni^{2+} concentration in the bath.

The nickel reduction on the cathodic surface can happen directly, following the reaction:

(1) $$Ni^{2+} + 2e^- \rightarrow Ni$$

Or in more steps passing through the hydrate form[83,84]:

(2) $$Ni^{2+} + H_2O \rightarrow NiOH^+ + H^+$$

(3) $$NiOH^+ + e^- \rightarrow NiOH_{ad}$$

(4) $$NiOH_{ad} + H^+ + e^- \rightarrow Ni + H_2O$$

The pH of the Watts solution is acidic and therefore protons are discharged simultaneously with nickel:

(5) $$2H^+ + 2e^- \rightarrow H_2 \uparrow$$

The hydrogen evolution occurs near to the cathodic surface and causes a local pH increase that could lead to the precipitation of nickel hydroxide according

82 E. Bertorelle, Trattato di galvanotecnica 1, fourth edition, Hoepli. 1974

83 A. Saraby-Reintjes and M. Fleischmann, Electrochim. Acta 29, (1984) 557

84 M. Matlosz, J. Electrochem. Soc. 140 (1993) 2272

to the reaction:

(6) $$Ni^{2+} + 2OH^- \rightarrow Ni(OH)_{2\ colloids}$$

These colloids can interact with the crystallization process or be embedded in the metallic layer making the coating rough and dark[85,86]. To avoid this problem the presence of the buffer is very important because it gives proton wherever there is any small and local change in the pH according to the reaction:

(7) $$H_3BO_3 \rightarrow H^+ + H_2BO_3^-$$

For the production of the composite coatings 20g/l of nanopowder were added into the electroplating bath which is treated with ultrasound for 1 hour and mechanically stirred for 24 hours before the electrodeposition. Mechanical stirring at 400 rpm was used also during the electrodeposition process. The bath temperature was maintained stable at 45°C using a thermostat.

[85] R.Winand, Electrocrystallization-theory and application, Hydrometallurgy, 29 (1992) 567

[86] A. Vicenzo and P.L. Cavallotti, Structure and Electrokinetic Study of Nickel Electrodeposition, Russian Journal of Elektrokhimiya (2008), Vol. 44, No.6, pp. 716-727

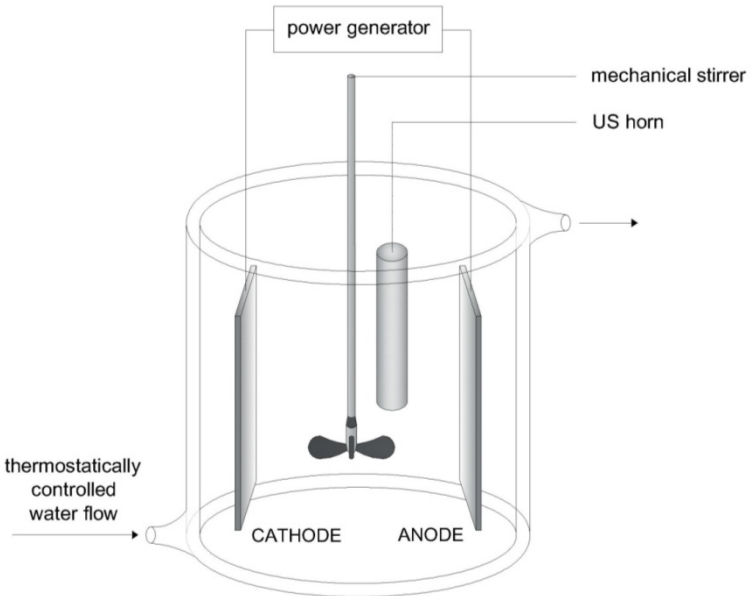

Fig 3.1. Deposition cell design

The geometry of the cell consisted in two vertical parallel plane electrodes, one in front of the other with the mechanical stirrer in between, see Fig 3.1.
This geometry ensures that the process is not affected by sedimentation. The mechanical stirring is necessary to maintain the powder in suspension during the deposition. An ultrasonic horn was introduced in the cell between the 2 electrodes whenever the stirring was performed by ultrasounds and for the deposition under ultrasonic vibration.

Current conditions

The deposition was carried out under galvanostatic control both under direct and pulse current. Pulse electrodeposition has been found to be effective in perturbing both the adsorption–desorption phenomena and electrocrystallization process, thus leading to an increase in the limit current density and to the opportunity to control the microstructure of nickel electrodeposits[87,88]. To achieve a significant grain refinement though, the pulse-off times should be at least as long as the pulse-on times[89,90].

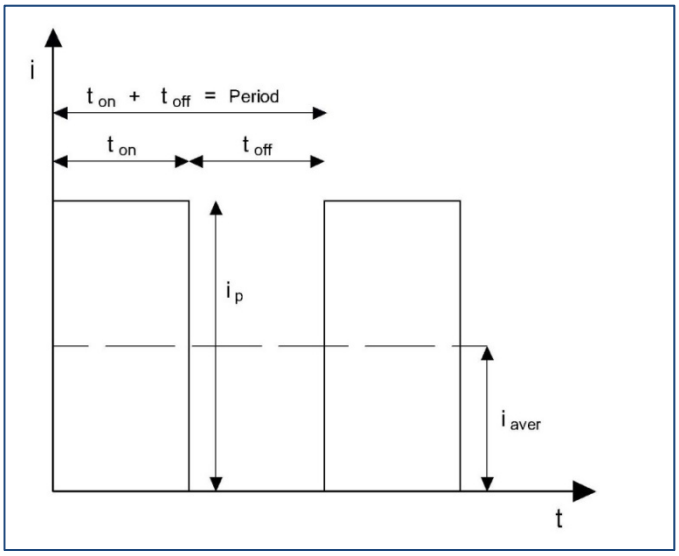

Fig 3.2. Schematic wave form and parameters

[87] N. Ibl, J.C. Puipe, H. Angerer, Surf. Coat. Technol. 6 (1978) 287.

[88] N. Ibl, Surf. Coat. Technol. 10 (1980) 81.

[89] E. Toth-Kadar, I. Bakonyi, L. Pogany, Surf. Coat. Technol. 88 (1996) 57.

[90] N.S.Qu., D.Zhu, K.C Chan, W.N.Lei, Surface and Coatings Technology 168 (2003) 123–128

A current density of 2 A/dm^2 was used for the specimens produced under direct current. The electrodeposition time was a function of the thickness of the deposits and the deposition rate under the above mentioned conditions was about 20μm/h.

The pulse current used had a square form (Fig 3.2) and a duty cycle of 50% (t_{on}=t_{off}). The minimum current density was 0, while the maximum current density was maintained at 2A/dm^2 in order to better compare the specimens with those produced under direct current. As above, the deposition time was dependant on the thickness of the deposits but in this case the deposition rate was 10μm/h because of the off-time.

The deposited mass can be calculated theoretically using the Faraday law:

$$m = \frac{MQ}{N_A z e} \qquad (8)$$

where:

m: deposited mass [g];

M: the atomic weight [g/mol];

Q: the total charge [C];

N_A: Avogadro number [mol^{-1}];

z: ion valence;

e: electron charge [C].

The deposited mass measured by weight gain was compared to the theoretical one calculated by Faraday law, thus leading to the calculation of the cathodic process efficiency as:

$$\varepsilon = \frac{m_{real}}{m_{th}} \qquad (9)$$

No differences due to the pulse current at different frequencies were observed in the process efficiency, while the addition of nanoparticles induced a slight

decrease on it. The mean value of the cathodic efficiency is about 94% for pure nickel and about 90% for codeposition process.

Substrate preparation

Q-panels of carbon steel (SAE 1008/1010; 0.13 max C, 0.25–0.60 Mn)[91] have been used as substrates for the production of both pure and composite coatings. Steel is much less noble than nickel and its corrosion products are clearly visible (red rust), providing an ideal substrate to evaluate the protective properties. Moreover, steel is one of the most common substrates usually coated by nickel, due to its mechanical properties and the low production cost. After being cut to the desired dimensions the Q-panels were mechanically polished using abrasive papers of 180, 500 and 800 grit and degreased by immersion in acetone and use of ultrasonic bath for 5 min. These procedure were necessary to be sure to remove any surface oxide and organic impurities. Then, to activate the surface, the substrates were etched using a 10%vol. of sulphuric acid at 60°C till the formation of a non adherent black oxide which covered the entire surface. This oxide was afterwards removed using distilled water and ultrasonic bath.

At this point the substrates were weighted and masked leaving free only the surface to be coated. Just before the immersion into the electroplating bath the masked substrate was again dipped in acid for few second and then rinsed with distilled water in order to remove the small amount of oxides which

[91] Q-panel techincal datasheet

might be formed during the exposure to the atmosphere while masking, since after etching the surface is extremely reactive.

After the deposition the tape used as mask was removed and the samples were rinsed in distilled water in an ultrasonic bath in order to remove any residuals of the galvanic bath, especially any loose adsorbed nanoparticles, from the surface and weighted again.

Organic additives

Wetting agents or surfactants, formulated specifically for nickel plating solutions, are almost always added to control pitting. Their function is to lower the surface tension of the plating solution so that air and hydrogen bubbles do not cover the cathodic surface hiding nickel formation and leaving pits and pores on this surface. The most used additive for Watts nickel plating bath is sodium dodecylsulphate (SDS)[92]. It is an anionic surfactant (Fig 3.3) with a tail of 12 carbon atoms, attached to a sulphate group. Its concentration into the deposition bath can vary from 0.01 to 1 g/l depending especially on the pH of the solution.

[92] E.Bertorelle, Trattato di galvanotecnica, Hoepli, Milano 1974

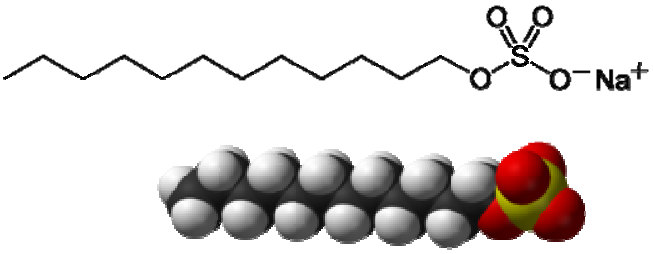

Fig 3.3. Schematic image of the SDS molecule

From an industrial point of view it is essential to use additives to avoid completely the pitting, because the pores could reach the substrate, in order to obtain an effective protective layer. Otherwise the defects could induce a more aggressive corrosion attack because of the galvanic couple formed between the metallic coating and the substrate.

Regarding the codeposition of metal matrix coatings via electrodeposition, surfactants and additives in general become even more important because they could affect and improve not only the metal deposition but also the powder suspension stability, its agglomeration degree especially if the size of the particles is in the nano range. The smaller inert particles are more difficult to embed into the deposition layer because they are hardly dispersed in the electrolyte[93,94,95].

The interaction mechanism between surfactants and electrolyte and between surfactant and ceramic powder is very complex and is very difficult to analyze.

[93] G. Maurin, A.Lavant, J.Appl. Electrochem., 25 (1995) 1113

[94] I.Garcia, J. Fransaer, J.P. Celis, Surf.Coat.Tchnol., 148 (2001) 171

[95] K.H,Hou, M.D.Ger, L.M.Wang, S.T. Ke, Wear, 253, (2002) 994

The deposition bath, in which the surfactant is added, has a high ionic concentration and the charged molecules interact with the ionic part of the organic additive. Moreover an electrical field is applied to the system and therefore an interpretation of the many process and interaction between the bath's components and the organic additive is complex.

When a surfactant is in contact with a partially charged solid surface, i.e. the ceramic nanoparticles in the electrolyte, it could be adsorbed onto the surface and interact with the surface charge. When the ionic coupling between the charge of the surface and the ionic part of the organic molecule is high, the zeta potential decreases until the surface charge is completely neutralized[96]. This could lead to the loss of stability of the suspension, since no electrostatic repulsion is possible any more.

On the other hand, the adsorption of organic molecules cause the alignment of the hydrophobic tie toward the electrolyte[97] and the surface becomes hydrophobic. The hydrophobic groups are not wetted by the electrolyte and recall other hydrophobic groups, thus continuing to adsorb organic molecules that are aligned in the opposite way with the non polar tie toward the particle and the ionic part toward the electrolyte. The charge is then preserved but with the opposite sign (Fig 3.4).

The effect of the organic additives on the codeposition process is not very clear and has been studied by several researcher groups.

[96] J.Goodwin, Colloids and Intefaces with surfactant and Polymers, Wiley 2004

[97] D. Myers, Surfactant science and technology, VCH Publishers, Inc., 1988

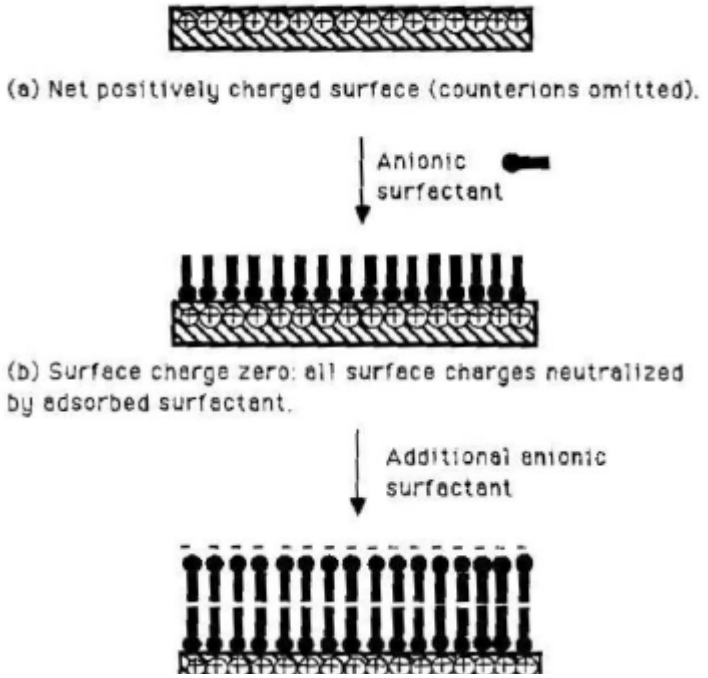

Fig 3.4. Mechanism of adsorption of surfactant on partially charged solid surface[16]

Since the mechanism of interaction between particles and surfactant is very complicated and depends on many variables, such as particle size, chemical composition, production technology, bath composition, etc., it is not easy to find a linear correlation between the variables of the studied system and the mechanism of surfactant–particles interaction. In fact there are opposite experiences. Ming-Der Ger[98] studied the system Ni/SiC (600nm) from a sulphamate bath containing CTAB (cetiltrimetilammonium bromide) as

[98] M.D. Ger, Materials Chemistry and Physics, 87 (2004) 67

cationic surfactant and showed that the embedded SiC fraction is proportional to the CTAB concentration, possibly because by increasing the positive zeta potential of the suspension, the embedded ceramic fraction will be increased. V.Terzieva et al.[99] on the contrary found that the cationic surfactant decreases the particles content in the deposited layer.

N. K.Shrestha, et al. [100] studied the influence of the length of the hydrophobic ties of cationic surfactant of AZTAB groups. They demonstrate that the shorter molecules were more effective in the codeposition process allowing the deposition of a larger amount of inert particles.

Effect of SDS on the SiC suspension stability

Since SDS is one of the most used organic additives for the pitting control in the industrial process, it is important to understand its effect on the powder suspension stability. Therefore the ζ-potential has been measured in suspension containing 0.1 g/l of SDS and in the same condition presented in chapter 2 (10^{-3} KCl and diluted Watts deposition bath).

[99] V. Terzieva, J. Fransaer, J.P.Celis, J. Electrochem Soc., 147 (2000) 198

[100] N.K.Shrestha, M.Masuko, T.Saji, Wear, 254 (2003) 555

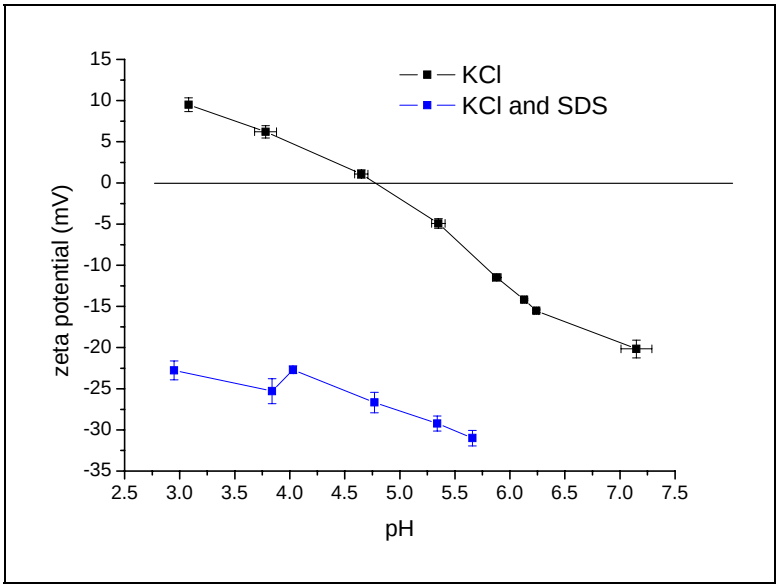

Fig 3.5. ζ–potential of SiC nanopowder in KCl with and without SDS

As the plot in Fig 3.5 shows, the addition of the SDS in the suspension changes the zeta potential of the silicon carbide powder towards more negative values. No IEP is visible in the pH range tested and the absolute ζ- potential value is always larger than 20 mV demonstrating a major stability of the suspension when the surfactant is added. The shift versus more negative values means that the particles' surface is surrounded by the additive molecules that are negatively charged. The negative charge could act as inhibitor for the codeposition process since the electrophoresis would move the particles towards the anode rather than the cathode, where the nickel layer is growing.

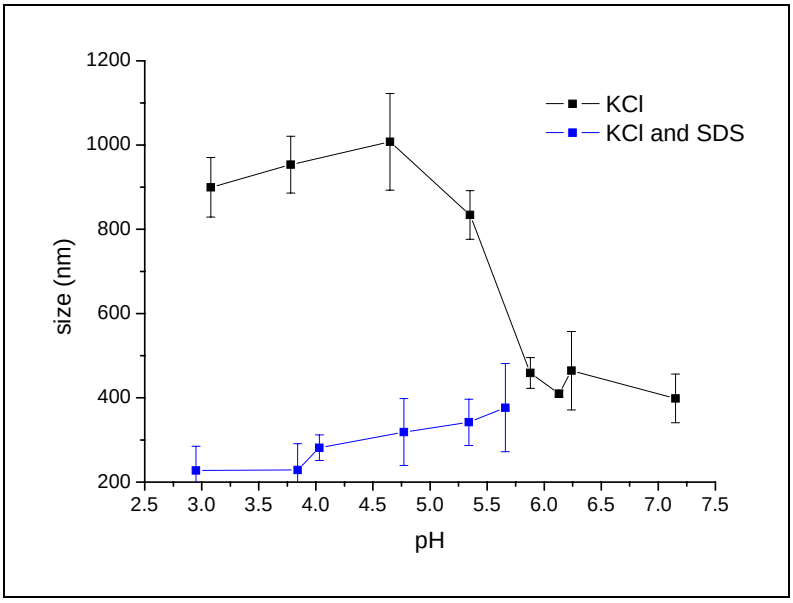

Fig 3.6. Mean size value of SiC nanoparticles in KCl solution with and without SDS

As the ζ-potential values suggested, the addition of SDS is active in improving both suspension stability and dispersion. As it can be appreciated in Fig 3.6 the agglomeration degree of the powder decreases of about one order of magnitude thanks to the anionic surfactant and the mean size increases slightly increasing the pH.

In the diluted Watts deposition bath (Fig 3.7), the absolute value of the ζ-potential is always less than 20 mV and therefore no stabile suspension is obtained in this solution both with and without SDS. As for KCl solution, when SDS is added to the solution no IEP point is visible in the pH range tested since the ζ- potential is always negative. ζ- potential slightly decreases increasing the pH of the solution. At the deposition pH of 4.5 the ζ- potential is about 0 in Watts solution and shifts down to -8 mV when the SDS additive is added. Of

course this means that in working condition the solution could be more stable with SDS, but not enough to avoid flocculation and sedimentation of the powder.

Moreover the more negative value of the powder ζ-potential could modify the electrophoresis and therefore the codeposition process.

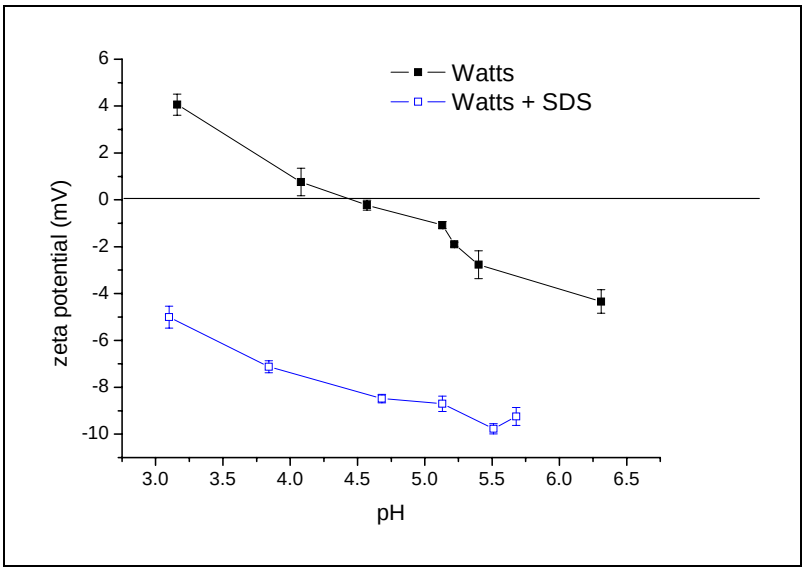

Fig 3.7. ζ- potential of SiC nanopowder in diluted Watts solution with and without SDS

Considering the mean hydrodynamic diameter (Fig 3.8), the addition of SDS provokes a slight increase of the mean size, even though the ζ-potential absolute value is higher.

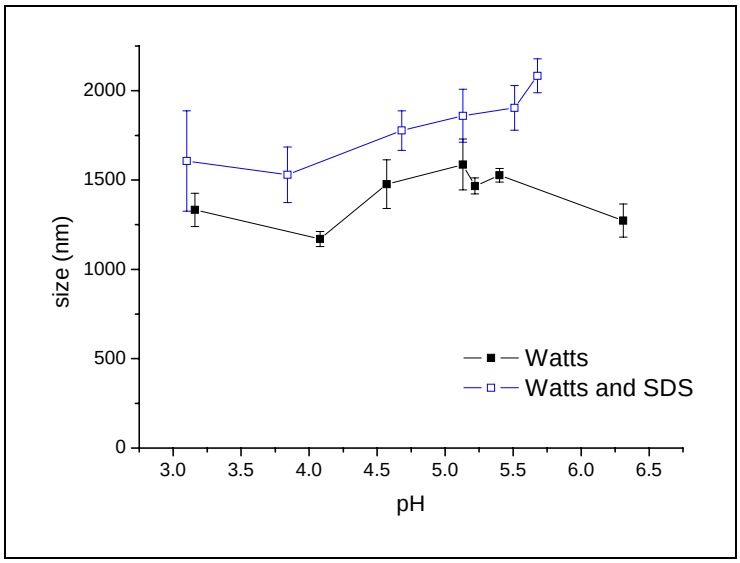

Fig 3.8. Mean size value of SiC nanoparticles in diluted Watts solution with and without SDS

Effect of SDS on the Al_2O_3 suspension stability

As for silicon carbide powder, the influence of SDS on the stability of alumina suspension was monitored by means of ζ- potential and hydrodynamic diameter both in KCl solution and diluted Watts deposition bath. In Fig 3.9 and Fig 3.10 are reported the plots of ζ- potential and hydrodynamic diameter as a function of the pH in KCl solution.

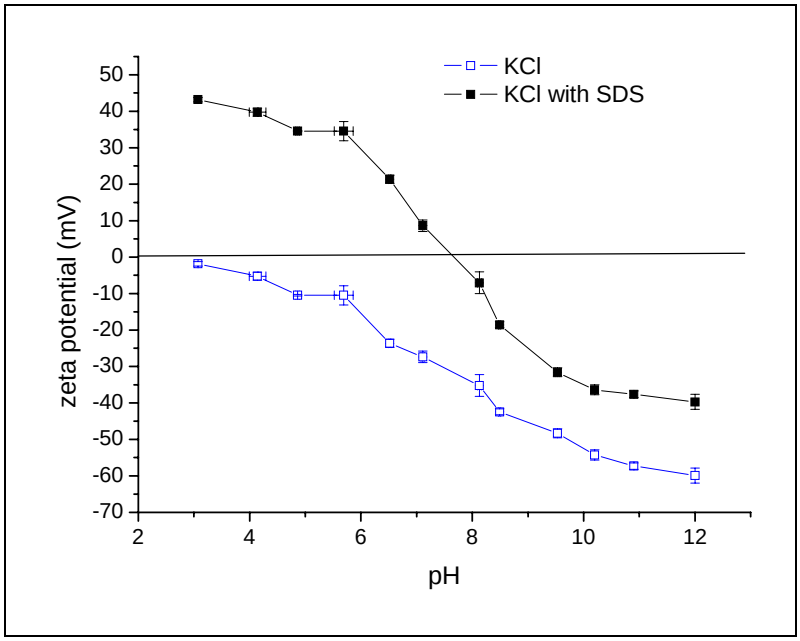

Fig 3.9. ζ- potential of alumina suspension in KCl solution with and without SDS

The ζ-potential shifts toward more negative values when the SDS is added, and the shift is more evident in the acidic pH range. The ζ-potential is negative from pH 3 to pH 12 and therefore no IEP is determined when SDS is added. The negative tie of the organic additive results to be adsorbed onto the ceramic particle's surface, thus modifying the sign of the potential from positive to negative in the range of pH from 3 to 7 and increasing the negative potential values in the range of pH from 7 to 12. With no additive the suspension is very stable, and the potential values is lower than 20 mV only in the proximity of neutral pH. When the SDS is added, the stability range changes and only above pH 6 the ζ- potential reaches values high enough to guarantee the stability.

The mean hydrodynamic diameter (Fig 3.10) decreases significantly

increasing the pH. According to the ζ-potential values the maximum value of hydrodynamic diameter corresponds to the lowest pH. Comparing these results to the values obtained in additive-free solution, it is clear that the agglomeration degree is higher in the presence of SDS. Considering the acidic pH range (pH 3-6), the additive-free solution shows a higher ζ-potential and therefore the mean size is much lower, more than one order of magnitude. For pH of 7-8, the alumina powder shows the IEP in the additive-free solution, while has a ζ-potential of -30 mV in KCl with SDS.

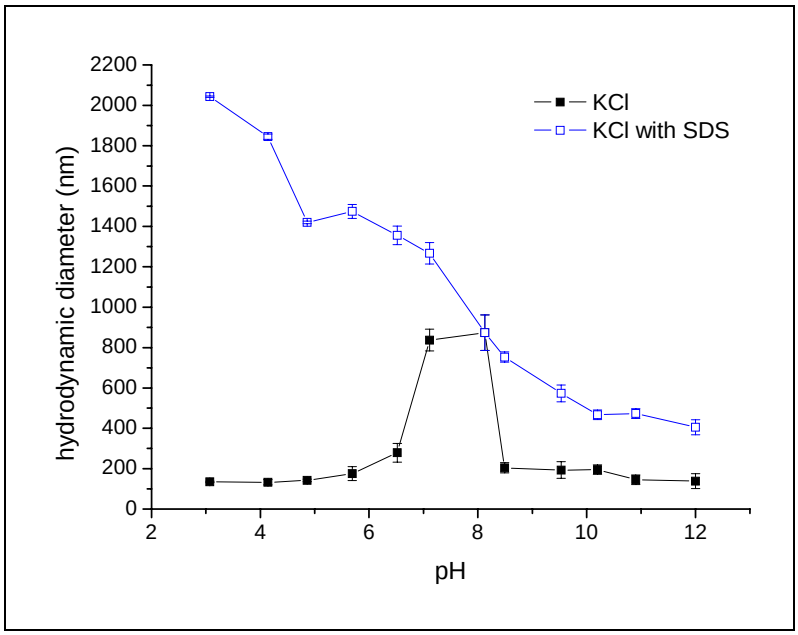

Fig 3.10. Mean hydrodynamic diameter of alumina suspension in KCl solution with and without SDS

However the mean size of the agglomerates is the same. In the alkaline range of pH the absolute value of the potential is higher in solution with SDS but the mean size does not reach the value of the size in additive-free bath.

These results demonstrate that even if the alumina powder is more stable for some pH values, the addition of the SDS leads to higher agglomeration rate. Moreover the SDS changes the sign of the zeta potential in the acidic range from positive to negative, thus leading to a possible change in the codeposition process.

The measurements were repeated also in diluted Watts solution with SDS and compared to the results obtained in the additive-free bath (see chapter 2).

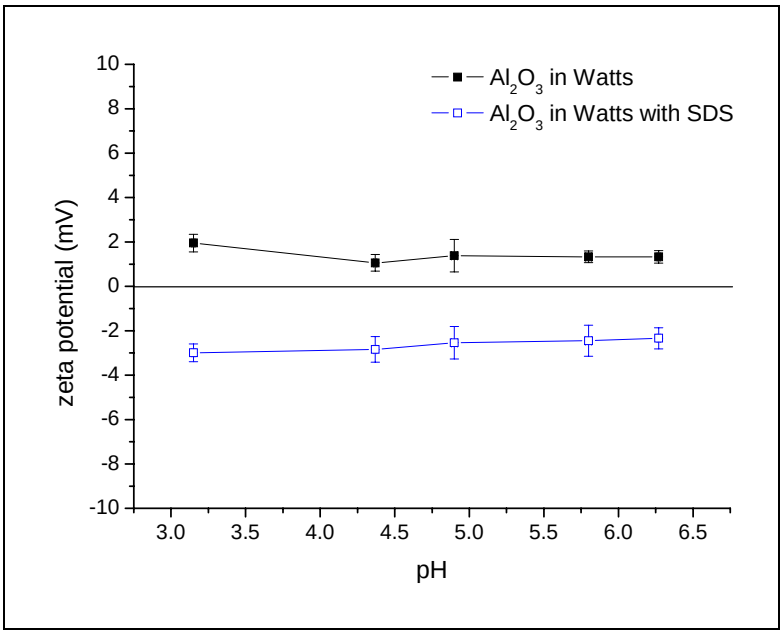

Fig 3.11. ζ- potential of alumina suspension in diluted Watts solution with and without SDS

The ζ-potential is more or less constant in the pH range tested and is very low (Fig 3.11), no IEP is visible and no stable suspension seems to be possible in this condition. Compared to the suspension in additive-free bath the ζ-potential has the same absolute value, but with the opposite sign. In this

condition the alumina powder is negatively charged.

Concerning the hydrodynamic diameter, plotted in Fig 3.12, the mean size does not change very much in the pH range tested and is about 0.9 μm. Compared to the mean size in additive-free bath, the alumina powder is more agglomerated in presence of SDS.

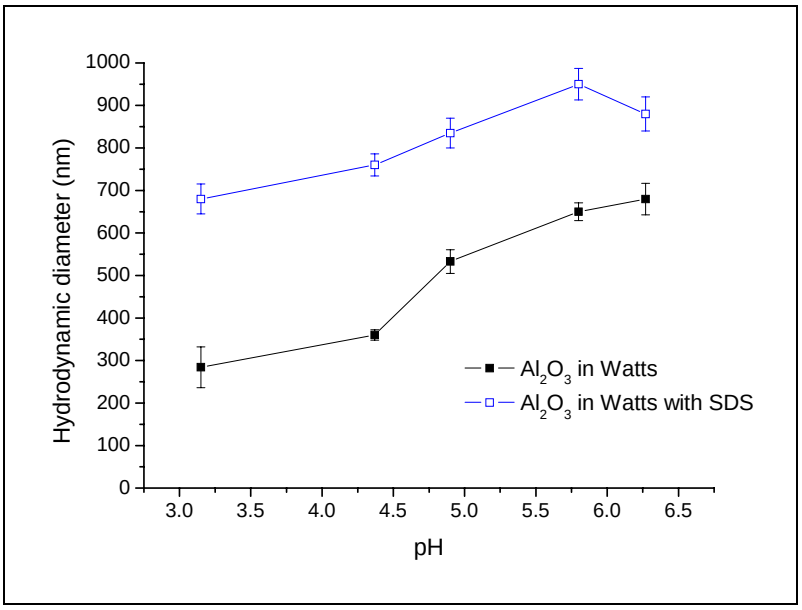

Fig 3.12. Hydrodynamic diameter of alumina suspension in diluted Watts solution with and without SDS

The use of ultrasounds in electrochemistry

Over the last few years a large number of articles has been published which describe the variety of applications of power ultrasound in chemical processes[101]. These include synthesis, polymer chemistry and some aspect of catalysis. Moreover ultrasounds have already a wide diffusion and applications on chemical engineering process, such as for dispersion of solids, crystallization and degassing processes.

Ultrasound was also shown to affect metal electrodeposition with benefit to the quality of the deposit, its adhesion and morphology, and also the diminution of brighteners and other additives needed in silent systems[102]. Generally the frequency region just above hearing is called 'power' ultrasound (20 – 100 kHz), and this is where ultrasonic cleaning bath are working. The effects of ultrasound in a liquid are to cause 'acoustic streaming' and/or the formation of cavitation bubbles, depending upon the parameters of ultrasonic power, frequency, sonic source characteristics, and solution phenomena such as viscosity, volatility, and the presence of dissolved gases or other nucleation sites[103]. The power of ultrasounds produces its effect via cavitation bubbles. These bubbles are generated during rarefaction cycle of the wave when the liquid structure is literally torn apart to form tiny voids which collapse in the compression cycle[104]. The formation and decay of cavitation bubbles involve transient extremes of temperature and pressure, and the bubbles can form

[101] T.j. Manson, Ultrasonics, 24 (1986) 245

[102] R. Walker, Advances in Sonochemistry, Manson ed.,JAI Press, 1993 vol 3

[103] T.J. Manson, J.P.Lorimer, Sonochemistry, Ellis Horwood, 1989

[104] M.A.Margulis, J.Phys. Chem., 50 (1976) 1

micro jets that impinge towards a surface.

A number of possible effects of ultrasound upon an electrochemical system may be predicted[105]:

- A general improvement of hydrodynamics and movement of species;
- The alteration of concentration gradients at various points in the reaction profile, and consequent switching of kinetic regimes with effect on mechanism and reaction products;
- A cleaning and abrading effect upon an electrode surface, thus obviating fouling problems, or else altering the nature of coatings that manage to form;
- Sonochemically-induced reactions of intermediate species that have been generated electrochemically;
- The sonochemical formation of species that react electrochemically in conditions where the silent system is electroinactive.

Regarding the electrodeposition of metals, these effects can be pointed out as[106]:

- rapid and effective removal of gas bubble from electrode surface thus avoiding pitting on the deposited layer;
- decrease of the double layer and of the diffusion layer thicknesses thanks to the agitation and the pressure waves;
- higher transport rate of the ions trough the double layer;
- Cleaning and activation of the electrodes surface that improve the process efficiencies, both cathodic and anodic.

[105] D.J. Walton, ARKIVOC (2002) 198

[106] T.J.Manson, J.P.Lorimer, Sonochemestry, Ellis Horwood, 1988

These factors are claimed to improve deposition rates and efficiencies and to have some benefits on the deposit hardness and on the adhesion to the substrate[107].

Much work has been carried out from an industrial point of view, empirically, in particular on metals important in electroplating technology such as zinc[108], iron[109], chromium[110,111], copper[112] and nickel[113]. Hyde and Compton[114] in their studies on the influence of ultrasounds on electrodeposition of metals, conclude that in electrodeposition under the influence of ultrasounds, the critical effect is the increase in mass transport, which may be high enough to change a diffusion controlled system into a charge transfer controlled system. In particular, in the case of nickel deposition from Watts bath under potential control, it has been found[115] that the exchange current density increases and the texture of the deposited film changes, increasing the (200) face rate and decreasing the (111) face rate. Moreover the charge transfer reaction is promoted by the use of ultrasounds.

The use of ultrasounds during electroplating of pure metals may improve the final properties of the films refining the microstructure and thus leading to a

[107] P.Lorimer, T.J. Mason, Electrochemistry, 67 (1999) 924

[108] P.B.S.N.Prasad, R. Vasudevan, S.K. Seshadri, Trans.Indian Met., 46 (1993) 247

[109] R. Walker, S.A. Halagan, Plat, Surf. Finish., 72 (1985) 68

[110] J.Dereska, E. Jaeger, F. Hovorka, J. Acoust. Soc. Am. (1957) 69

[111] E. Namgoong, J.S. Chun, Thin Solid Films, 120 (1984) 153

[112] RT. Walker, C.T. Walker, Ultrasonic, 13 (1975) 79

[113] J.K.Klima, C.Bernard, C. Degrand, J. electroanal. Chem., 367 (1994) 297

[114] M.E. Hyde, R.G. Compton, J. Electroanal. Chem., 531 (2002) 19

[115] K.Kobayashi, A. Chiba, N. Minami, Ultrasonics, 38 (2000) 676

harder more compact layer [116,117].

Few studies have been performed on the use of the ultrasounds during the electrocodeposition of ceramic nano-particles. Qu et al.[118] demonstrated that the ultrasonic vibrations promote the uniform distribution of Al_2O_3 wiskers but decreases the ceramic content embedded in the nickel matrix. Resrazi[119] used ultrasounds to improve the codeposition rate of PTFE particles in gold matrix; Zheng[120] used the ultrasonic treatment to improve the content and uniformity of nano Al_2O_3 in NiZn alloy matrix. Lee et al[121] found out that ultrasonic vibrations enhance the de-agglomeration of Al_2O_3 and CeO_2 in Cu matrix specially in low concentrated baths. Very few studies consider how ultrasounds affect the codeposition, and no systematic studies have been performed on the final properties, both mechanical and protective.

Effect of US on the suspension stability

The efficiency of the ultrasonic vibrations on the disagglomeration of the powder in suspension has been monitored measuring the mean diameter of agglomerates in the same 2 suspensions described in chapter 2: the 10^{-3} M KCl solution and the diluted Watts deposition bath at pH of 4.5 that corresponds to the deposition pH. The powder was suspended in the solution and

[116] J.C. Ball, R.G.Compton, Electrochemistry, 67 (1999) 912

[117] L.Martins, J.I. Martins, A.S. Romeira, M.E. Costa, J. Costa, M.Bazzaoui, Mater. Sci.Forum, (2004) 455

[118] N.S.Qu, K.C.Chan, D.Zhu, Scripta Mater. , 50 (2004) 1131

[119] M. Rezrazi, M.L.Doche, P.Bercot, J.Y.Hihn, Surf.Coat. Tech., 192 (2005) 124

[120] H.Y. Zheng, M.Z. An, J. Alloys and Compounds, 459 (2008) 548

[121] D. Lee, Y.X.Gan, X. Chen, W.J. Kysar, Mat. Scie. Eng. A, 447 (2007) 209

mechanically stirred for 12 hours before the first measurement, in order to simulate the codeposition bath preparation procedure. Then the suspension was stirred by ultrasonic vibrations for different times and then the size distribution was monitored after 5, 10 , 30 and finally 60 minutes of US treatment. Of course the measurement has been carried out just after the US stirring, without any vibration.

In Fig 3.13 the mean size values of SiC powder are plotted for both the 2 suspensions. At the working pH the differences between the hydrodynamic diameter in KCl and Watts deposition bath are very limited. At this pH in fact, both suspensions show a very small ζ- potential (see chapter 2). The ultrasound treatment is practically useless in the neutral solution, no big changes in the mean size are visible after 60 minutes of US stirring. Probably, the US can break the SiC agglomerates during the stirring, but at this pH the powder has a ζ- potential vale near to 0 (it is at its IEP indeed) and therefore the suspension tends to agglomerate again when the ultrasound source is turned off for the measurement.

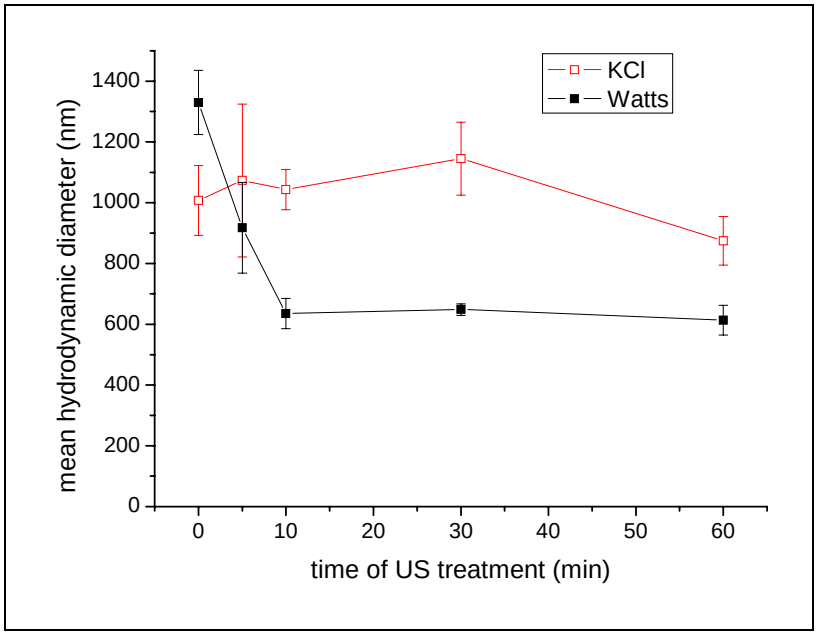

Fig 3.13. Hydrodynamic diameter of SiC powder in suspension in Watts and KCl solution before and after the US treatment

The suspension in Watts deposition bath, on the contrary, is positively affected by the US treatment and the agglomerate mean size decreases during the first 10 minutes of stirring from 1400 nm to about 600 nm and then remains stable for longer treatment. At the working pH of 4.5 the SiC ζ-potential is near to the IEP and therefore it can be supposed that the efficiency of US treatment would be higher at different pH, but when the stirring is turned off the suspension tends to agglomerate again.

In the graph of Fig 3.14 of the mean size values of the alumina suspension in the 2 different solutions during the US treatment are plotted.

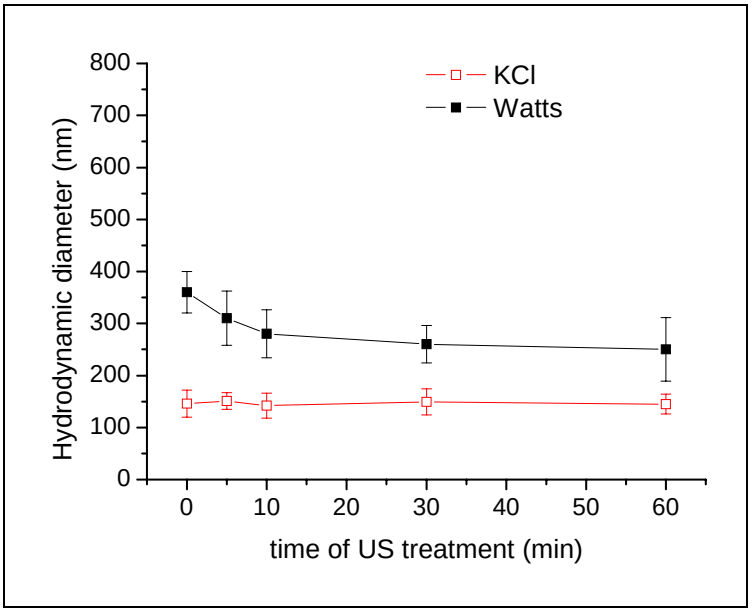

Fig 3.14. Hydrodynamic diameter of Al_2O_3 powder in suspension in Watts and KCl solution before and after the US treatment

The alumina powder in KCl solution at pH 4.5 (Fig 3.14) is already well dispersed and the mean diameter is about 150 nm. The US treatment does not affect the mean size that is already very small. The alumina in Watts solution has a slightly bigger dimension that after 10 minutes decreases from about 350 nm to about 280 nm; longer US treatment does not further affect the agglomeration degree. Since the alumina powder is already very well dispersed in both solutions, the US are not so effective in decreasing the agglomeration degree of the alumina suspensions.

Summary and comments

A first general comment has to be done comparing the results obtained in KCl solutions to the ones of diluted Watts bath. The ζ- potential measured in the neutral environment is often very different from the values measured in the real working solution. This fact is due to the presence of the metallic cations or generally to the high concentration of ions in a galvanic bath that interact with the particles in suspension, changing their charge and their stability. The measurement in KCl could be important to understand the as-received state of the powder and therefore to monitor the initial agglomeration degree, but in order to understand the real behaviour it is always important to make the measurements in the real environment.

The effect of one of the most used organic additive on the pitting control has been tested by means of ζ-potential measurements and mean hydrodynamic diameter. The results of the previous paragraphs demonstrate that the SDS decreases the ζ-potential of the particles, both SiC and Al_2O_3. For SiC powder, this shift toward more negative values corresponds to an increase of powder stability and therefore a decrease in the mean size. For Al_2O_3 the presence of SDS leads even to a change in the sign of the potential especially for pH<7 and this shift brings the ζ-potential from stable values down to values too low to guarantee the stability of the suspension, thus leading to the increase in the mean diameter. A very important factor is that SDS increases in certain cases the stability of the suspension, but decreases the zeta potential values that become negative. Having a negative surface charge, the powder could not be electrophoretically brought to the cathode surface and this could lead to an inhibition of the codeposition process.

The SDS has to be removed from the galvanic bath in order not to interfere with the codeposition process.

A possible alternative to SDS in avoiding pitting on cathode surface is to use ultrasounds: their degassing properties can help in removing the hydrogen bubbles leading to the formation of a pore-free deposit and moreover the US could deagglomerate the nanopowder during the deposition process. Again this last effect has been monitored by means of hydrodynamic diameter by DLS and the results show that US are effective in decreasing the mean size of agglomerate in Watts solution, while for SiC no effect is visible in KCl solution. The alumina powder is already well dispersed and therefore no big effects of US are visible on its agglomeration degree.

From these starting results the powder agglomeration inside the metal deposits and how ultrasounds affect the dispersion in the metal matrix will also be evaluated.

4. Preliminary optimization of some process parameters

An important issue in the research on the nanocomposites produced by electrodeposition is the nanopowder content in the final layer. Contrary to the micro-powder, the nanopowder is hardly codeposited and several data and papers[122,123] in the literature confirm that. The embedded fraction is in inverse proportion to the size of the particles added to the bath[124,125].

Before discussing in details the deposition process and the properties of the nanocomposite layers, it is important to decrease the number of the variables of the process itself. For this reason in this part of the work some process parameters will be studied in order to optimize the embedded ceramic fraction. Therefore the ceramic content in the deposited layer and the microhardness will be presented as a function of different process parameters such as the current density, the presence of SDS for the pitting control, the

[122] S.-C. Wang, W.-CJ., Wei, Mater. Chem. Phys.,78, (2003), 574

[123] H.-K.Lee, H.-Y. Lee, J.-M. Jeon, Surf. Coat. Tech., 201, (2007), 4711

[124] I.Garcia, A,Conde, G. Langelaan, J. Fransaer, J.P. Celis, Corrosion Science, 45, (2003), 1173

[125] G. Maurin, A. Lavanant, J. Appl. Electrochem., 25, (1995), 1113

frequency of pulse current and the powder loading. In each case the best condition will be chosen for the further work.

Current condition

The deposition has been carried out both under direct current and pulse current. The pulse current has a square wave form and the duty cycle is fixed at 50%. The two parameters that can be varied are the frequency of the pulse current and the current density.

First, different current condition have been tested, changing from direct current to pulse current and testing different frequencies: 0.01, 0.1, 1 ,10 Hz.

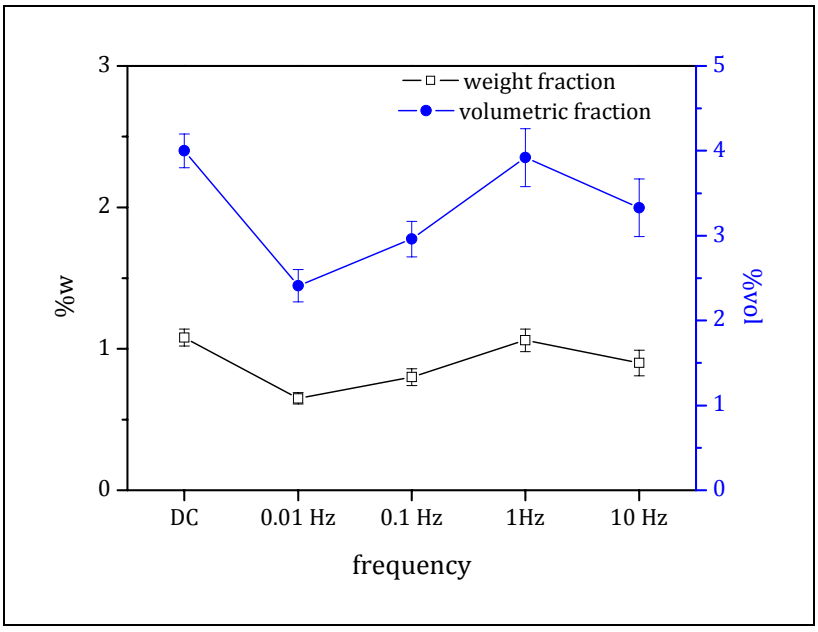

Fig 4.1. Embedded SiC fraction in nickel deposited at 2 A/dm² from Watts bath with 20 g/l of powder

In Fig 4.1 and in Fig 4.2 are presented respectively the plots of weight percent and volumetric fraction of embedded SiC and the microhardness of the composite layer at different current conditions.

The plotted ceramic powder content values are the mean values of 5 different measurements performed by GDOES, while the microhardness values are the results of the average of 30 measurements onto two different specimens for each deposition condition.

Nickel matrix composites show the best embedded rates under direct current and/or pulse current at 1 Hz. For Ni/SiC system all the other frequencies show a decrease in the ceramic content and the minimum is obtained at the lowest frequency of 0.01 Hz. An increase of the frequency of the pulse current causes an increase of the ceramic content up to the frequency of 1 Hz, and then at 10 Hz a slight decrease is observed.

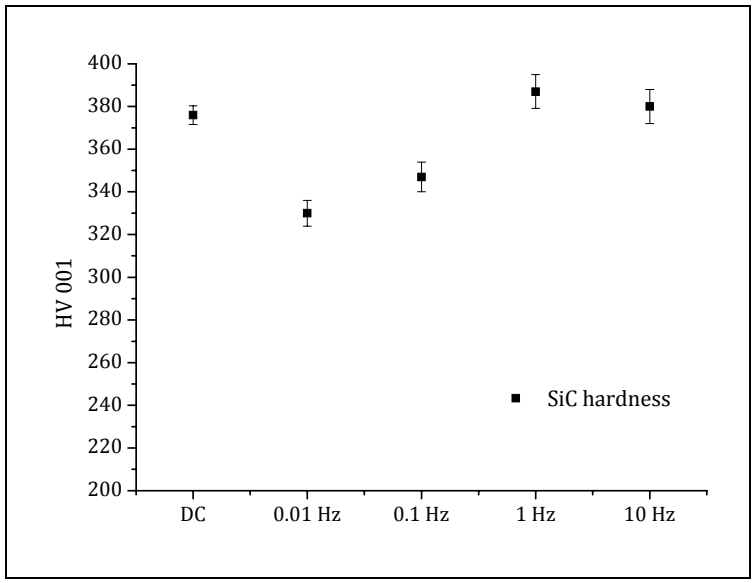

Fig 4.2. Microhardness of Ni/SiC coating as a function of the current condition

The microhardness values show the same trend as the powder content, confirming that the more promising current conditions are DC and PC at 1 Hz.

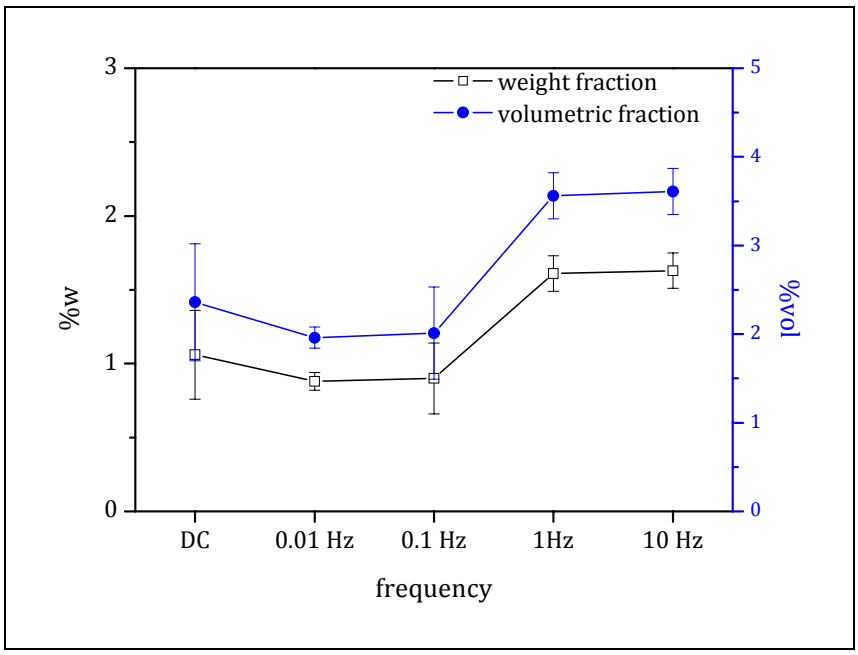

Fig 4.3. Embedded Al_2O_3 fraction in nickel deposited at 2 A/dm² from Watts bath with 20 g/l of powder

The Fig 4.3 show both weight and volumetric content of embedded alumina as a function of the deposition current conditions. The Ni/Al_2O_3 system shows only a slight decrease in ceramic content passing from direct current to pulse current at 0.01 and 0.1 Hz, while the use of the pulse current at 1 and 10 Hz leads to a substantial increase in ceramic content.

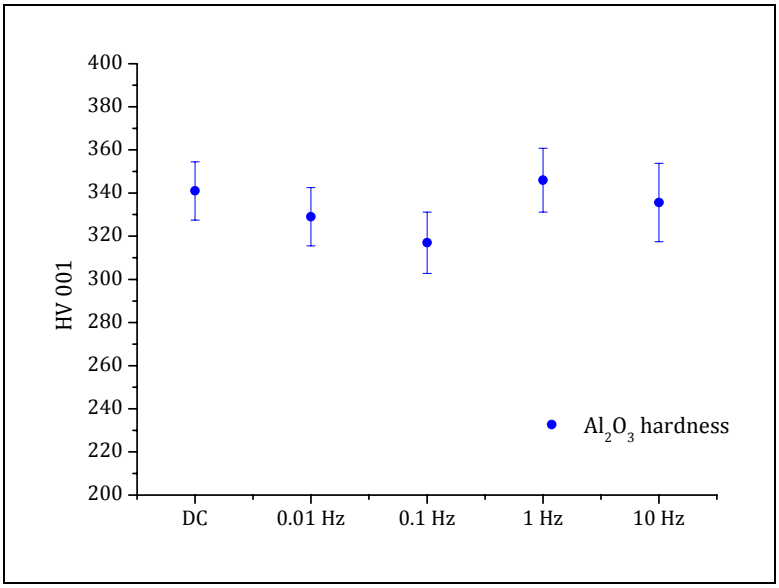

Fig 4.4. Microhardness of Ni/Al_2O_3 coating as a function of the current condition

The microhardness values plotted in Fig 4.4 do not vary very much by the frequency variation, but confirms that the DC and PC at 1 Hz are the conditions leading to the more promising final properties.

Both SiC and Al_2O_3 nickel matrix composites show the best embedded rates under direct current and/or pulse current at 1 Hz.

Regarding the current density, the Watts type bath used can work in a range from 1 to 10 A/dm^2 according to the literature[126]. Therefore different current densities are used first of all for the deposition of pure nickel in order to verify the good results as for aspect, adhesion, roughness and homogeneity. Current density values lower than 2 A/dm^2 lead to burned deposits, while for current densities higher than 7 A/dm^2 the deposits tend to present a low adhesion to

[126] E. Bertorelle, Trattato di galvanotecnica, Hoepli, Milano 1974

the substrate and a fair homogeneity on the surface.

To optimize the current density value for the production of composite layers, deposition was carried out maintaining constant the powder loading into the bath and applying current densities of 2, 4, 6 A/dm^2 for direct current and the same values as peak density for pulse current. The ceramic content has been evaluated by GDOES. In the following graphs it is possible to appreciate the variation of both silicon carbide and alumina content as a function of the current density under direct current condition and pulsed condition at 1 Hz, the two conditions that seem to be more promising in term of ceramic powder content.

Considering Ni/SiC composites (Fig 4.5), no big differences are visible between direct current condition and pulse current at 1Hz. Both current conditions lead to similar silicon carbide content. Increasing the current density from 2 to 4 A/dm^2, the embedded powder increases and then remains more or less stable for higher current densities.

The Ni/Al_2O_3 system (Fig 4.6) on the other hand is only slightly affected by the current density: only under direct current condition a slight alumina increase is visible increasing the current density. Under pulse current condition the embedded Al_2O_3 content is almost constant for all the current densities used.

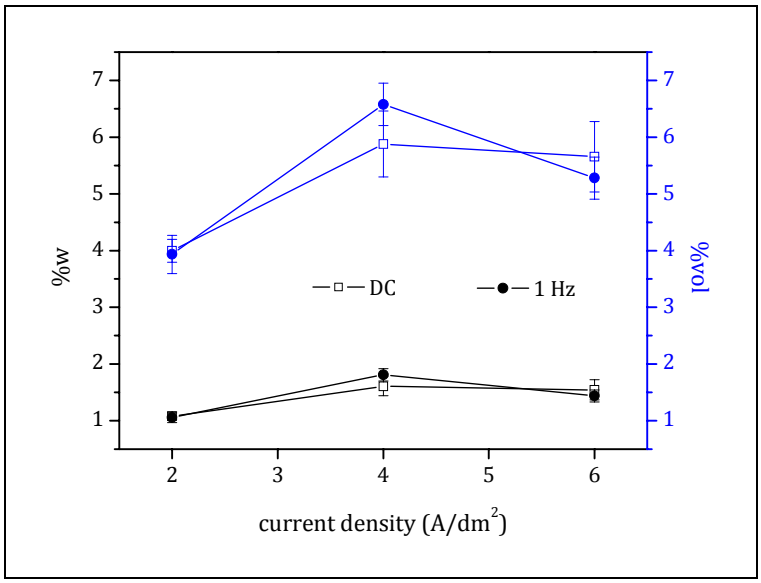

Fig 4.5. SiC content in Ni/SiC deposited under DC and PC with 20 g/l of powder

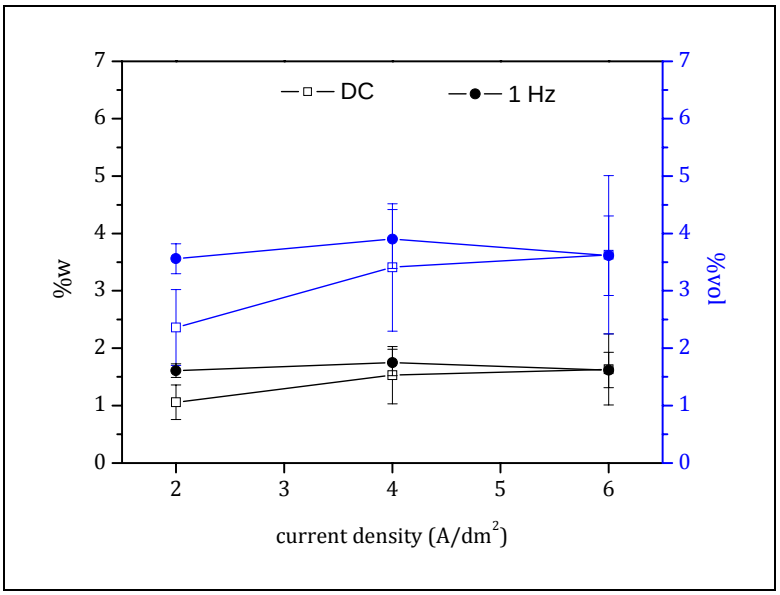

Fig 4.6. Al_2O_3 content in Ni/Al_2O_3 deposited under DC and PC with 20 g/l of powder

The results of the alumina system has a higher standard deviation. Generally the codeposited Al_2O_3 weight fraction is higher than SiC, but because of the different density, the %vol of SiC is much higher than the alumina one. Since the final properties of the composites are affected by the volume fraction of the loading phase and not by its weight %, SiC is probably more efficient than alumina in producing hardening. Moreover some studies indicates[127],[128] that the efficiency of the codeposition is related to the number of codeposited particles and thus the codeposited SiC amount results to be even higher since silicon carbides particles are smaller than alumina ones.

Effect of SDS additive on the codeposition

The first parameter to check is the influence of the organic additive usually used for the pitting control on the codeposition efficiency. Therefore the deposits produced from an additive-free bath have been compared with the deposits produced from a Watts bath with the addition of 0.5 g/ of SDS in term of ceramic content. In Fig 4.7 the mean value of 5 measurements of the SiC content is plotted as a function of the current condition, the current density used is $2A/dm^2$, both for direct current density and for peak current density in case of pulse current, and the measurements have been carried out by GDOES, while Fig 4.8 represents the hardness as a function of the current density of layer obtained in the same conditions. Regarding the microhardness, the

[127] I. Garcia, J. Fransaer, J-P. Celis, Surf. Coat. Tech., 148, (2001), 137

[128] E.A. Pavlatou, M. Stroumbouli, P. Gyftou, N. Spyrellis, J. Appl. Electroche., 36, (2006), 385

plotted values are the average results of 30 measurements onto two specimens for each deposition conditions.

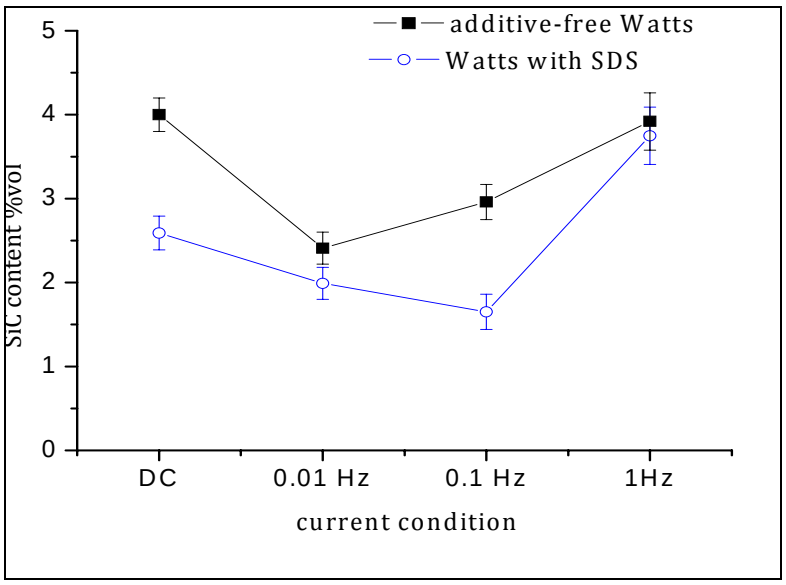

Fig 4.7. Comparison between SiC content from Watts bath with and without SDS addition

These results show that the SDS decreases the powder content in the deposited layer. The shift versus negative values of the zeta potential due to the presence of SDS in the bath partially inhibits the codeposition process thus leading to a minor content of ceramic particles in the final layer. Except for the nickel layer deposited under DC with SDS, the microhardness measurements are coherent with the SiC content results.

The microhardness confirm that generally the additive-free bath allows a higher incorporation rate of SiC powder. The major difference is shown under DC condition, as the microhardness values confirm. Probably, the pulse

current minimizes the inhibition effect of the SDS to the ceramic nanopowder codeposition.

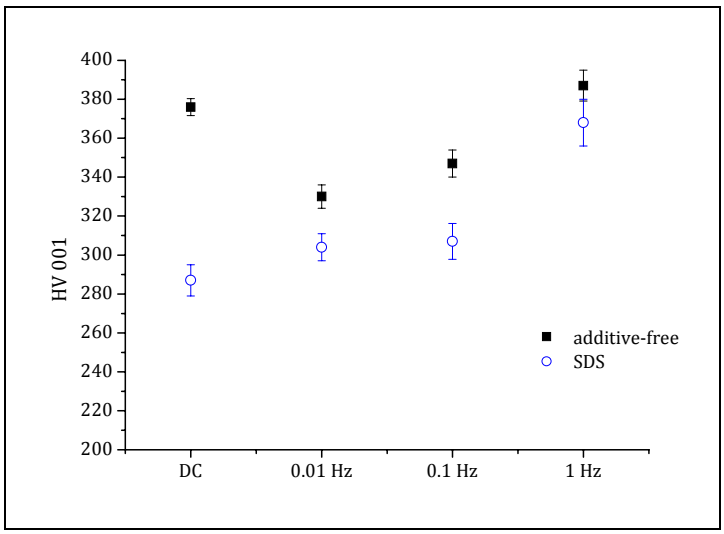

Fig 4.8. Hardness of the layers deposited from Watts bath with and without SDS

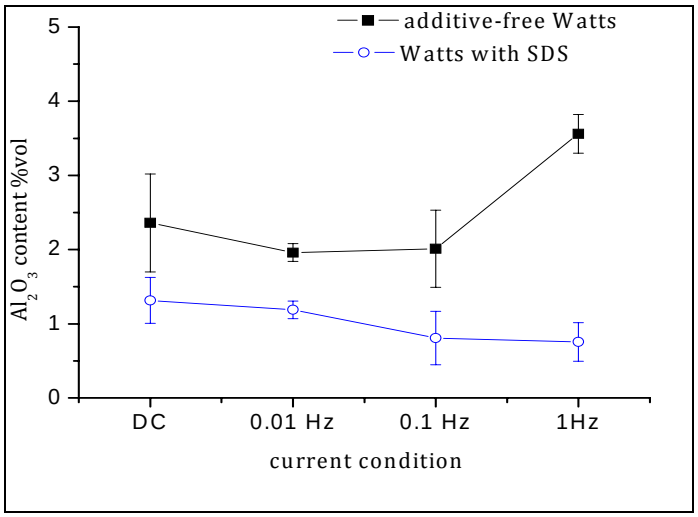

Fig 4.9. Comparison between Al_2O_3 content from Watts bath with and without SDS

The Fig 4.9 reports the results of the Al_2O_3 content as a function of the deposition parameters obtained with the same procedure. The presence of the SDS leads to the decrease of the embedded ceramic fraction more evidently than for the silicon carbide powder. In Fig 4.10 the mean values of the Ni/Al_2O_3 microhardness are plotted as a function of the current conditions.

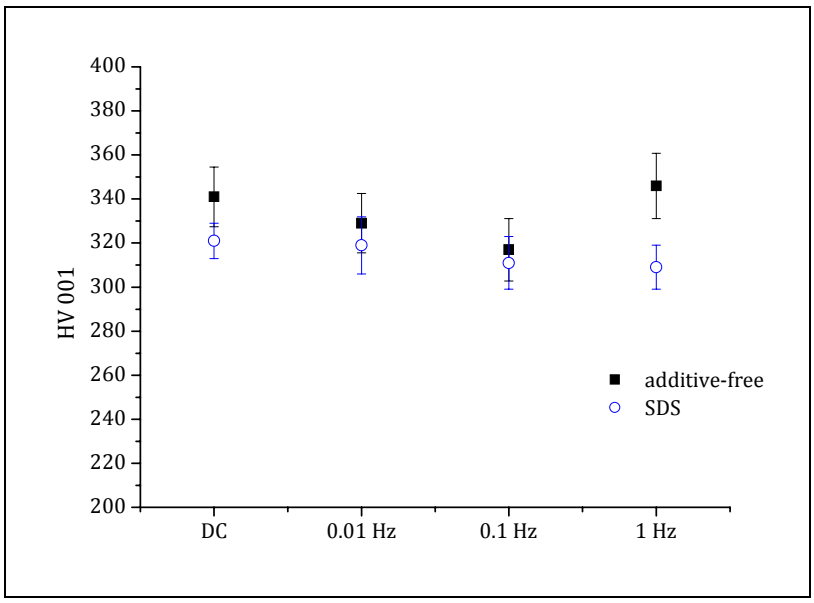

Fig 4.10. Comparison betweenAl_2O_3 content from Watts bath with and without SDS

Unlike the particles content, the microhardness values do not show such a big difference: the hardness values are only slightly higher for the layers deposited from the additive-free bath, despite the alumina content increases noticeably. The biggest difference between additive-free bath and SDS containing bath is produced under PC at 1 Hz.

The further work was therefore carried out on coatings produced from additive-free baths.

Powder loading

The powder content in the deposition bath can strongly affect the ceramic content in the final layer. It is very difficult to evaluate the relationship between powder loading in the galvanic bath and the final embedded ceramic fraction, because it depends on many factors such as agglomeration degree, shape and chemical composition of the particles, pH and chemical composition of the deposition bath. Moreover the geometry of the electrochemical cell and the fluidodynamics are very important parameters that can strongly affect the codeposition process and its efficiency. Therefore each system should be tested in order both to understand how the powder loading changes the codeposition rate and to optimize the quantity of ceramic particles to add to the galvanic bath.

The plot of Fig 4.11 shows both the SiC and Al_2O_3 content in the deposited nickel layer as a function of the powder addition into the Watts bath. Applying a direct current of 2 A/dm^2 the results report a slightly increasing codeposition rate increasing the powder loading

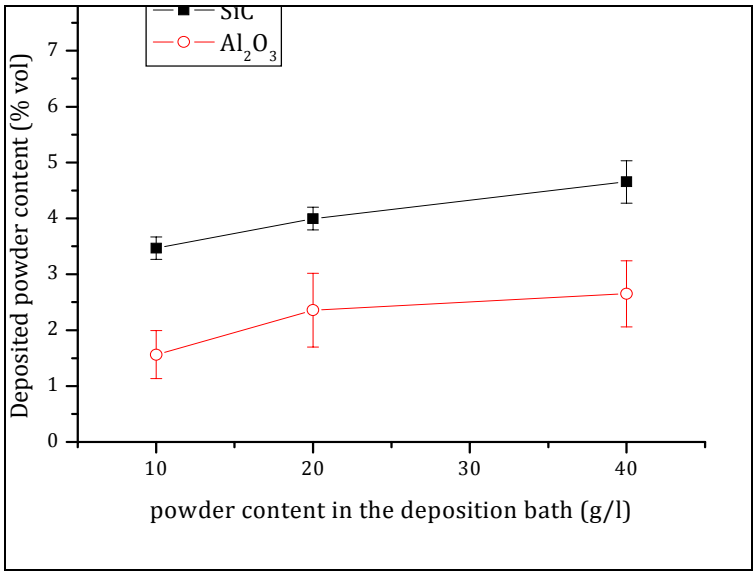

Fig 4.11. Correlation between powder content in the bath and in the layer under DC

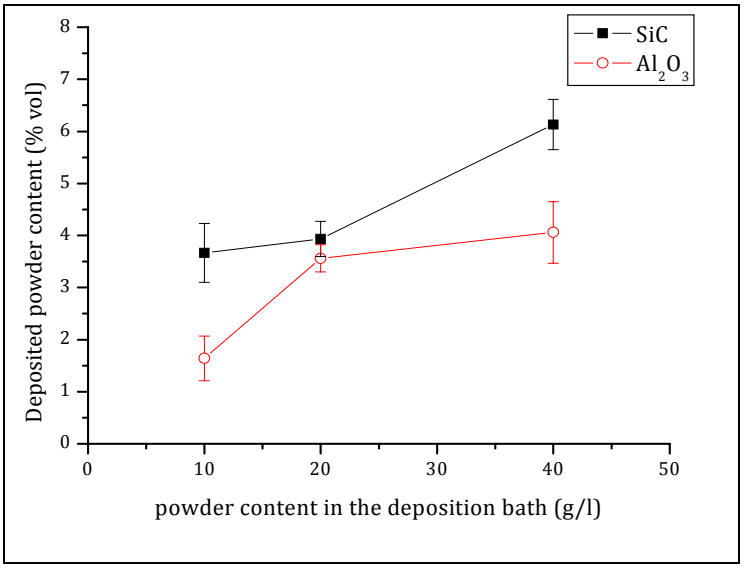

Fig 4.12. Correlation between powder content in the bath and in the layer under PC

In Fig 4.12 the results obtained under pulse current at 1 Hz with a peak current density of 2 A/dm^2 are plotted.

Also for this set-up, the increase of the powder loading in the deposition bath induces an increase of the embedded ceramic fraction in the final layer for both Ni /SiC and Ni/ Al_2O_3 systems.

In term of volumetric fraction the silicon carbide powder is always more effective in the codeposition process, only in the condition of 20 g/l of powder the alumina reaches similar results as silicon carbide.

Embedded SiC fraction-Parameters maps

Repeating these measurements varying all experimental conditions, it is possible to build a 3D map that gives a correlation between the different parameters discussed before. In this case there are three process variables to optimize in order to maximize the codeposition of ceramic particles: current density, current type and powder loading. The 3D maps have been built as a function of two parameters: powder loading and current density and maintaining constant the current conditions. For the Ni/SiC system, that demonstrated to be the more effective, a map has been built under both DC and PC condition at 1 Hz. In these maps it is possible to appreciate the behaviour of the SiC powder and how the codeposition process is affected by the combination of different process parameters.

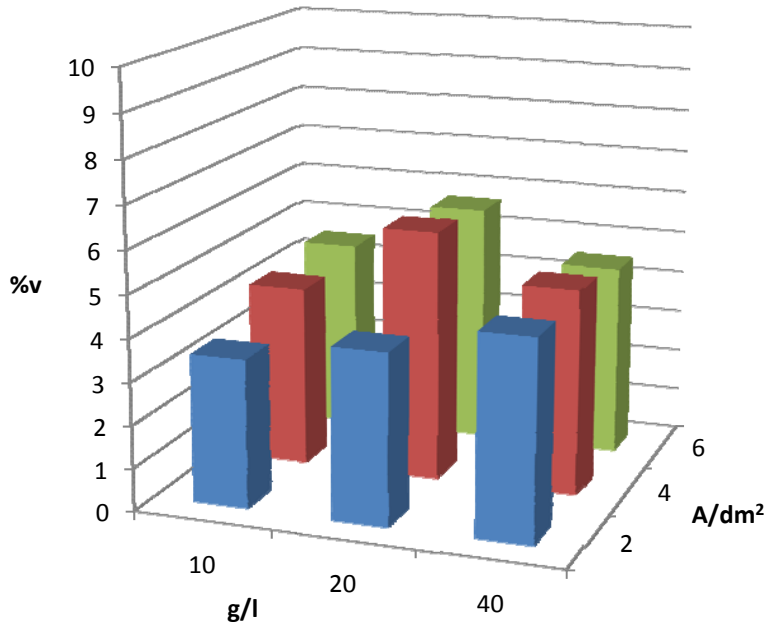

Fig 4.13. SiC-Parameters map under DC condition

In the Fig 4.13 the results of codeposited SiC under DC condition are reported. This graph shows that there is a proportionality between powder loading and embedded powder only at 2 A/dm^2, in which condition an increase in the powder loading leads to an increase of the embedded SiC fraction as discussed before. For higher current densities though, the maximum of embedded fraction is reached for 20 g/l of powder loading.

On the other hand, only for a powder loading of 10 g/l an increase of the current density corresponds to an increase of the powder content in the final layer. For 20 g/l of SiC there is an increase in embedded powder content passing from 2 to 4 A/dm^2, but a further increase of the current density has no beneficial effect on the codeposited SiC fraction. Moreover for higher powder

loading no effect of current density is visible on the codeposition process efficiency.

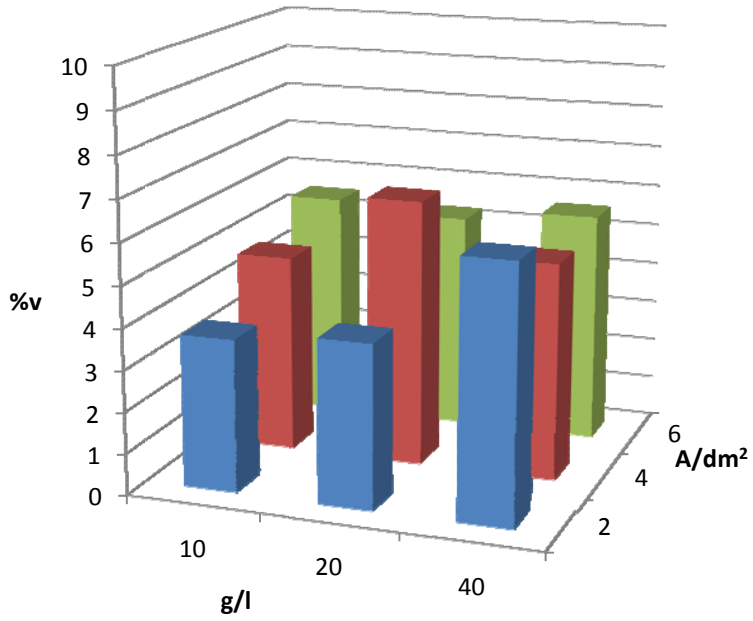

Fig 4.14. SiC-Parameters map under PC condition at 1 Hz

In Fig 4.14 the map of codeposited SiC under PC condition at 1 Hz is reported. Again this graph shows that there is a proportionality between powder loading and embedded powder only at 2 A/dm^2, as under DC condition. And also in this case only for a powder loading of 10 g/l an increase in the current density corresponds to an increase in the powder content in the final layer. The trend of ceramic particles content is uncertain for the 40 g/l or the 6 A/dm^2 deposition conditions, there are no correlations between the parameters variation, and the final particle content that remains more or less constant. The maximum of embedding rate is obtained by the use of 20 g/l of

powder in the plating bath and applying a current density of 4 A/dm^2 .

The codeposition process seems to be affected both by powder loading and current density separately: for low current density, the powder loading has a strong effect on the codeposition efficiency; on the contrary for low powder loading, the influence of current density on codeposited SiC fraction is clearly visible. Increasing both parameters contemporary, at maximum current density and maximum powder loading no beneficial effect is obtained on the embedded SiC fraction. This trend has been observed in both DC and PC condition at 1 Hz and in both cases the most effective deposition set-up is at 20 g/l and 4 A/dm^2.

Comments

A preliminary optimization of the working parameters has been carried out considering only the final deposited SiC fraction and the microhardness values. The tests and the results presented in this chapter show how important the process parameter are for the codeposition process and its efficiency.

For the Ni/SiC codeposits, the correlation and the building of a 3D map has been important to understand that there is a strong synergic effect of the parameters and it is not easy to separate the influence of each ones. For example the increase of the deposition current density does not always correspond to an increase in SiC content because it depends also on the powder loading and type of current.

After these experiments it can be concluded that for high powder loading or high current densities the system is not affected by the change in the other

working parameters, while for low powder loading and low current densities any small change in working parameters strongly affects the final result.

In order to maximize the ceramic content the best conditions are to work at the "medium values" of the considered parameters, where changes of one parameter does not affect very much the final ceramic content value. Moreover in this way the deposition process results more consistent and the reproducibility of the layers is higher. On the other hand the ceramic content is not the single parameter to be taken into account. The coatings need to be also suitable as for the corrosion protection and therefore no defects and pores should be present. The major pores source is the hydrogen evolution during the deposition that is proportional to the deposition current density. Especially in the case of additive-free plating bath the hydrogen evolution has to be maintained under control and limited.

A compromise between the maximization of powder codeposition rate and low current density to limit hydrogen evolution has to be chosen. Therefore for the further work, the condition of 20 g/l and 2 A/dm^2 were considered to be the optimum set-up.

5. Microstructures

This chapter focuses on the study of the microstructures of pure nickel, Ni/nano-SiC and Ni/nano-Al_2O_3 coatings deposited under the optimized parameter, i.e. deposited under DC and PC at 1 Hz from additive-free bath containing 20 g/l of nanopowder. The influence of deposition parameters and the application of ultrasounds on the surface morphology, the grain size and powder agglomeration will be discussed.

The surface microstructure and morphology of the coatings has been studied by Scanning Electron Microscopy (SEM) and Atomic Force Microscopy (AFM). The roughness of the coatings were also characterized by profilometer.

Moreover the samples have been cut in cross-section, embedded in resin and etched with an acid solution (50% lactic acid, 50% nitric acid) in order to evidence the grainborders. The etched cross-sections have been observed by SEM in order to study the growth of the columnar grains, typical of this kind of deposits and powder agglomeration.

Finally some samples have been observed by Transmission Electron Microscopy (TEM) in order to see the nanoparticles inside the metal layers.

Macroscopic porosity

The ultrasonic treatment applied during the deposition is beneficial for all the specimens eliminating the pores and defects left on the surface by the hydrogen evolution. The degassing properties of the ultrasonic vibrations remove the hydrogen bubbles formed onto the cathode surface before they reach the critical diameter and therefore they remain onto the substrate surface for shorter time. As a result the metal layer is not blocked in its growth and can coat homogeneously the surface.

In Fig 5.1 a sample produced without ultrasound is compared to a sample produced with ultrasound treatment.

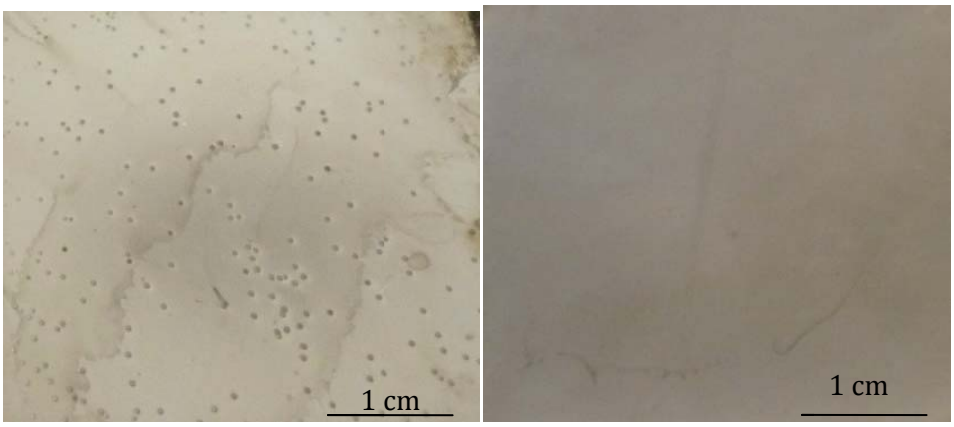

Fig 5.1. Surface of nickel deposited under DC without (left) and with (right) US

The small dots visible in the image in the left part of the Fig 5.1 are the pores due to the hydrogen bubbles. The specimen produced in the same current conditions but with the US is pore-free. This is a clear demonstration that US can replace organic additives in order to avoid pitting when hydrogen evolution is an issue.

Roughness

To evaluate the effect of the process parameters on the surface finishing, the roughness of the coatings were measured by a MarSurf PS1 contact roughness measuring instrument among a distance of 0.5 cm.

The R_a results are presented as an average value of 10 measurement on each sample in table 5.1 .

Table 5. 1 roughness values of different deposits.

deposition current condition	roughness [μm]		
	pure Ni	Ni/SiC	Ni/Al_2O_3
DC	0.38±0.4	0.31±0.6	0.28±0.6
DC US	0.31±0.5	0.29±0.3	0.28±0.4
1 Hz	0.29±0.7	0.27±0.2	0.29±0.4
1 Hz US	0.25±0.4	0.22±0.2	0.24±0.5

The roughness values show that the pulse current as well as the ultrasonic vibrations tend to decrease the roughness for all the type of coatings. The composite coatings deposited under silent conditions are generally less rough compared to pure nickel but the application of the ultrasounds make the films flatter and the influence of the particles codeposition is negligible.

Surface morphology - SEM and AFM

Pure nickel layers

Pure nickel deposits have been observed on the surface after been rinsed in distilled water with ultrasounds in order to clean the surface from any impurities and bath residuals.

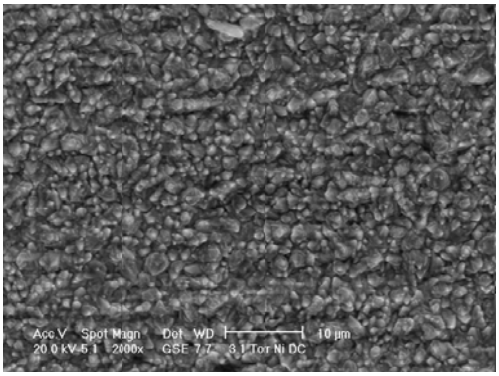

Fig 5.2. Pure Ni deposited under DC

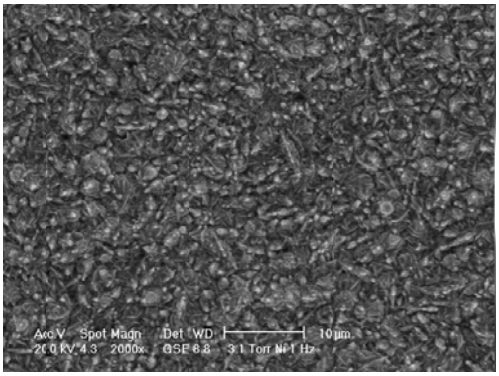

Fig 5.3. Pure Ni deposited under PC

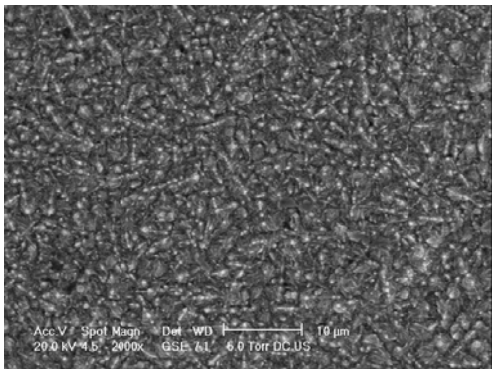

Fig 5.4. Pure Ni deposited under DC and ultrasounds

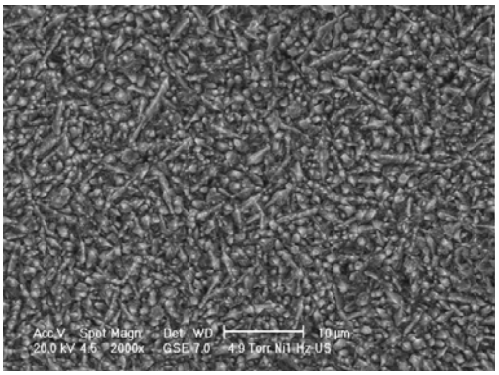

Fig 5.5. Pure Ni deposited under PC and ultrasounds

Representative surface micrographs of pure 20 μm thick deposits are presented. The analyzed samples are produced under DC and PC at 1 Hz with and without the ultrasound treatment.

The figures from Fig 5.2 to Fig 5.5 show the surface of the pure nickel coatings at low magnifications in order to see the homogeneity of the morphology and microstructure. All the samples are homogeneous and flat. In these micrographs the grains appear different in the 2 configurations with and without the ultrasound treatment. The ultrasounds tend to form acicular grain aggregates and a sort of short lines of grains are visible on the surface.

The atomic force microscopy (AFM) can provide some more information regarding the microstructure because it is a vertical analysis of the surface morphology. Two different areas were observed by AFM: a 80 μm x 80 μm area and a 15 μm x 15 μm area corresponding more or less to the area observed by the scanning electron microscope.

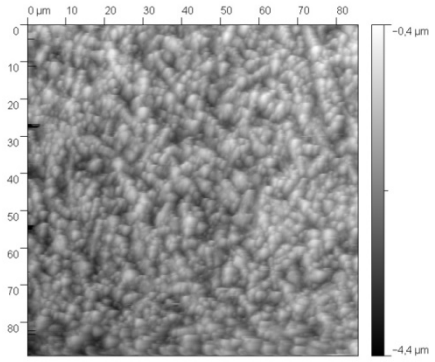

Fig 5.6. AFM 2D image of pure Ni deposited under DC

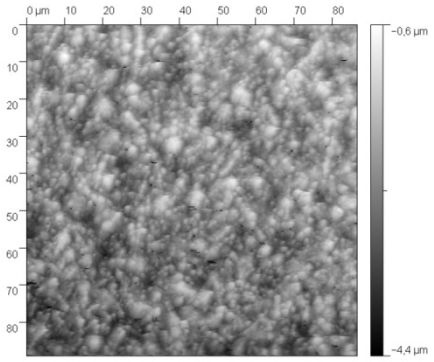

Fig 5.7. AFM 2D image of pure Ni deposited under PC

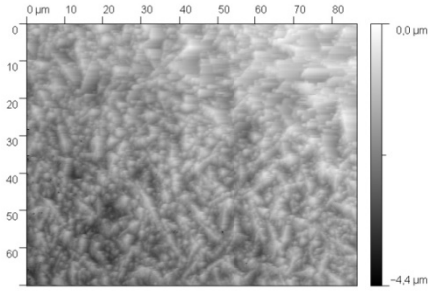

Fig 5.8. AFM 2D image of pure Ni deposited under DC and US

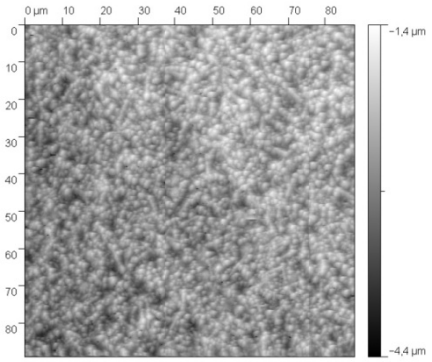

Fig 5.9. AFM 2D image of pure Ni deposited under PC and US

The bigger area is represented as 2D images from Fig 5.6 to Fig 5.9 and gives the information about the homogeneity of the surface morphology and the vertical growth. The images confirm that the application of the ultrasounds refines the microstructure and decreases the surface roughness. The grains height is evidenced by the colour in the AFM images and the surfaces of the films deposited under US vibrations seem to be more homogeneous.

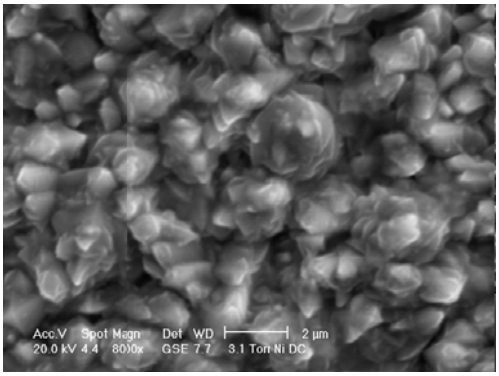

Fig 5.10. Pure Ni DC

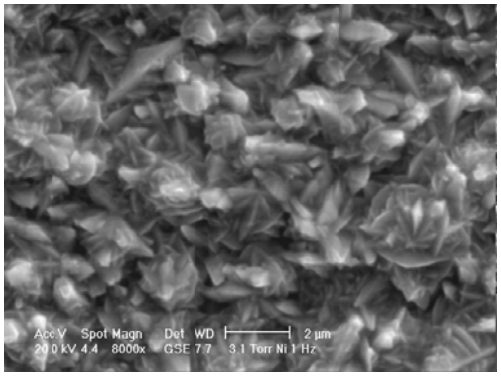

Fig 5.11. Pure Ni PC

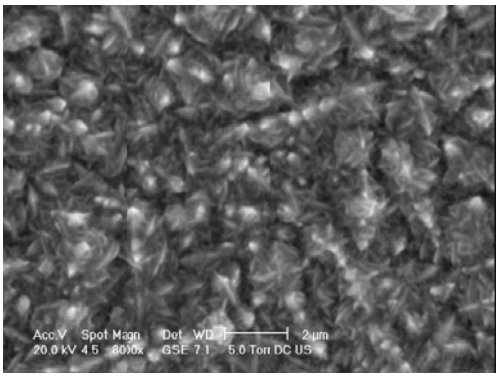

Fig 5.12. Pure Ni deposited under DC and ultrasounds

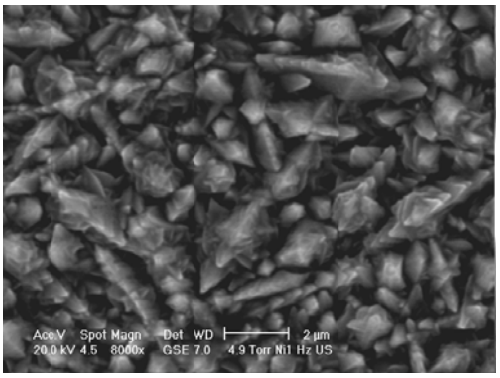

Fig 5.13. Pure Ni deposited under PC and ultrasounds

At higher magnifications it is possible to appreciate the grain shape and size. The sample produced under DC conditions (Fig 5.10) shows large columnar grains with some voids among them due to the vertical growth, typical for this type of process. The application of a pulse current (Fig 5.11) leads to a refinement of the microstructure and to a change in the grains shape. There are small plates aggregated in larger columns. The application of ultrasounds during deposition leads to a big refinement under DC conditions and also in this case the grains seem to assume a plates form. The influence of the ultrasonic treatment is more evident in the DC case and leads to a finer microstructure than under PC conditions.

On the other hand the smaller area observed by AFM is plotted in a 3D image from Fig 5.14 to Fig 5.17 to give a better idea of the vertical growth of the grain agglomerates.

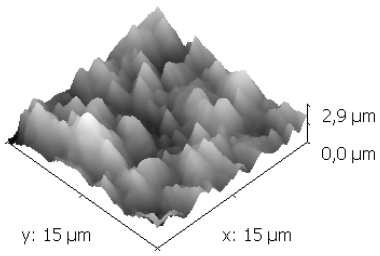

Fig 5.14. AFM 3D image of pure Ni deposited under DC

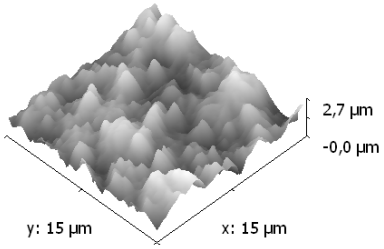

Fig 5.15. AFM 3D image of pure Ni deposited under PC

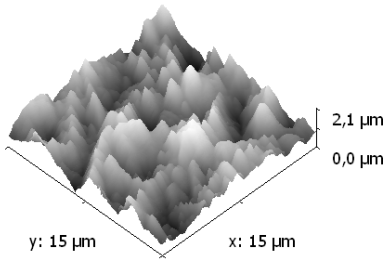

Fig 5.16. AFM 3D image of pure Ni deposited under DC and US

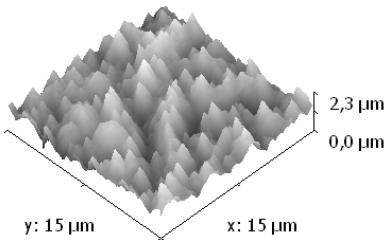

Fig 5.17. AFM 3D image of pure Ni deposited under PC and US

These images are clearerregarding the vertical profile of the deposit, but can not be representative of the surface roughness since the scanned area is too small. The application of the pulse current make the grain aggregates more homogeneous regarding the vertical growth, while the ultrasonic vibrations lead to a slight reduction of the aggregates height.

Ni/SiC nanocomposite layers

The nickel-nanoSiC coatings, produced under the same conditions as the pure nickel seen previously, were observed by SEM and AFM in order to study how the codeposition of nano silicon carbide powder affects both the output microstructure and surface morphology.

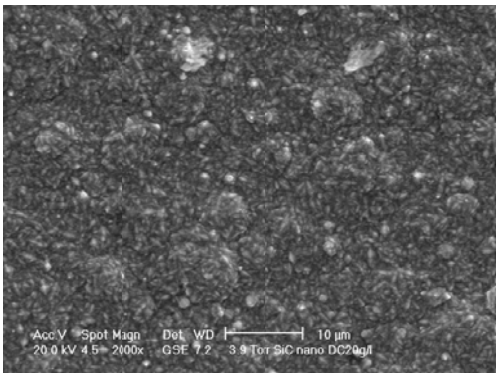

Fig 5.18. Ni/SiC deposited under DC

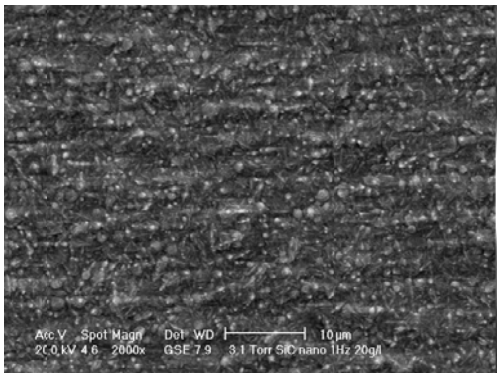

Fig 5.19. Ni/SiC deposited under PC

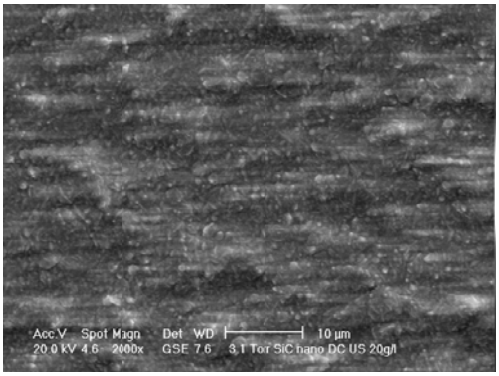

Fig 5.20. Ni/SiC deposited under DC and ultrasounds

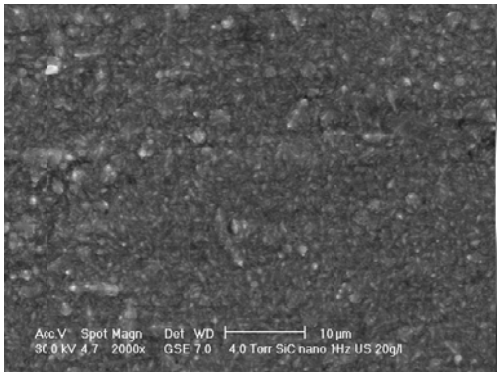

Fig 5.21. Ni/SiC deposited under PC and ultrasounds

At low magnifications it is possible to appreciate the uniformity and homogeneity of the surfaces, even though the sample deposited under DC conditions is less flat than pure nickel layers. The surface of the sample deposited under DC and silent condition (Fig 5.18) shows round globular grains aggregates and therefore the surface results more irregular than the pure nickel ones but also more compact. When the US are applied the aggregates are much smaller and therefore the surface results flatter as shown in Fig 5.20. The layer produced under pulse current, represented in Fig 5.19, shows a quite homogeneous and flat surface, no grain agglomerates are visible and when the US are applied during deposition the surface becomes even flatter and more homogeneous. The corresponding AFM micrographs are reported in the figures from Fig 5.22 to Fig 5.25. The same grain aggregates shown in the SEM micrographs on the surface of the sample deposited under DC, can be found in the AFM micrograph (Fig 5.22) where the vertical dimension is more reliable.

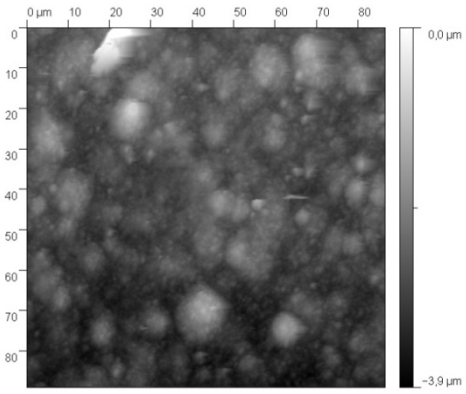

Fig 5.22. AFM 2D image of Ni/SiC deposited under DC

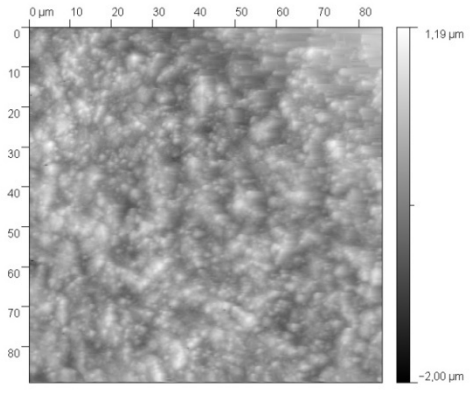

Fig 5.23. AFM 2D image of Ni/SiC deposited under PC

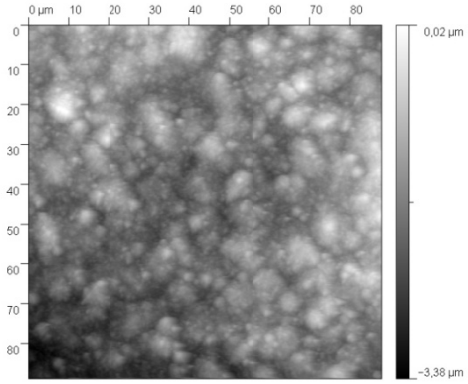

Fig 5.24. AFM 2D image of Ni/SiC deposited under DC and US

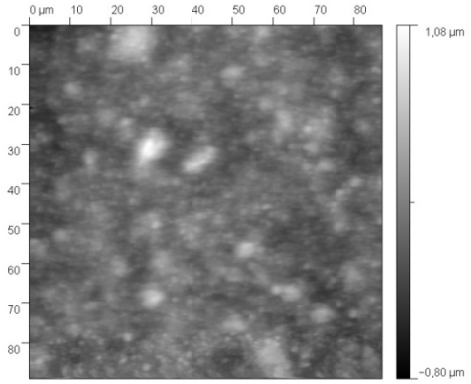

Fig 5.25. AFM 2D image of Ni/SiC deposited under PC and US

The AFM evidences the presence of similar agglomerates also in the sample deposited under DC and US even if they are smaller. The samples produced under pulse current on the contrary are much more homogeneous and the grains are finer. Considering the vertical scale, it has to be underlined that the sample deposited under pulse current and ultrasonic vibrations shows the smaller vertical range. The surface is flatter with a much lower roughness.

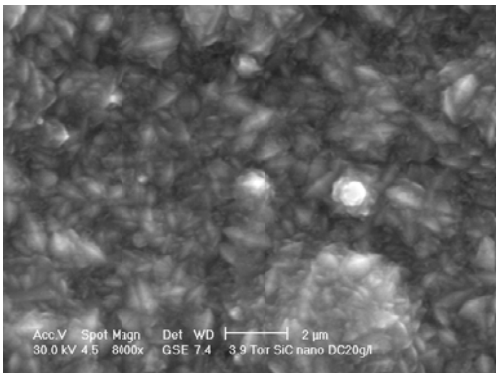

Fig 5.26. Ni/SiC deposited under DC

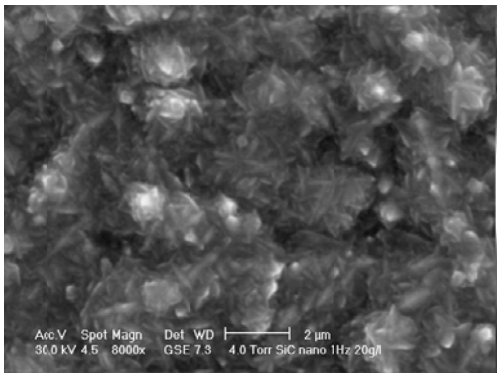

Fig 5.27. Ni/SiC deposited under PC

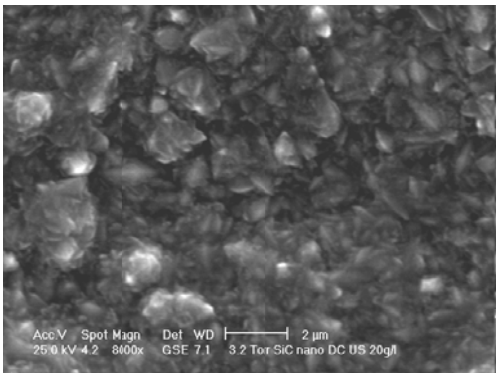

Fig 5.28. Ni/SiC deposited under DC and US

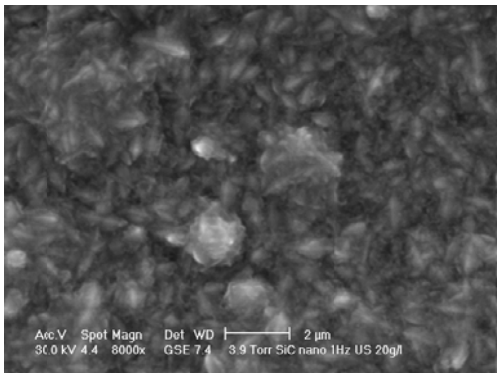

Fig 5.29. Ni/SiC deposited under PC and US

At higher magnifications the grains are clearly visible and it is possible to appreciate how fine the microstructure is in the case of Ni/SiC nanocomposites. In all deposition conditions the grains have acicular shape and are much smaller than 1 micron. In the case of US treatment, the surface microstructure seems more compact (Fig 5.28 and Fig 5.29) since there are no voids or gaps between grains agglomerates. The 3D micrographs obtained by AFM (Fig 5.30 - Fig 5.33) are even clearer about the surface morphology.

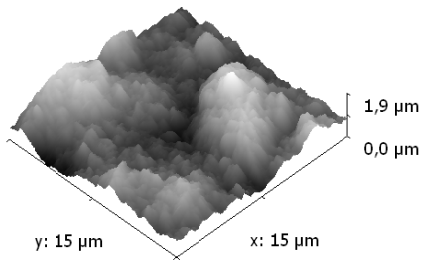

Fig 5.30. AFM 3D image of Ni/SiC deposited under DC

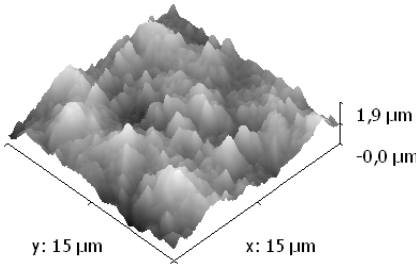

Fig 5.31. AFM 3D image of Ni/SiC deposited under PC

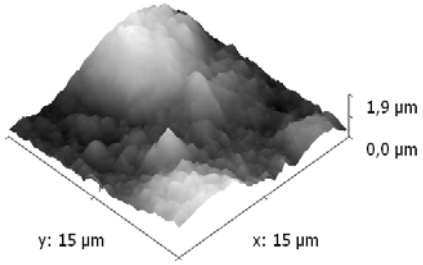

Fig 5.32. AFM 3D image of Ni/SiC deposited under DC and US

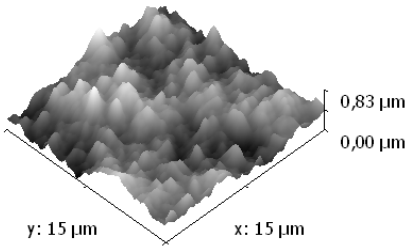

Fig 5.33. AFM 3D image of Ni/SiC deposited under PC and US

The grains aggregates, present on the surface of DC samples, have a globular shape with a considerable vertical growth respect to the film surface. The application of the pulse current destroy the formation of these grains aggregates and the synergic effect of pulse current and ultrasonic vibrations make the film surface even more flat and homogeneous. The vertical axes of Fig 5.33 indeed is reduced by 50% compared to the other micrographs.

Comparing these micrographs to the pure nickel ones a big refinement in the microstructure is noticed. Moreover the structure appears more compact and homogeneous. The presence of the second phase and the change in the crystallization process due to the codeposition lead to a big change in the final microstructure, and this gap is much more important than the differences due to the deposition current conditions. Moreover the synergic effect of pulse current and ultrasonic vibrations in the case of codeposition of silicon carbide nanoparticles leads to the formation of a homogeneous and flat surface with a very fine and compact microstructure.

Ni/Al_2O_3 nanocomposite layers

The nickel-nanoAl_2O_3 coatings, produced under the same conditions as the pure nickel and nanocomposite with SiC seen previously, were observed in order to study how the codeposition of nano alumina powder affects both final microstructure and morphology.

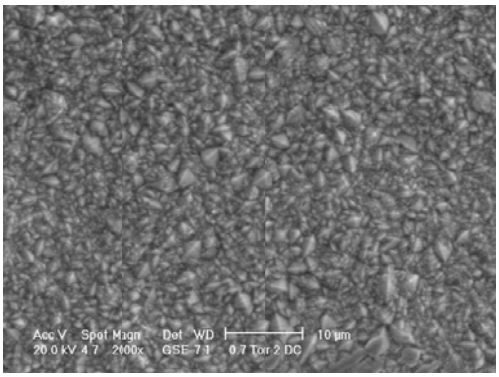

Fig 5.34. Ni/Al_2O_3 deposited under DC

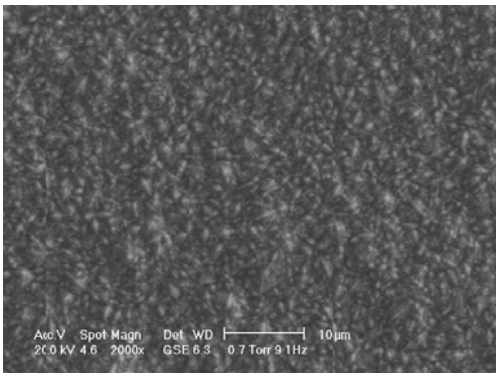

Fig 5.35. Ni/Al_2O_3 deposited under PC

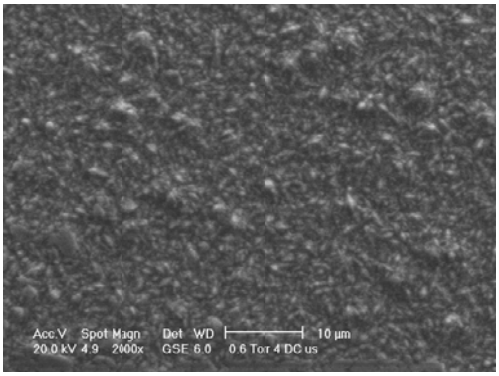

Fig 5.36. Ni/Al_2O_3 deposited under DC and ultrasounds

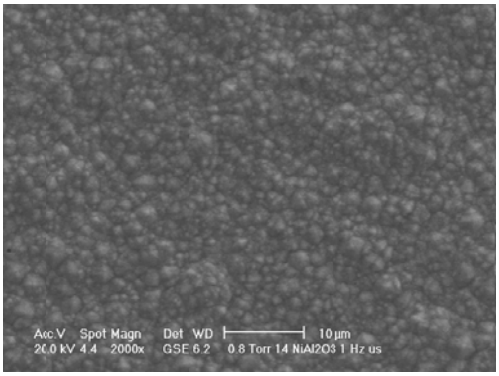

Fig 5.37. Ni/Al_2O_3 deposited under PC and ultrasounds

In the top-view SEM micrographs (Fig 5.34 - Fig 5.37), the surfaces of the Ni/ Al_2O_3 nanocomposite coatings appear flat, homogeneous ad compact. Only the sample produced under DC conditions shows a wide grain size distribution: near to bigger grains with a size greater than 1 micron, very small ones grow.

The AFM micrographs, presented in the figures from Fig 5.38 to Fig 5.41, evidence the changes in the surface morphology seen in the SEM images. Since the vertical growth is considered in the colour of these images more differences are visible between the different deposition conditions. The sample produced under DC present small grains and a homogeneous and flat surface.

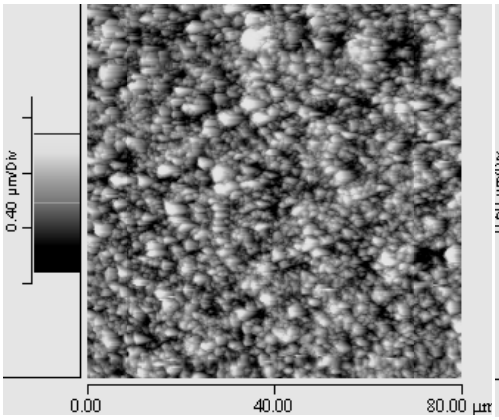

Fig 5.38. AFM 2D image of Ni/Al_2O_3 deposited under DC

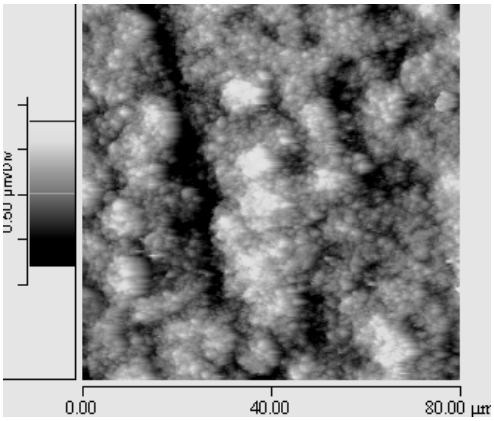

Fig 5.39. AFM 2D image of Ni/Al_2O_3 deposited under PC

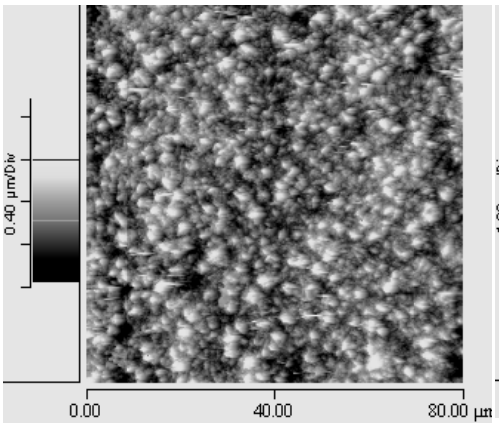

Fig 5.40. AFM 2D image of Ni/Al_2O_3 deposited under DC and US

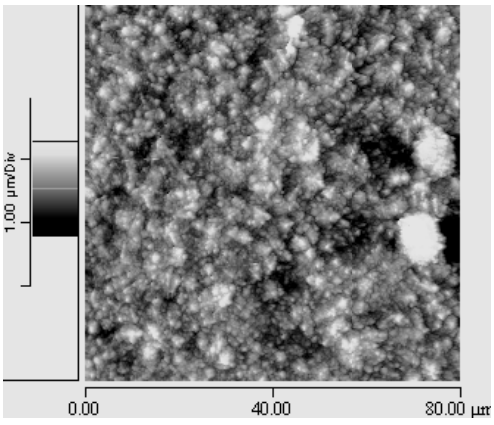

Fig 5.41. AFM 2D image of Ni/Al_2O_3 deposited under PC and US

The application of the pulse current refines the grains and the grain size is more homogeneous but some heterogeneity in the vertical profile are present. The application of the ultrasounds results to be efficient in avoiding these small surface defects. A smaller area has been observed both by SEM and AFM in order to see smaller details of the surfaces.

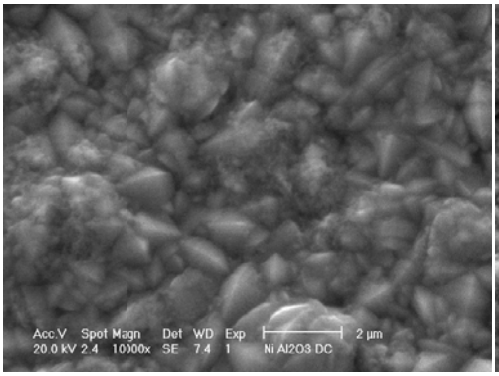

Fig 5.42. Ni/Al_2O_3 deposited under DC

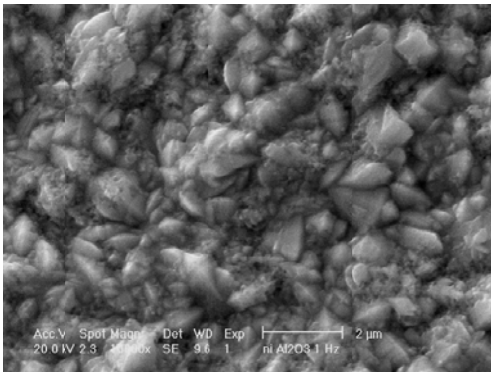

Fig 5.43. Ni/Al_2O_3 deposited under PC

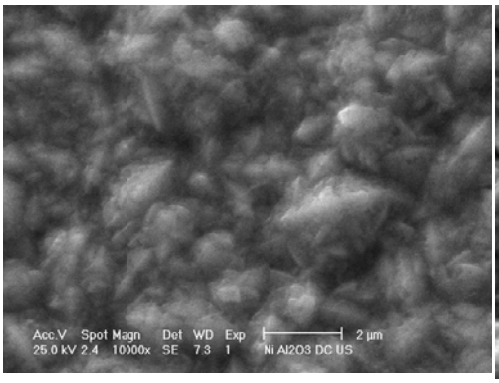

Fig 5.44. Ni/Al_2O_3 deposited under DC and ultrasounds

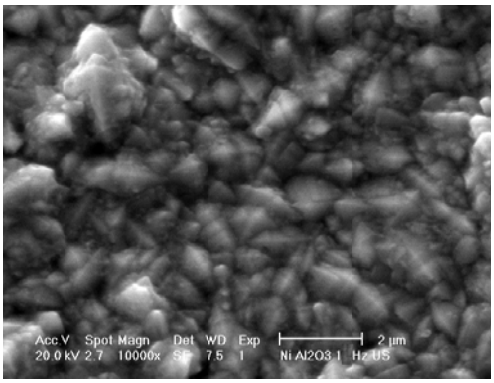

Fig 5.45. Ni/Al_2O_3 deposited under PC and ultrasounds

At higher magnifications it is possible to distinguish the grain shape and a wide size distribution in grain size is visible especially under PC conditions (Fig 5.43). In this kind of nanocomposites no big differences are visible on the specimens surfaces, changing the current conditions, or applying the ultrasonic treatment during the codeposition. The Ni/Al_2O_3 layers show a different grain shape compared to the pure nickel and Ni/SiC, and a wider grain size distribution since large grains are still present .

Moreover looking at the samples at very high magnifications it is possible to see powder residuals on the surface of Ni/Al_2O_3 layers deposited under silent conditions. The Fig 5.46 shows a detail of the surface of the codeposit produced under DC. Over and among the metal grains are visible small round particles corresponding to the alumina powder.

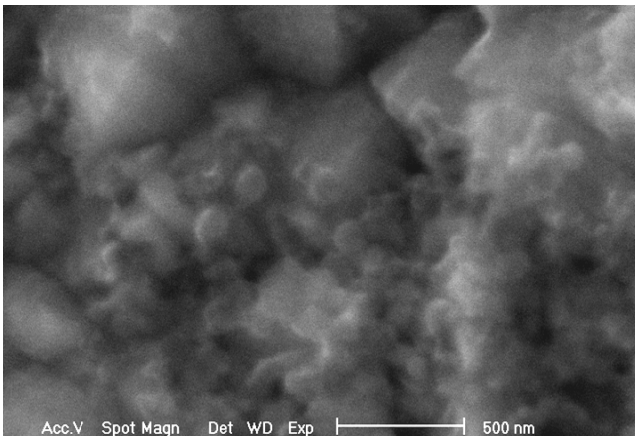

Fig 5.46. Detail of the surface of Ni/Al_2O_3 deposited under DC

This kind of partially embedded or loose adsorbed powder agglomerates are present only on the surface of the Ni/Al_2O_3 samples produced under silent conditions and are visible also in the AFM micrographs (Fig 5.47 and Fig 5.48).

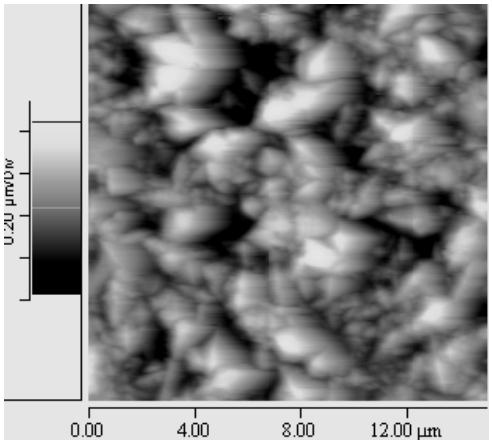

Fig 5.47. AFM 2D image of Ni/Al_2O_3 deposited under DC

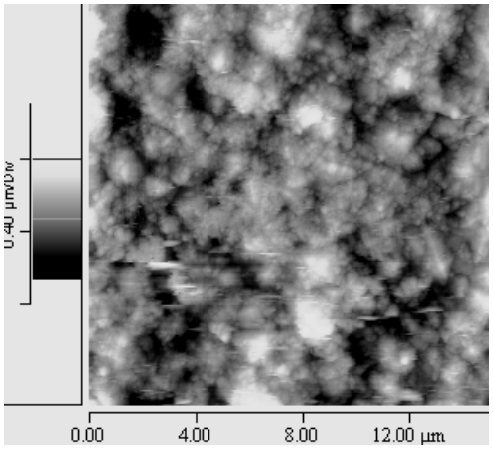

Fig 5.48. AFM 2D image of Ni/Al_2O_3 deposited under PC

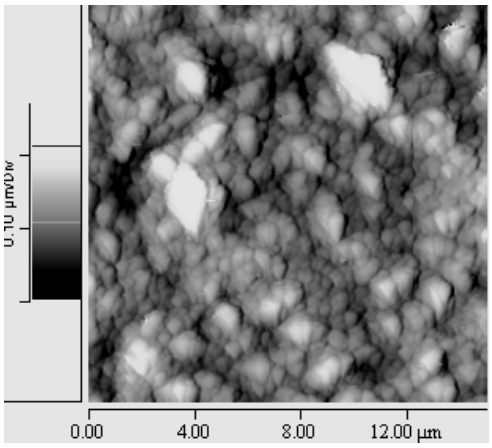

Fig 5.49. AFM 2D image of Ni/Al_2O_3 deposited under DC and US

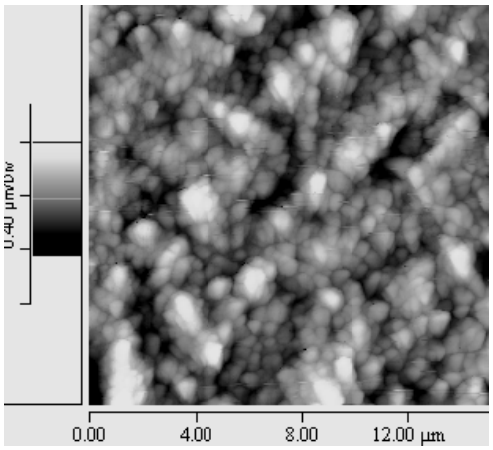

Fig 5.50. AFM 2D image of Ni/Al_2O_3 deposited under PC and US

The samples produced under US on the contrary present a clean and flat surface with small grains.

Compared to pure nickel deposits the microstructure is finer and more homogeneous and compact since no voids or space are visible among the grains. Comparing these micrographs to the Ni/SiC systems though, the microstructure is slightly coarser for the Ni/Al_2O_3 but the surface is flatter and the metallic grains do not form aggregates on the surface.

Comments

In order to give an overall idea of the influence of the codeposition process of different nanopowders, the sample produced under DC condition are put side by side.

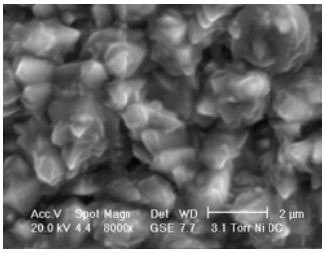

Fig 5.51. Ni DC

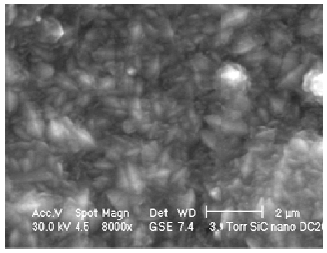

Fig 5.52. Ni/SiC DC

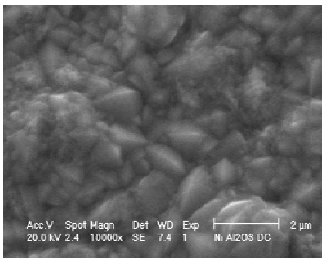

Fig 5.53. Ni/Al_2O_3 DC

The microstructure obtained under DC condition are very different in the three systems. The columnar grains of the pure coating are destroyed by the addition of the ceramic powders and SiC seems to be more effective in refining the microstructure than Al_2O_3, but the Al_2O_3 leads to a more planar and flatter surface. Both powders though lead to the formation of a more compact layer avoiding the formation of gaps between the grains. The application of of the pulse current leads to more homogeneous and flatter surfaces and the differences between the samples are smaller but still present.

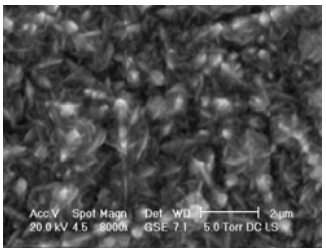

Fig 5.54. Ni DC US

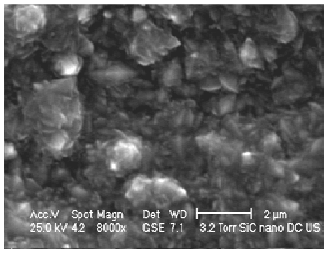

Fig 5.55. Ni/SiC DC US

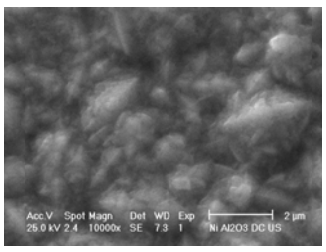

Fig 5.56. Ni/Al_2O_3 DC US

Moreover the application of the ultrasonic vibrations during deposition induces a further refinement of the microstructures in both pure and composite layers. Of course the major effect is observed on the pure layers since there are a bigger room for improvement. The composite layers show

already a fine microstructure under silent conditions and therefore the application of the US only leads to a slight refinement and to flatter surfaces. The influence of ultrasounds is very important not only because they avoid the pits left by the hydrogen evolution, but they can induce refinement of the metal microstructure and make the surfaces flatter and more homogeneous.

Cross-section microstructure

To evaluate the cross-section structure of the deposits, metallographic specimens were produced. The samples were cut in cross-section embedded in resin for the mechanical polishing procedure with silicon carbide paper and diamond powder until the surface reaches a mirror-like finishing. The samples were then etched for 90 sec with an acidic solution containing 50% lactic acid and 50% nitric acid in order to evidence the bordergrains or grains agglomerates.

Pure nickel layers

As can be observed in Fig 5.57-Fig 5.60, the pure nickel deposits consist of columnar grains growing perpendicular to the substrate and parallel to the applied electric field. This kind of microstructure is typical for nickel deposited from Watts bath and it is specific of an electrocrystallization process under mass transport control. The use of the pulse current leads to the formation of shorter and thinner columns which are still field-oriented.

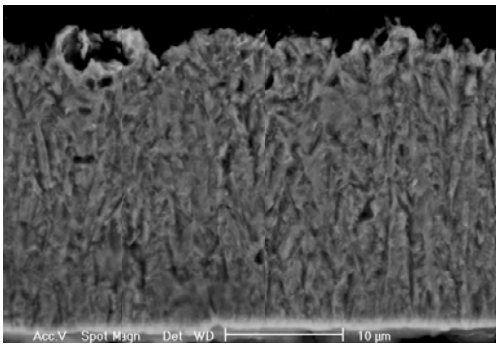

Fig 5.57. Etched cross section of pure Ni layer deposited under DC

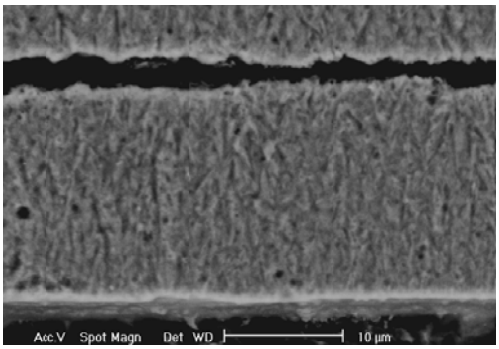

Fig 5.58. Etched cross section of pure Ni layer deposited under PC

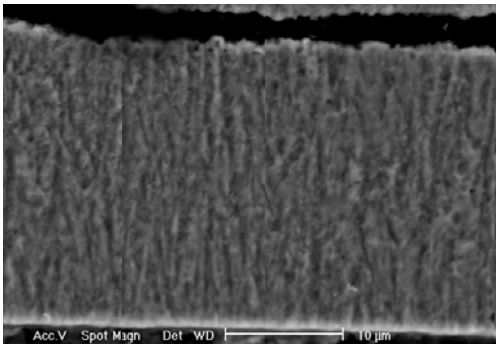

Fig 5.59. Etched cross section of pure Ni layer deposited under DC with US

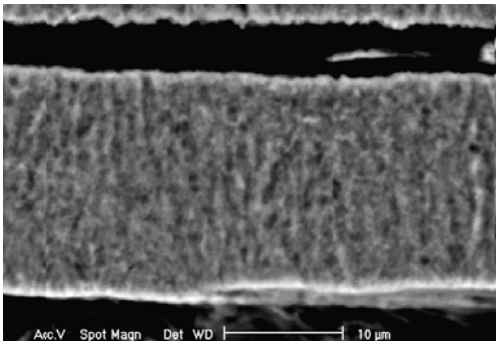

Fig 5.60. Etched cross section of pure Ni layer deposited under PC with US

The specimens produced under US treatment are more reactive during the etching and therefore more difficult to attack. They were etched for shorter time and the microstructure could appear more corroded. The application of the US during the deposition leads to a further grain refinement and the sample cross-sections result more compact. Moreover the grains result more parallel to the electric field direction.

Ni/SiC nanocomposite layers

The cross-section micrographs of the Ni/SiC layers were observed after etching are reported from Fig 5.61 to Fig 5.64.

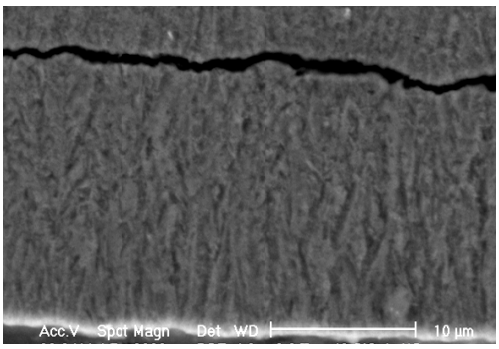

Fig 5.61. Etched cross section of Ni/SiC layer deposited under DC

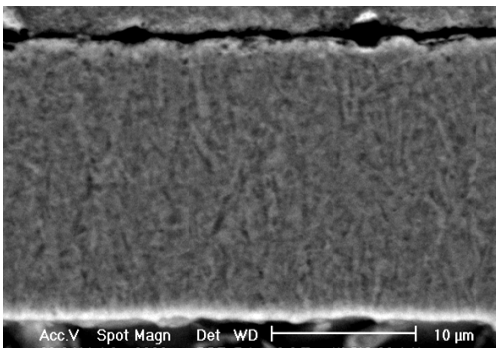

Fig 5.62. Etched cross section of Ni/SiC layer deposited under PC

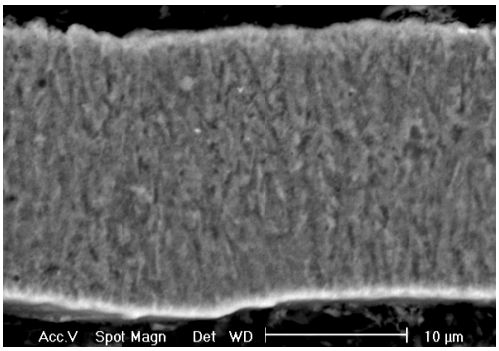

Fig 5.63. Etched cross section of Ni/SiC layer deposited under DC with US

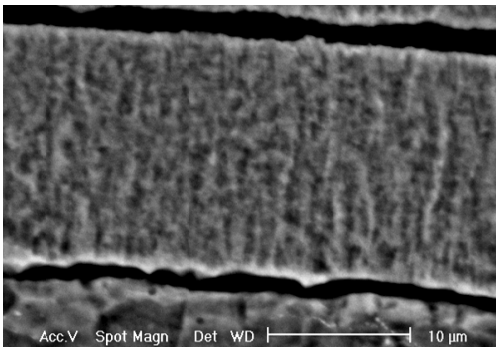

Fig 5.64. Etched cross section of Ni/SiC layer deposited under PC with US

The cross-section observations confirm that the Ni/SiC nanocomposites show a very fine microstructure. The sample produced under DC conditions, shown in Fig 5.61, is formed by very fine grains and field-oriented columns that are

thinner and shorter compared to pure nickel samples. Applying the pulse current (Fig 5.62) the grains are even finer and no field orientation is distinguishable. The application of the US leads to a further refinement under DC leading to a very compact and fine microstructure. The field orientation is only lightly visible. On the other hand the US applied together with the pulse current increase the field orientation of the grains but the layer is more reactive to the metallographic attack and therefore it is not easy to distinguish the grainborders. No powder agglomeration was detected both by SEM and LOM.

Ni/Al_2O_3 nanocomposite layers

The following SEM micrographs refer to the etched Ni/Al_2O_3 cross-sections. In Fig 5.65 the DC deposit shows a very large columnar structure that is strongly field oriented. These columns are about 1 micron wide and arise from the substrate-film interface to the surface. Applying a pulse current the columns become narrower and shorter, but the microstructure is still columnar and field-oriented. The off-time of the pulse current interrupts the growth of the columns but does not change the mechanism of crystallization.

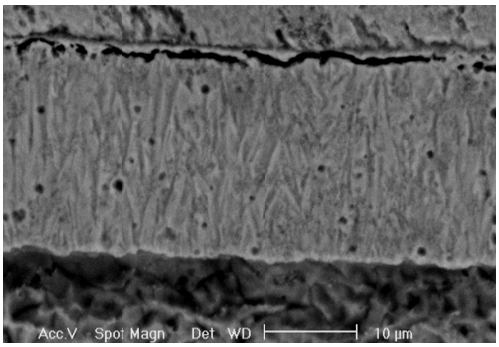

Fig 5.65. Etched cross section of Ni/Al_2O_3 layer deposited under DC

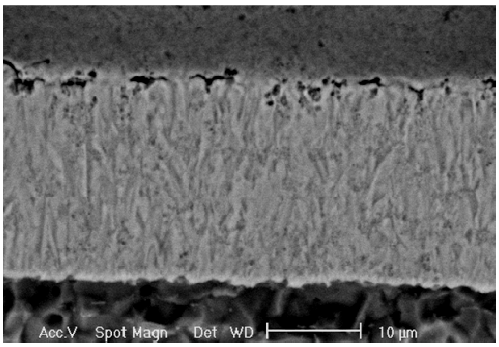

Fig 5.66. Etched cross section of Ni/Al_2O_3 layer deposited under PC

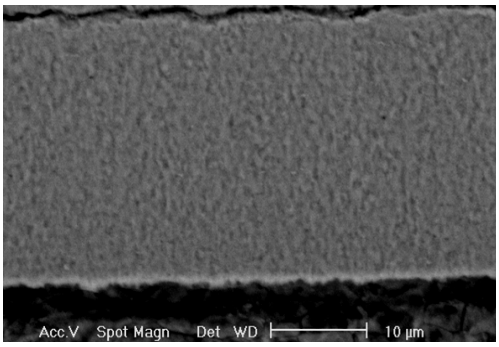

Fig 5.67. Etched cross section of Ni/Al_2O_3 layer deposited under DC with US

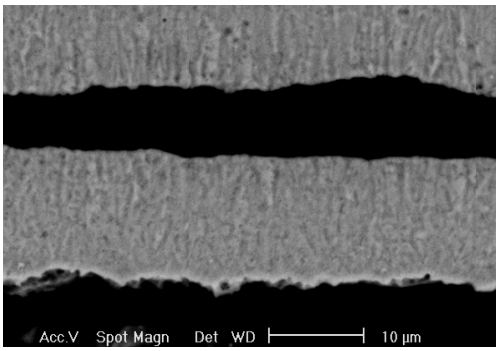

Fig 5.68. Etched cross section of Ni/Al_2O_3 layer deposited under PC with US

The application of the ultrasounds during the deposition induces severe changes in the microstructure: the columnar structure of the sample produced under DC is completely destroyed and replaced by a dispersed unoriented-type microstructure with small round grains as visible in Fig 5.67. The microstructure is very fine and the grain size is less than 1 micron. Also under PC conditions the US induce such a microstructural change as demonstrated in the Fig 5.68.

In Fig 5.65 and Fig 5.66 among the columns and the metal grains a sort of shadow clouds are visible. Looking at higher magnifications in Fig 5.69, the agglomerates of alumina are recognizable.

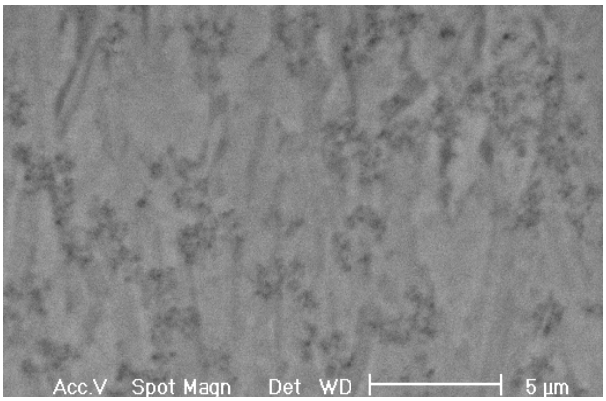

Fig 5.69. Detail of the microstructure of Ni/Al_2O_3 cross-section

Moreover the Ni/Al_2O_3 cross-section were observed by the light optical microscope (LOM) in order to verify the powder agglomeration and the distribution of the embedded ceramic particles.

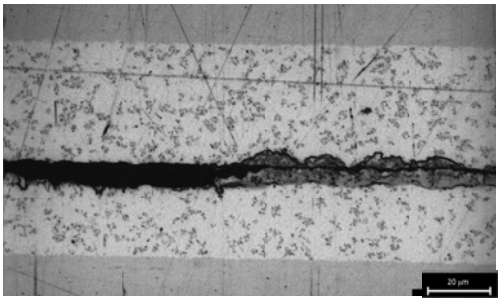

Fig 5.70. LOM image of Ni/Al_2O_3 deposited under DC

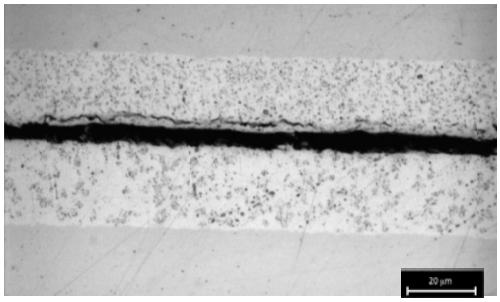

Fig 5.71. LOM image of Ni/Al_2O_3 deposited under PC

The alumina distribution is quite homogeneous in the layer but very agglomerated. Even at the optical microscope the ceramic agglomerates are visible as reported in Fig 5.70 and Fig 5.71, and their dimension is about some micron. These micrographs show that the pulse current decreases the agglomeration degree, but does not avoid it.

Fig 5.72. LOM image of Ni/Al_2O_3 deposited under DC with US

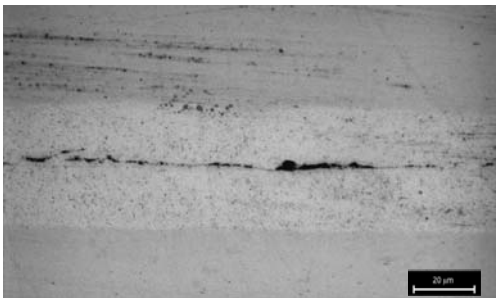

Fig 5.73. LOM image of Ni/Al_2O_3 deposited under PC with US

On the other hand the use of ultrasounds sharply decreases the agglomeration degree of the embedded ceramic powder (Fig 5.72 and Fig 5.73) but does not achieve to avoid it completely. Moreover, since the agglomerate size is smaller, the dispersion of the powder in the metallic layer seems to be more homogeneous.

TEM micrographs

Since no ceramic particles have been detected by SEM and LOM, the Ni/SiC samples, were observed by transmission electron microscopy (TEM) to see how the SiC particles have been codeposited and to evaluated the agglomeration degree. Some Ni/SiC specimens were prepared first by

mechanical thinning with abrasive papers and then by ionic gun thinner. The sample preparation could induce some modification in the microstructure of the metal matrix, but in this case we were interested only in the detection of the particles and how they are embedded in the metal matrix. The Fig 5.74 and Fig 5.75 correspond to the samples produced under direct current and silent condition, while in the Fig 5.76 and Fig 5.77 the micrographs of the pulse plated specimens are reported.

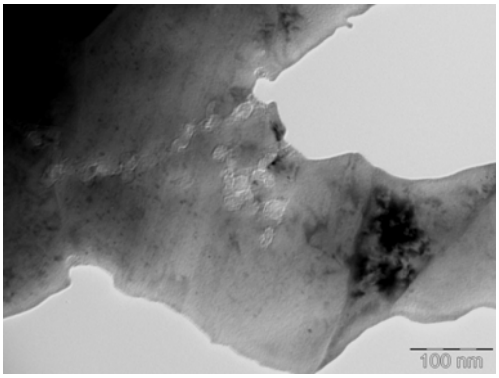

Fig 5.74. TEM image of Ni/SiC DC

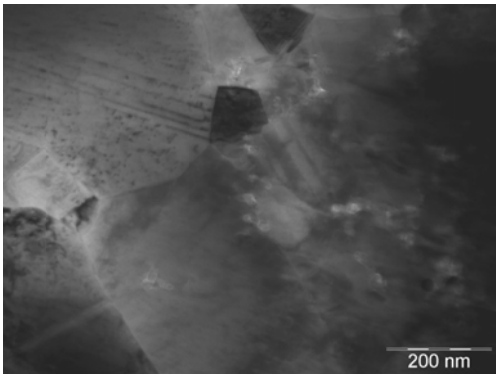

Fig 5.75. TEM image of Ni/SiC DC

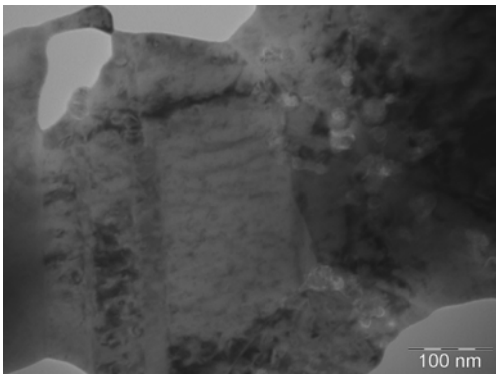

Fig 5.76. TEM image of Ni/SiC PC

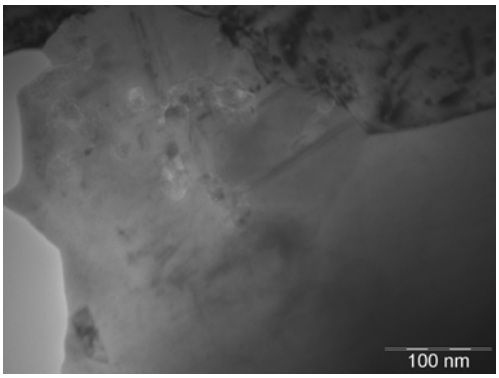

Fig 5.77. TEM image of Ni/SiC PC

The SiC nanoparticles are codeposited in the nickel matrix with a low agglomeration degree, despite the powder tends to agglomerate in the galvanic bath. The particles aggregates formed by 20-30 particles are clearly visible both inside the metal grains and near to the bordergrains. The pulse current does not influence the dispersion of the powder.

Applying the ultrasonic vibrations during the electrodeposition the aggregates size decreases and small aggregates formed by 5-10 particles are still present (from Fig 5.78 to Fig 5.81). The application of the pulse current does not induce further deagglomeration: no significant differences are visible among samples deposited under different current conditions.

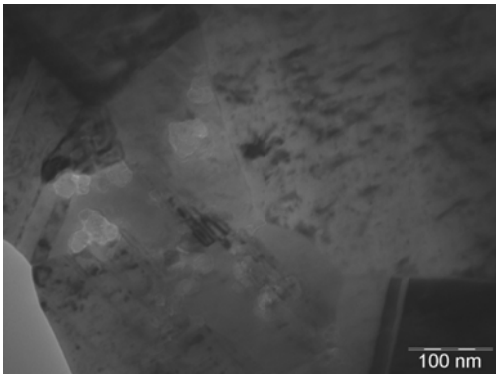

Fig 5.78. TEM image of Ni/SiC DC US

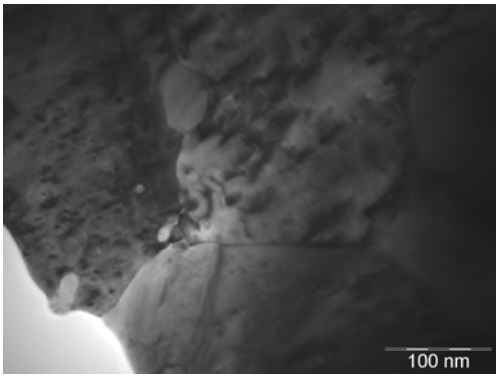

Fig 5.79. TEM image of Ni/SiC DC US

Fig 5.80. TEM image of Ni/SiC PC US

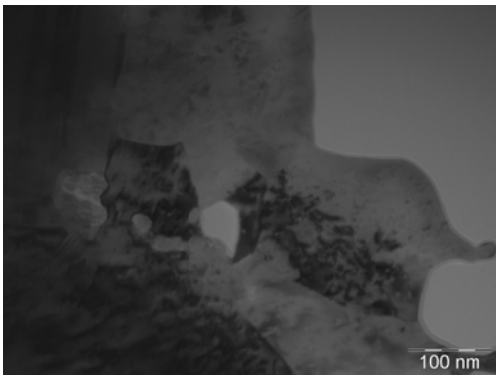

Fig 5.81. TEM image of Ni/SiC PC US

These micrographs show that some particles are individually codeposited and the aggregation is limited. The most of the particles are located along the grainborders or next to them.

Comments

The microstructure analyses of the samples cross-section give a lot of interesting information about the coating growth and how it is affected by the codeposition of nanoparticles or by the current conditions. Generally nickel films present vertical columnar grains grown parallel to the applied electric field. The codeposition of the ceramic powder partially interrupts the growth of the columns. In the case of codeposition of silicon carbide powder the application of the pulse current or the ultrasonic vibrations leads to a more refined structure were the columns are not more present, but the vertical orientation is still lightly visible. In the case of alumina nanoparticles

codeposition, only the application of the ultrasounds is able to interfere with the columnar growth whereas under silent condition the films present large columnar grains and big ceramic agglomerates. The ultrasonic vibrations and the consequential better dispersion of the alumina particles change completely the electrocrystallization process leading to an unoriented microstructure both under direct and pulse current.

Despite SiC tends to agglomerate more in the galvanic bath compared to alumina, the Ni/SiC film results to be more dispersed and homogeneous. On the contrary, the deposited alumina particles are strongly agglomerated and only the application of the ultrasounds decrease partially this problem.

The agglomeration degree of codeposited particles is an important property of the composite coating since smaller agglomerates are better distributed in the whole matrix compared to bigger ones and the reinforcement could be more homogeneous and more effective. Moreover the smaller the particles the higher is their influence on the electrocrystallization process and therefore on the final microstructure of the coatings.

Ceramic content

In order to evaluate the real ceramic embedded fraction two different analyses were carried out: EDXS spectra on the layer surface and GDOES in order to have a concentration profile along with the coating thickness. EDXS provides a semi-quantitative analysis and therefore could not be used to calculate the composite phase composition but is a very fast test and gives a lot of important information. Moreover this is the technique commonly used in the field of composite electrodeposition to study the layer composition and

therefore has been used in order to better compare the results with the literature data. Two main limits of this technique have to be underlined: first, as already mentioned, this is a semi-quantitative analysis and especially for very low concentrations the results are affected by a high error, second these measurements are usually carried out on the surface of the coating and therefore the results refer to a very particular region of the layer. The surface suffers in fact of the contamination due to the loose adsorbed powder and usually results richer in ceramic particles. The results are presented as an average value of five measurements performed onto two different samples.

GDOES is more precise in detecting and quantifying the elements contained in the deposits and gives also a concentration profile among the thickness. This is a very important information as it is possible to monitor the particles distribution. The GDOES analyses were carried out using a JY RF-GD PROFILER HR instrument, manufactured by Horiba Jobin-Yvonne, Longjumeau, France. The instrument is equipped with a standard 4 mm diameter anode, a polychromathor with 28 acquiring channels and a Quantum XP software. The source conditions were Ar pressure of 650 Pa and 35 W applied power. These conditions are necessary to obtain a flat crater in order to increase the depth resolution. All results shown were obtained with the same source conditions and with the same calibration method. The calibration was performed with 21 samples selected among SUS and CRM's. The results are presented as an average value of five measurements on two different specimens.

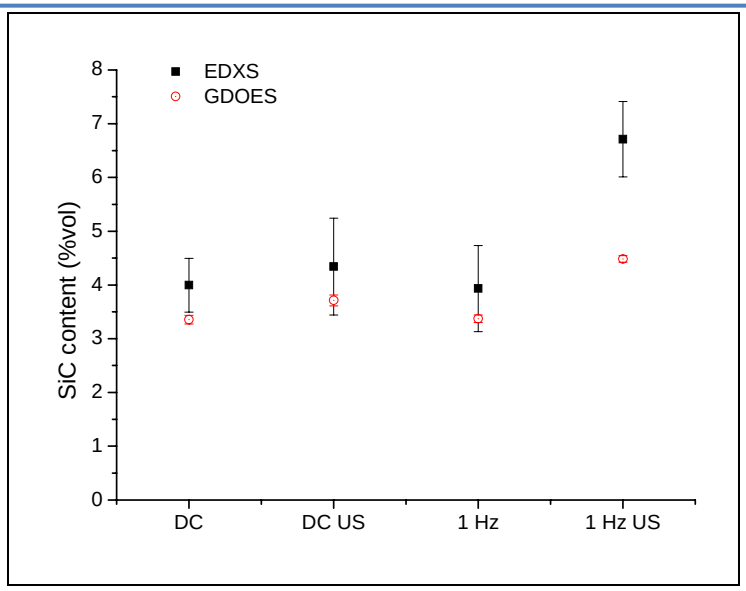

Fig 5.82. Volumetric content of embedded SiC particles

In Fig 5.82 the average values of SiC content in the deposits are plotted for different deposition current conditions, measured both by EDXS and GDOES. First of all the results demonstrate that the EDXS detects a higher content of ceramic particles and, more important, has a higher standard deviation. The embedded SiC content is much higher if compared to the systems containing a surfactant for the pitting control, but is still limited to some percentages.

The specimens produced under DC deposition contains about 3.5%vol of ceramic particles and the application of the pulse current does not change the incorporation rate. Moreover the use of the ultrasonic vibrations during the deposition has a beneficial effect on the codeposition process. Under DC conditions the samples show only a slight increase in the SiC content , but the coatings produced under PC reach values of about 4.5% according to GDOES analyses. Additionally representative concentration profile of the deposits are

plotted in the figures from Fig 5.83 to Fig 5.86. In the plots the concentration of each element is plotted versus the depth from the surface. The signals of both Si and C amounts follow the same trend and the SiC is homogeneously distributed along the whole thickness of the deposit. The higher amount on the surface of the deposit is attributed to the absorption of the SiC particles on the surface of the deposit due to the immersion in the plating bath and to the roughness. The profile of the Si and C of the sample produced under silent conditions are homogeneous and constant along the whole thickness, demonstrating the good dispersion of the silicon carbide particles.

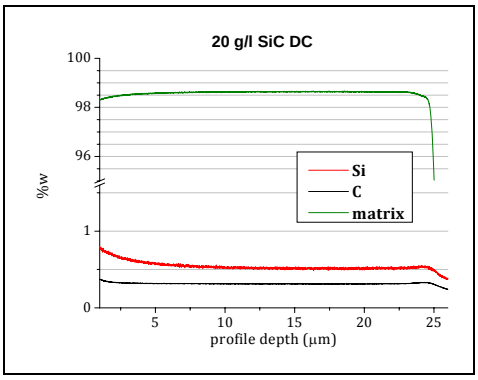

Fig 5.83. GDOES profile concentration of Ni/SiC sample produced under DC

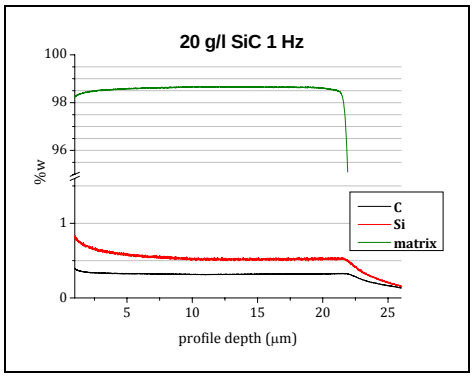

Fig 5.84. GDOES profile concentration of Ni/SiC sample produced under PC

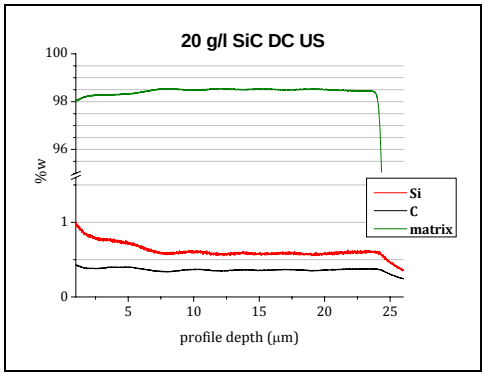

Fig 5.85. GDOES profile concentration of Ni/SiC sample produced under DC with US

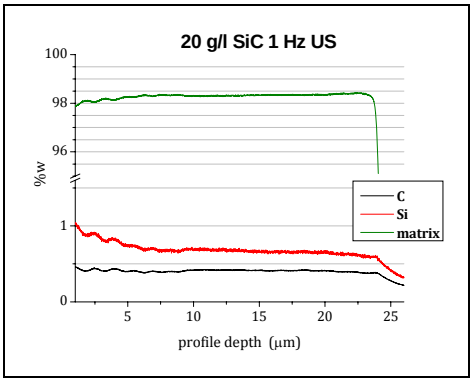

Fig 5.86. GDOES profile concentration of Ni/SiC sample produced under PC with US

On the other hand the samples produced with the application of the ultrasonic vibrations have a wavy concentration profile of Si and C especially in the outer part of the coating.

Concerning the Ni/Al_2O_3 deposits, Fig 5.86 shows the average value of the particles content evaluated both by EDXS and GDOES. Again the EDXS results show a higher content of ceramic particles in the case of the specimens produced under pulse current, while for the specimens deposited under DC conditions the EDXS and GDOES give comparable values.

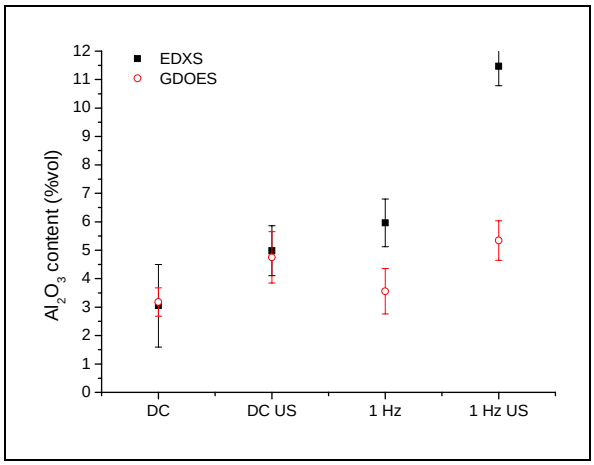

Fig 5.87. Volumetric content of embedded Al_2O_3 particles

The alumina content in the samples deposited under DC conditions is about 3%vol and increases slightly by the application of a pulse current under silent conditions. The use of the ultrasounds, on the contrary, has a substantial effect on the embedding of ceramic particle and induces an increase from 3% to about 5%, under both DC and PC conditions. In all the measurements the standard deviation is quite high, even for the results of GDOES, probably due to a more heterogeneous distribution of the powder into the metallic matrix. Some representative GDOES concentration profiles are reported in figures from Fig 5.88 to Fig 5.91 and give more information about the ceramic content in the nickel matrix. Since oxygen is an element with a very difficult calibration, the plots report only the signal of Al and Ni as weight percent. The calculation of the alumina content were carried out with the hypothesis that the powder is stechiometric. The concentration profiles of aluminium codeposited under silent conditions is almost constant among the coating thickness as shown in Fig 5.88 and Fig 5.89. The area interested by the

measurement has a diameter of 3 mm and therefore the results do not detect the alumina distribution heterogeneity. However the depth resolution is very high and the results show a good homogeneity along the coating thickness.

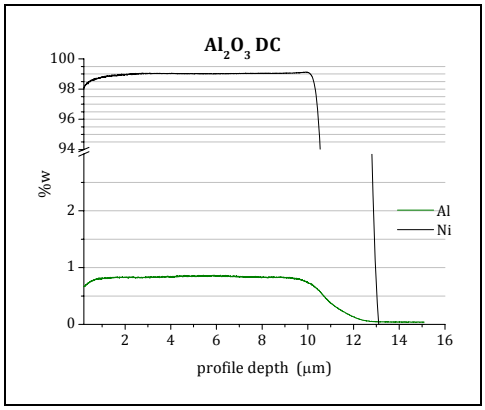

Fig 5.88. GDOES profile concentration of Ni/Al_2O_3 sample produced under DC

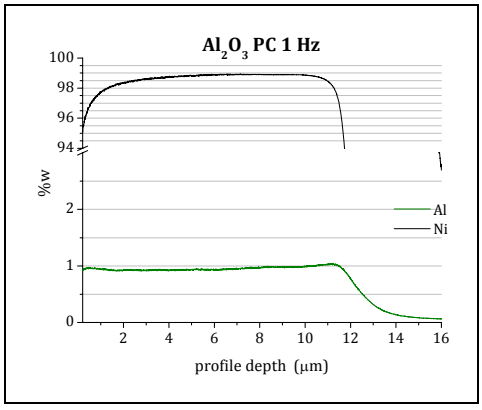

Fig 5.89. GDOES profile concentration of Ni/Al_2O_3 sample produced under PC

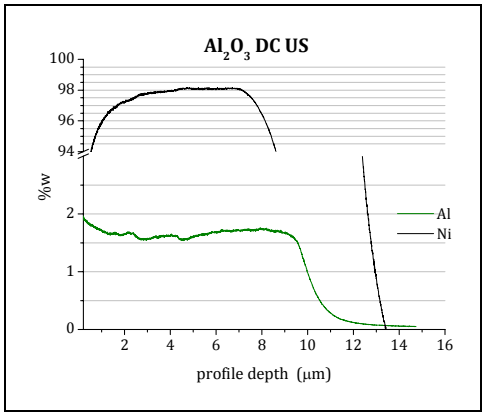

Fig 5.90. GDOES profile concentration of Ni/Al_2O_3 sample produced under DC US

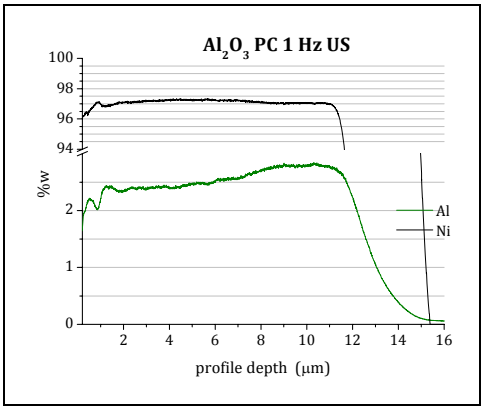

Fig 5.91. GDOES profile concentration of Ni/Al_2O_3 sample produced under PC US

The GDOES spectra of the samples produced with the ultrasonic vibrations

reported in Fig 5.90 and Fig 5.91, on the contrary, show an irregular concentration profile. These results demonstrate that the ultrasounds induce some variations into the codeposition process and in the final distribution of the embedded particles.

Comments

Considering the ceramic fraction, alumina is more easily codeposited in the nickel matrix compared to SiC and more influenced by the deposition condition like pulse current and ultrasounds. The application of the ultrasonic vibrations induces an increase of the embedded powder in all current condition and for both SiC an Al_2O_3. The increase is higher in the case of alumina and accompanied by a decrease of the agglomeration degree. Since the ultrasounds could break the powder aggregates in the electrolyte, it can be conclude that the agglomeration tends to decrease the codeposition rate of the solid second phase. A well dispersed powder should be codeposited at a higher rate than an agglomerate one.

6. Mechanical properties

The changes induced by the application of the US and the codeposition of the ceramic powder lead to the refinement and the optimization of the layer microstructure and as a consequence the mechanical properties should be enhanced. Since these deposits are applied on the surface of mechanical devices the most important features are the surface properties such as hardness and abrasion resistance. In order to quantify the reinforcement due to the ceramic particles and the microstructural changes, the Vickers microhardness 001 and the abrasion resistance by Taber Abraser of the layers were tested.

Microhardness

The Vickers microhardness was measured in cross section to avoid the influence of the substrate. The applied force was 0.1 N and the dwell time 10 s. The values reported in the Fig 6.1 are the average values of 30 measurements performed onto 2 different specimens. The pure nickel layers deposited under DC show a microhardness of about 270 HV both under silent condition and with ultrasounds. As can be observed, the use of the pulse current during the

deposition of pure nickel deposits leads to a slight microhardness increase.

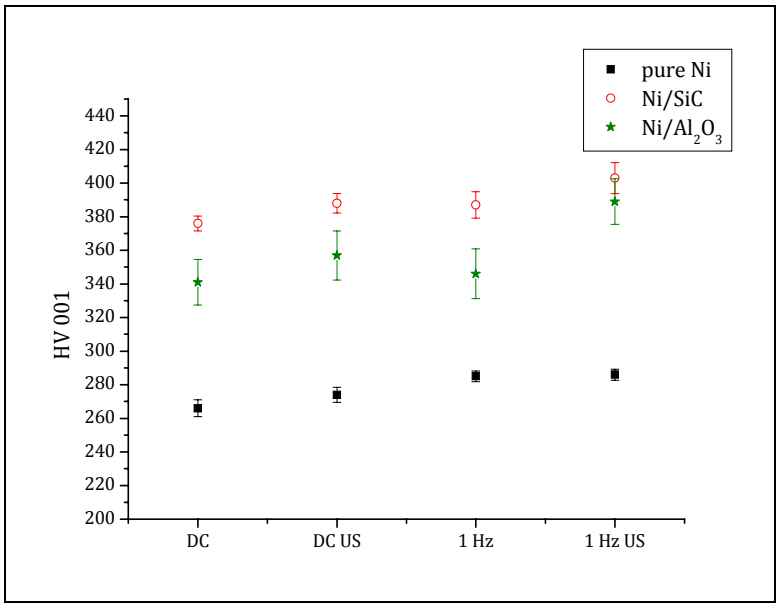

Fig 6.1. Vickers microhardness of different layers

The grain refinement caused by the use of pulse current and the consequent increase of the grain borders extension lead also to an increase of the microhardness due to the strain hardening effect. The application of the ultrasounds though does not affect the microhardness values.

The addition of the SiC nanoparticles induces a substantial increase of the hardness of the layer of about 100 HV partially due to the presence of the harder second phase and partially caused by the microstructure changes caused by the codeposition process as exposed in chapter 5. As for pure nickel layers, also for Ni/SiC systems the use of a pulse current induces an increase in the hardness due to refinement of the microstructure and therefore to the strain hardening. Moreover by the synergic effect of the pulse current and the

ultrasonic vibrations the hardest layer is produced.

The codeposition of the alumina nanopowder as well is beneficial for the microhardness which increases of about 80 HV. The layers containing alumina do not reach the hardness of the ones containing silicon carbide, only the sample produced under pulse current and US vibrations reaches a comparable hardness. Moreover the Ni/Al_2O_3 hardness values are affected by a higher standard deviation. This large error can be correlated to the high agglomeration degree and heterogeneity in the alumina dispersion into the metallic layer as shown in the cross-section micrographs in chapter 5. The Ni/Al_2O_3 specimens show the same trend in the hardness values as Ni/SiC layers: the US slightly increase the hardness and the synergic effect of pulse current and ultrasounds induces a substantial hardening effect.

In order to check if there is a relationship between the particles content and the microhardness in Fig 6.2 the microhardness of the nanocomposite layers are plotted as a function of the embedded particle volume fraction. From this graph is clear that the silicon carbide particles codeposition leads to harder coatings even if the embedded particles content is comparable to the alumina powder. There are too few points for each system to determine which kind of relationship correlates the particles content to the hardness, but from these data a linear proportionality seem to be present.

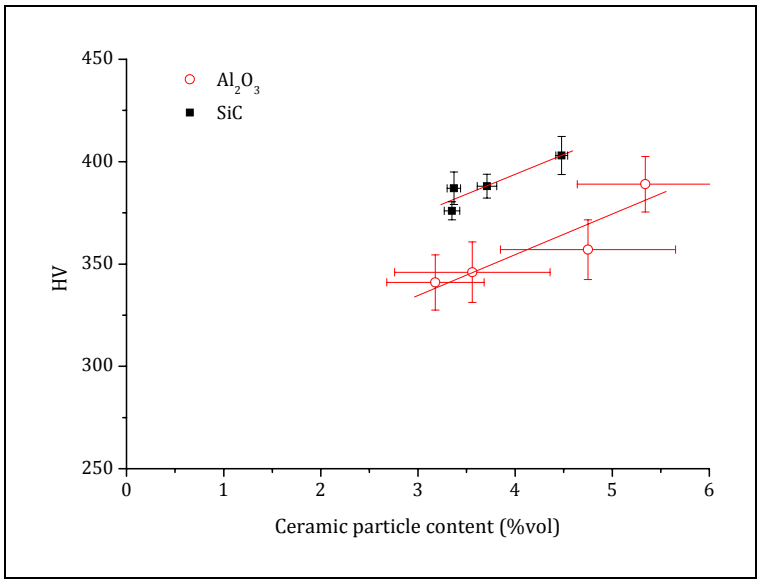

Fig 6.2. Correlation between particles content and microhardness

To better understand if there is a good correlation between hardness and ceramic particles content it is better to plot all the hardness data measured and previously exposed in chapter 4, relative to all the different deposition conditions previously tested.

In the Fig 6.3 Ni/SiC particles microhardness values are plotted as a function of the SiC content, while the Fig 6.4 reports the Ni/Al_2O_3 microhardness value as a function of the alumina content.

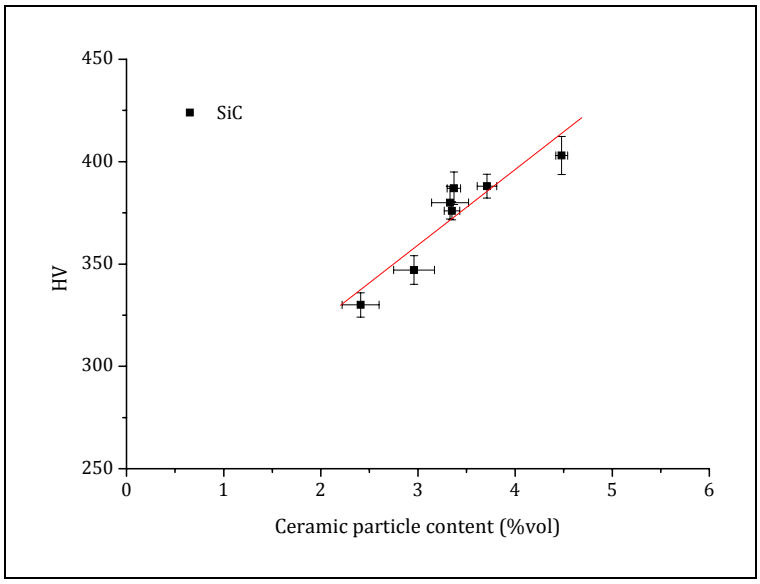

Fig 6.3. Correlation between SiC content and microhardness

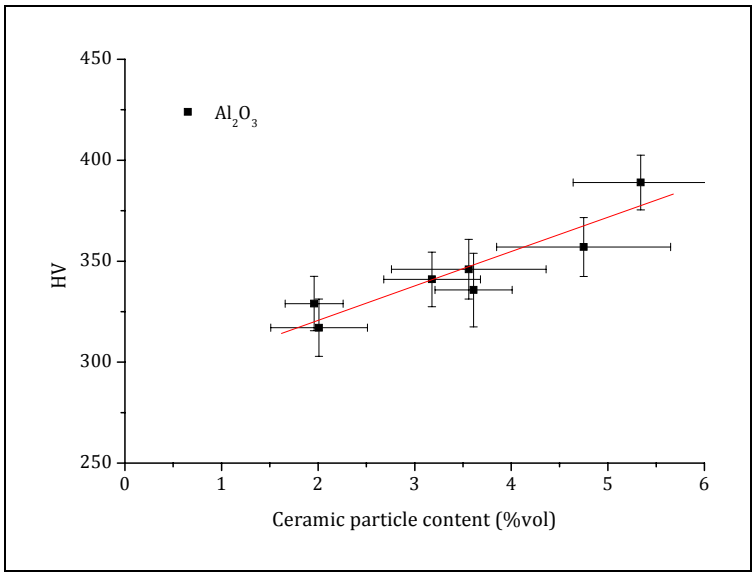

Fig 6.4. Correlation between Al_2O_3 content and microhardness

Both the two graphs show that exists a linear proportionality between the final hardness and the ceramic particles content. However, this relationship is different for the 2 systems. The microhardness is not related only to the hard phase content, but also to its hardness, its dispersion degree and to the modifications that the particles induce in the metal matrix.

The hardening obtained by SiC codeposition is higher than Al_2O_3 even if the embedded SiC amount is smaller, moreover fitting the points with a straight line, the Ni/SiC system shows a higher rate of hardening than the Ni/Al_2O_3 one.

The silicon carbide nanopowder is not only harder than alumina, but its codeposition leads to a finer and more homogeneous dispersion of the particles into the metal layer. Furthermore the SiC powder induces a substantial grain refinement even under silent conditions as shown in chapter 5. All these characteristics improve the effectiveness of the SiC nanopowder in hardening, thus leading to a higher rate of the hardness-particle content relationship. However also the alumina powder shows a linear proportionality between particles content and hardness, but due to its agglomeration the hardening is smaller and the increase in the particle content leads to a smaller increase in the hardness.

Abrasion resistance

Specimens of 10x10 cm and with a deposit thickness of 50 μm were prepared for this test. The specimen is placed onto a disk which rotates at a steady speed of 60 rpm and is abraded under the weight that is inflicted by two abrasive wheels which rotate in opposite directions as shown in Fig 6.5.

The wheels used were CS10 type and the additional weight was 1 kg. The test was interrupted every 500 cycles to weight the samples and to clean the wheels with an abrasive paper. Three tests were performed on different specimens and in the following figures representative plots are reported. The abrasion resistance is expressed by the rate of the mass loss during the abrasion process.

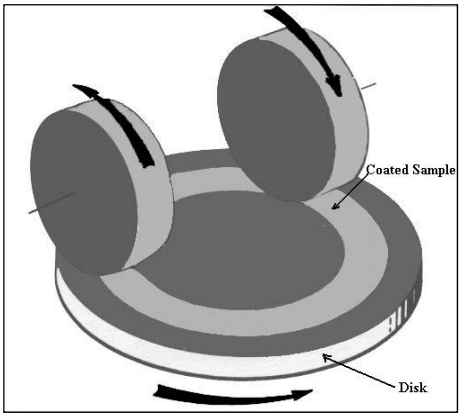

Fig 6.5. Schematic design of Taber Abraser test

The mass loss as a function of the number of cycles for pure deposits produced under different current conditions for both silent and sonicated processes is reported in Fig 6.6 in order to evaluate the influence of the process parameters on the abrasion resistance of the deposits. All the specimens show a similar abrasion resistance.

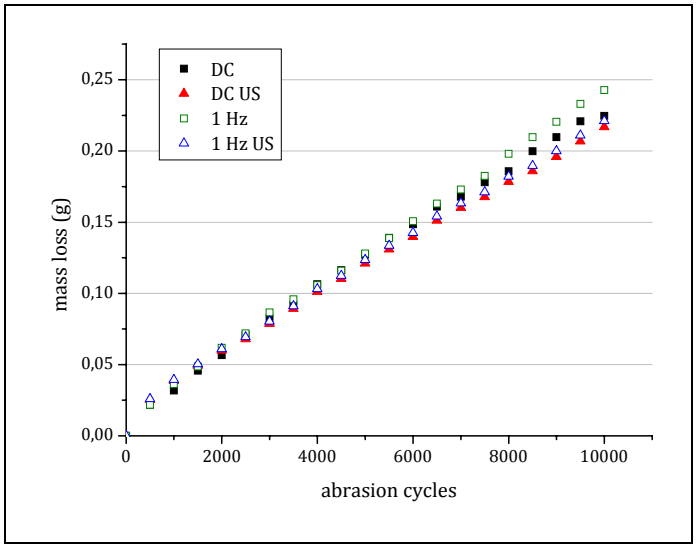

Fig 6.6. Mass loss during abrasion test of pure nickel layers

The pure nickel layers lose from 0.22 to 0.24 g at the end of the test of 10000 cycles and the abrasion rate is summarized in Table 6. 1. No big differences are noticed between pure nickel layers produced under different deposition conditions. The curves corresponding to the deposits produced under direct current and under pulse current at the frequency of 1Hz are similar even if they consist of completely different grain size microstructures.

Table 6. 1 Abrasion rate of pure nickel layers.

deposition conditions	abrasion rate
DC	2.21 E-5 ± 8.4 E-7
DC US	2.03 E-5 ± 8.2 E-7
1 Hz	2.33 E-5 ± 7.4 E-7
1 Hz US	2.07 E-5 ± 8.3 E-7

The abrasion rates reported in Table 6. 1 are very similar for each kind of pure nickel deposit. Only a slight decrease in the abrasion rate is visible for the samples produced under ultrasonic vibrations.

In the Fig 6.7 representative plots of the mass loss during the abrasion test for Ni/SiC deposits are plotted.

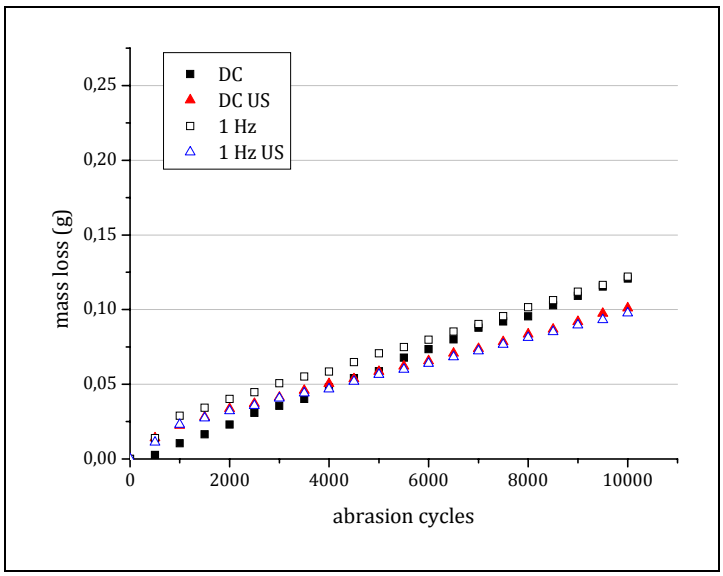

Fig 6.7. Mass loss during abrasion test of Ni/SiC layers

The abrasion resistance of the Ni/SiC layers is much higher compared to the pure nickel ones and after 10000 cycles of abrasion the samples produced under silent conditions loose 0.12 g, while the specimens produced with the ultrasonic vibrations loose only 0.10 g. The most important parameter is the abrasion rate that is summarized in Table 6. 2 for the Ni/SiC layers.

Compared to pure nickel layers, the abrasion rate is reduced of about 50% for Ni/SiC produced both under DC and PC silent conditions and even more for the samples produced under ultrasonic vibrations.

Table 6. 2 Abrasion rate of Ni/SiC layers.

deposition conditions	abrasion rate
DC	1.23 E-5 ± 1.14E-7
DC US	8.66 E-6 ± 2.14E-7
1 Hz	1.06 E-5 ± 2.7E-7
1 Hz US	8.46 E-6 ± 2.47E-7

This improvement has to be related to the presence of the ceramic powder, its dispersion and to the microstructural changes that the powder induces into the metal matrix and it is generally correlated to the hardening effect of the codeposition process. The application of the ultrasounds improves the abrasion resistance because the ceramic content increases in the deposits but also because the vibrations increase the homogeneous dispersion of the powder.

In the Fig 6.8 representative curves of mass loss as a function of the abrasion cycles of Ni/Al_2O_3 layers are plotted.

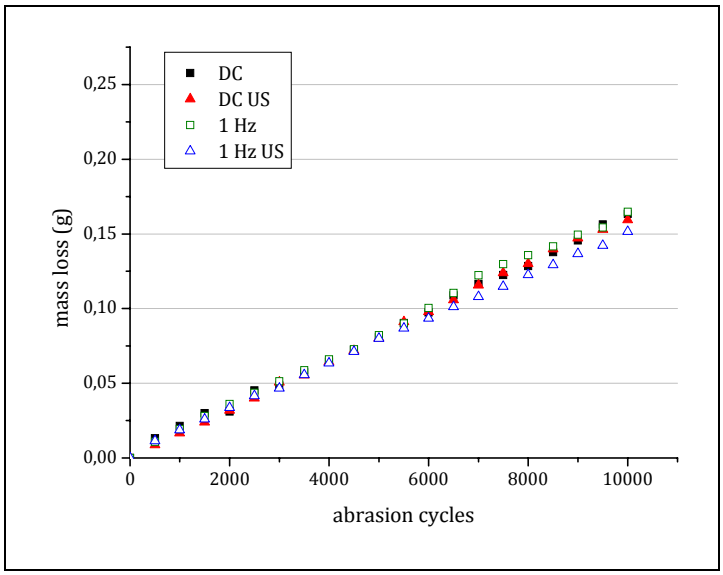

Fig 6.8. Mass loss during abrasion test of Ni/Al_2O_3 layers

No differences between the nanocomposites containing alumina produced under different conditions are visible. The mass loss after 10000 cycles is about 0.15 g for each specimen. Comparing these results to the pure nickel ones a considerable increase of abrasion resistance is to notice. Comparing them to the Ni/SiC ones, on the contrary, the abrasion resistance is much lower.

The Table 6. 3 reports the mean values of the abrasion rate of the Ni/Al_2O_3 deposits. The values are very similar for deposits produced under different conditions; the only slight increase in the abrasion resistance is offered by the synergic effect of pulse current and ultrasonic vibrations.

Table 6. 3 Abrasion rate of Ni/Al_2O_3 layers.

deposition conditions	abrasion rate
DC	1.60 E-5 ± 5.6 E-7
DC US	1.59 E-5 ± 5.0 E-7
1 Hz	1.63 E-5 ± 5.7 E-7
1 Hz US	1.48 E-5 ± 3.0 E-7

In order to have a complete overview of the abrasion resistance, Fig 6.9 reports the representative plots of all the specimens. From this plot the differences between the 3 systems in the abrasion resistance are clear.

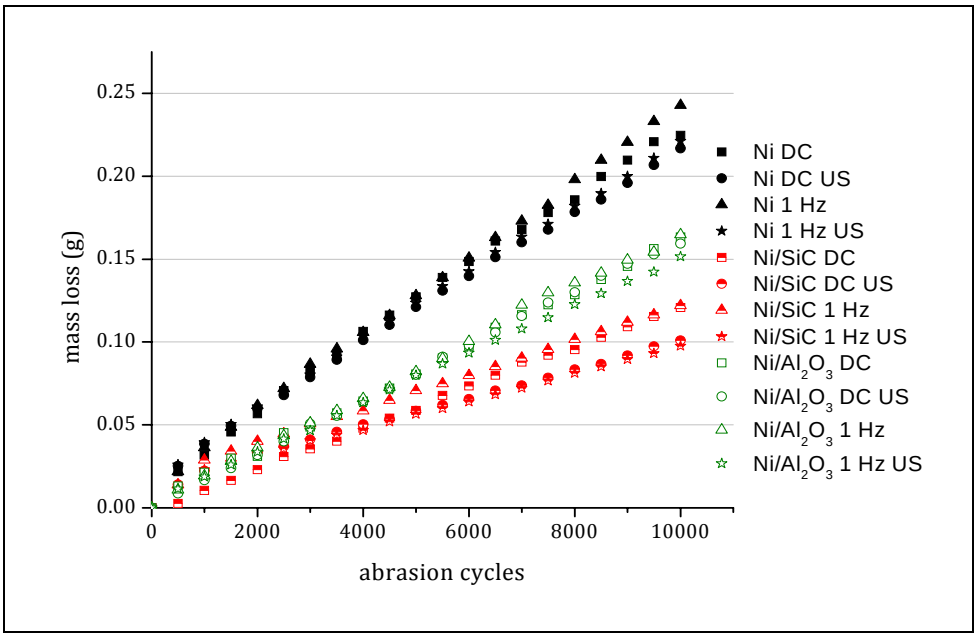

Fig 6.9. Comparison of the mass loss during abrasion of all specimens

The mass loss is linearly proportional to the abrasion cycles for all specimens, small variation from this behaviour are to be correlated to the mass measurements errors. As the microhardness values have pointed out, the Ni/Al_2O_3 coatings are not reinforced as the Ni/SiC ones. The abrasion resistance indeed is enhanced by the addition of the ceramic particles, both silicon carbide and alumina, but the increase due to the silicon carbide is much higher. In order to find out if a relationship between hardness and abrasion resistance is definable, in the Fig 6.10 the abrasion rate are plotted as a function of the hardness of the layers.

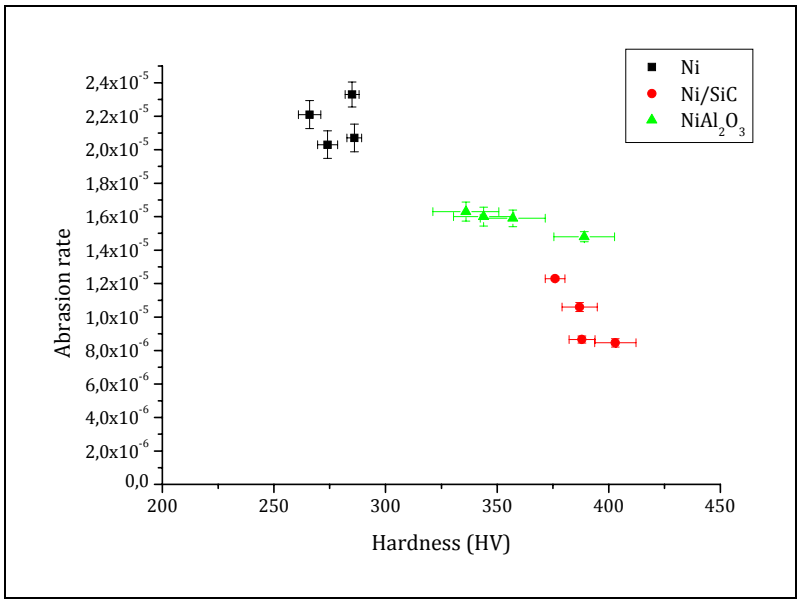

Fig 6.10.Correlation between abrasion rate and hardness

A sort of correlation between these two properties is absolutely evident, the harder the layer, the lower the abrasion rate. The Ni/SiC deposits indeed are harder and also more resistant to abrasion. On the contrary the pure nickel

layers show the highest abrasion rate and therefore the lowest resistance to abrasion. Considering the pure nickel layers though, the layers produced under different conditions do not show any kind of proportionality since the difference both in hardness values and in the abrasion rate are slight and therefore all the data points are very near.

The values of the nanocomposite on the other hand have different behaviour depending on the type of embedded particles. The Ni/Al_2O_3 layers show a limited decrease in the abrasion resistance corresponding to a quite large increase of the hardness, the Ni/SiC on the contrary, for a small variation of the hardness value shows a substantial decrease in the abrasion rate.

The correlation between the abrasion resistance and the hardness is therefore not unique and not definable.

The abrasion resistance is correlated not only to the microhardness but also to the dispersion of the particles inside the metal matrix. The homogeneity of the dispersion and the absence of agglomeration is much more important for abrasion resistance than for the hardening.

Comments

The mechanical properties that were tested and presented in this chapter provide information about the improvement of the final properties due to the codeposition process and about its mechanism. As for all the composites, the mechanical properties depend on the reinforcement phase, on its quantity and on its dispersion. In the case of electrodeposited composites the presence of the second phase influences also the electrocrystallization process and induces changes in the metal microstructure. Therefore the mechanical

properties depend also on the capability of the particles to interact with the electrocrystallization process.

As shown in the previous chapter the presence of the second phase induces a severe refinement of the grains and if well dispersed can change completely the microstructure avoiding the columnar field-oriented grains growth and promoting a non-oriented round shape grains nucleation and growth.

As shown in chapter 5 the Al_2O_3 particles have a high agglomeration degree when codeposited into the nickel layer, while the SiC particles are codeposited homogeneously and well dispersed. As a consequence, the mechanical properties of the Ni/SiC layers are more promising than the Ni/Al_2O_3 ones.

The SiC powder is more effective in hardening: not only the Ni/SiC layers are harder than Ni/Al_2O_3 layers for the same content of ceramic particles, but also the rate of the proportionality between hardness and ceramic content is higher.

However, the Ni/Al_2O_3 coatings are noticeably improved by the application of the ultrasonic vibrations during the deposition, since they promote the dispersion of the powder inside the metal and lead to the deposition of a harder and more resistance coating.

Since the agglomeration degree of the powder is an issue and influences negatively the final mechanical properties, the US result to be very effective in improving the final properties of the deposits, both decreasing the agglomeration, as for alumina, and increasing the particles content, both for alumina and nickel.

7. Electrochemical properties

Metal matrix composite coatings are usually applied on those surfaces subjected to mechanical load in order to improve their resistance, but usually their corrosion resistance is not considered. For example, the micro-composite coatings are widely industrialized and applied especially in the automotive industry because of the improved wear resistance and higher hardness, but they present a worse corrosion resistance if compared to the pure metals. They indeed present some weak points. During the electrodeposition process the micro-particles are not easily embedded and covered by the growing matrix thus presenting some voids among the particle-matrix interfaces. Moreover the presence of partially embedded particles on the surface is a barrier for the continuity and the homogeneity of the natural protective oxide for passive metals. Nanocomposite coatings seem to be a good alternative for those devices that work in aggressive environments and need both corrosion protection and improved mechanical properties.

In this study the corrosion resistance of the nickel matrix deposits was studied by potentiodynamic curves in different environments and by exposure to the salt spray cabinet combined by Electrochemical Impedance Spectroscopy

measurements (E.I.S.). The different testing environments have been chosen in order to evaluate the resistance to both uniform and pitting corrosion. The electrochemical interface used for the measurements is a Potentiostat/Galvanostat EG&G model 273 coupled with a frequency response analyzer Solartron model 1255 for EIS tests.

Polarization tests

The polarization tests allow considerable information on the surface electrochemical processes to be acquired. Through the potentiodynamic polarization technique, information on the corrosion rate, pitting susceptibility and passivity are possible to be obtained, thus giving information of both thermodynamics and kinetics of the electrochemical process.

In order to monitor the electrochemical behaviour 3 polarization test for each sample have been performed and in this chapter some representative plots are presented. For the electrochemical tests the samples have been embedded in resin in order to mask the substrate and the uncoated part and leave free only the coated surface to be tested. The measurements have been performed using a three electrode system (working electrode: specimen embedded in resin, reference electrode: Ag/AgCl 3M, counter electrode: platinum).

The resistance to uniform corrosion was evaluated by the potentiodynamic curves performed in an acidic (pH 3) electrolyte.

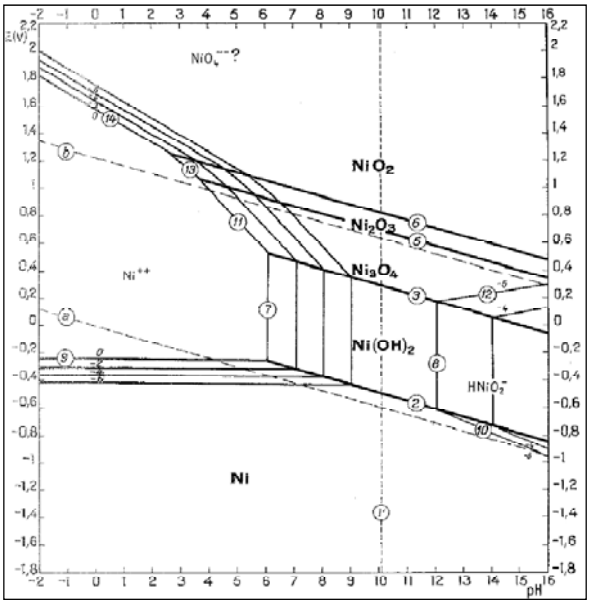

Fig 7.1. Pourbaix diagram of nickel.

The electrolyte used was a 0.5M Na_2SO_4 aqueous solution in which sulphuric acid has been added until the pH reached the value of 3. The specimens have been immersed in the electrolyte till the stabilization of the measured potential before the test and the potential scanning was performed from -250mV vs. OCP up to 1.1V vs. Ag/AgCl. The scanning rate was 0.2mV/s.

In the Fig 7.2 the polarization curves of pure nickel deposits produced under direct current with and without ultrasonic vibrations are presented.

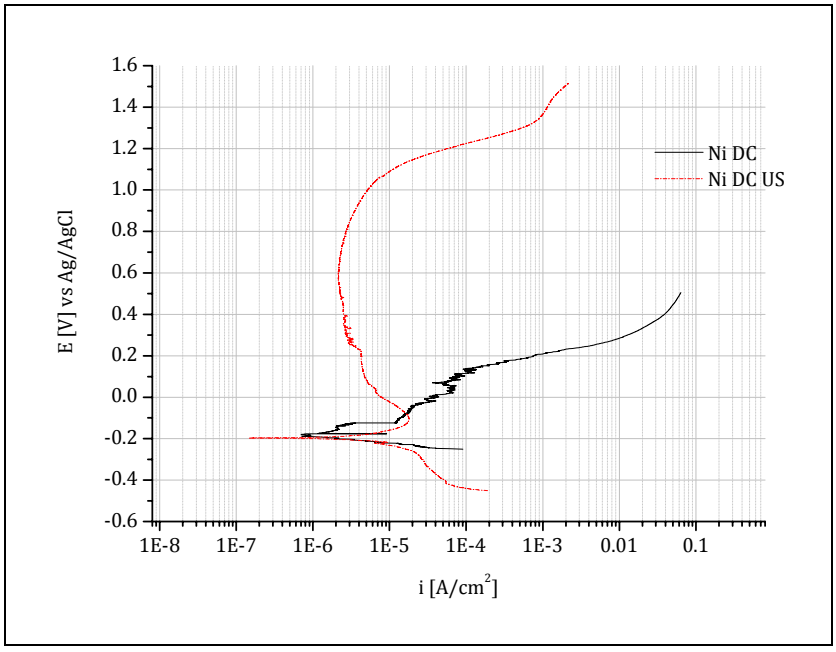

Fig 7.2. Polarization curves at pH 3 of pure nickel coatings deposited under DC with and without US

Despite both the coatings have the same free corrosion potential of -200 mV (vs Ag/AgCl), the coating produced under silent condition has an active behaviour, while the coating produced under ultrasonic vibrations has an active-passive transition and shows a passivity region from -100 mV to the breakdown potential of about 1,1 V. This great difference in the electrochemical behaviour is due to the presence of pores and defects in the coating that could pass through the whole thickness of the deposited layer or offer weak points for the corrosion attack.

As already pointed out in the previous chapters the samples produced under silent conditions suffer from porosity due to the hydrogen evolution on the cathodic surface. These surface defects are very dangerous for the corrosion point of view because nickel is generally more noble of the substrates on

which is deposited and therefore a more severe corrosion will take place due to the galvanic coupling. The potentiodynamic plots of Fig 7.2 show indeed that not only the passive region is completely disappeared but also that the current densities of the anodic branch are very high, confirming that a porous coating can not protect from corrosion but even improves the corrosion rate of the substrate. Therefore in order to compare and study the electrochemical behaviour of the deposits only the coatings produced under ultrasonic vibrations are tested.

In the following graph the polarization curves of the pure nickel samples are presented.

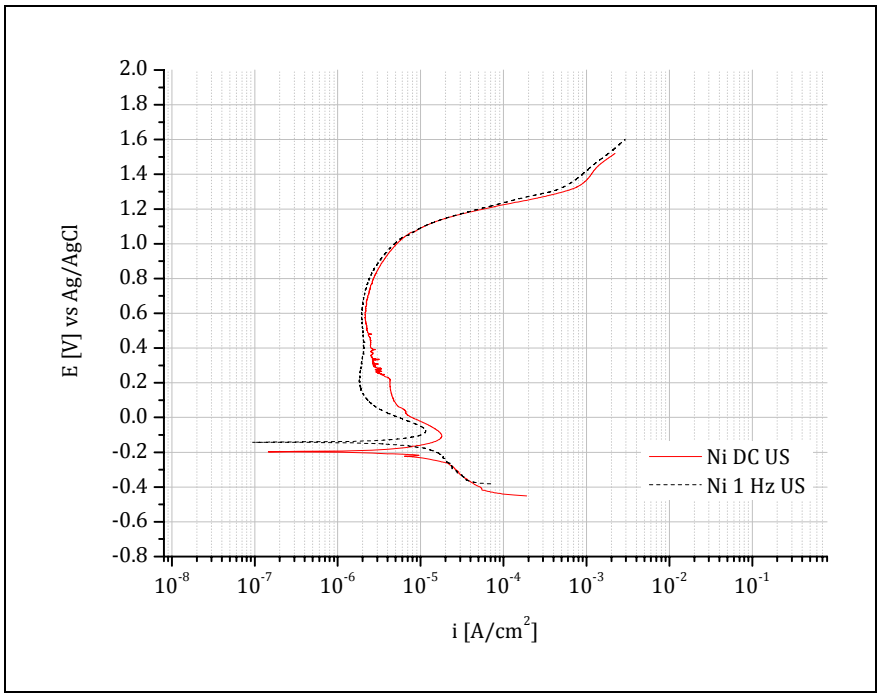

Fig 7.3. Potentiodynamic curves of pure nickel coatings at pH 3

The curves plotted in Fig 7.3 show that pure nickel coatings produced with

ultrasonic treatment under both direct and pulse current present an active-passive behaviour. The passive range is quite wide and well defined. The pulse plated layer shows a slightly more stable passive oxide with a constant passive current density, while the layer deposited under direct current shows a passive current density that decreases increasing the applied potential demonstrating a progressive stabilization of the passive oxide film. The electrochemical parameters are summarized in Table 7. **1** . The Ni/SiC nanocomposite coatings have an electrochemical behaviour similar to the pure nickel in acidic electrolyte as shown by the graphs of Fig 7.4.

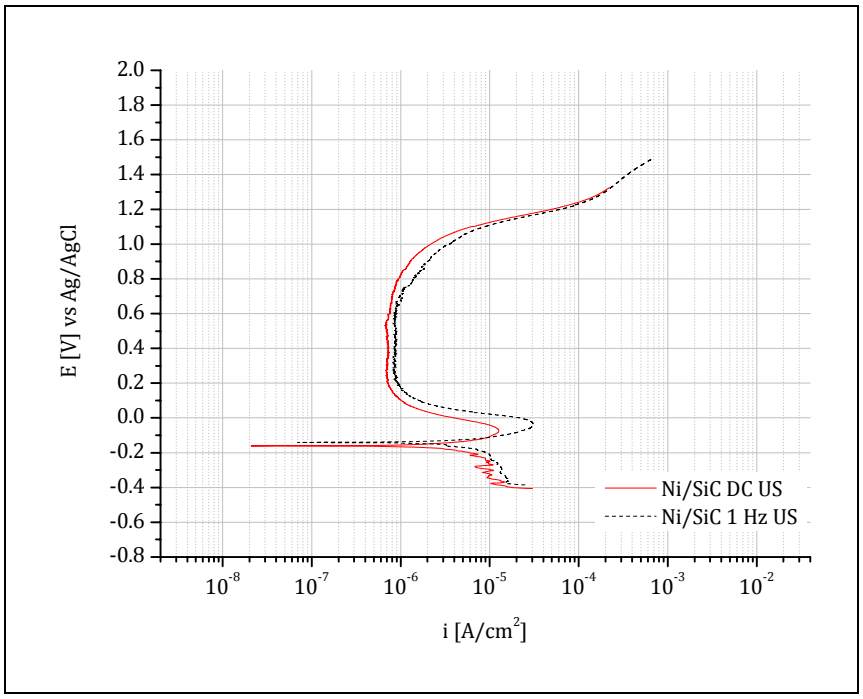

Fig 7.4. Potentiodynamic curves of nanocomposite Ni/SiC coatings at pH 3

Both the Ni/SiC nanocomposite coatings show an active-passive transition and there are no substantial differences between the deposits. The corrosion

potential and current density as well as the passive current density are equal for both deposits produced under direct and pulse current.

The active parts of the curves are almost overlapped and there are only small differences in the critical current density. The passivity zone is stable and both kind of specimens present the same passive range.

The electrochemical behaviour in acidic electrolyte of the Ni/Al_2O_3 nanocomposite coatings is shown by the polarization curves of Fig 7.5.

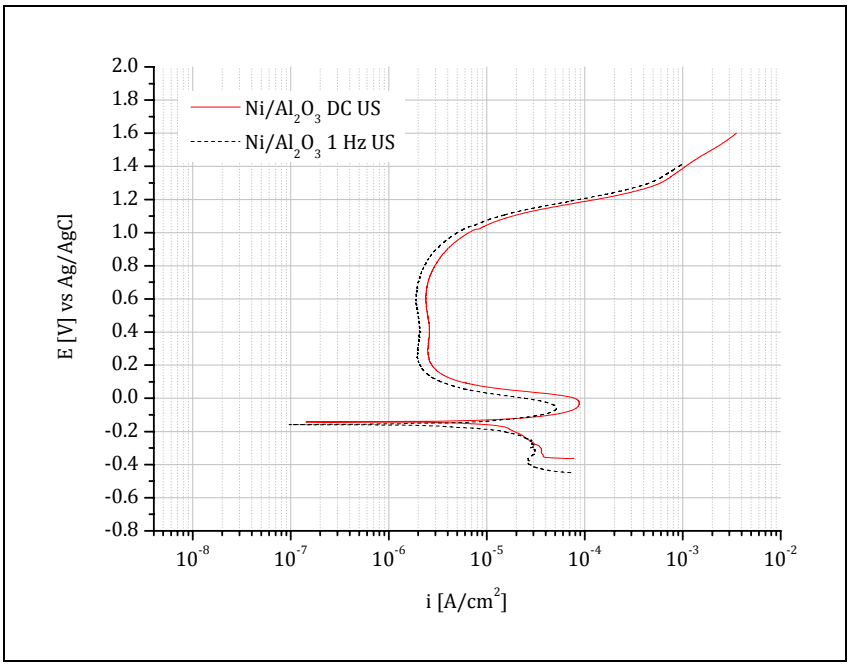

Fig 7.5. Potentiodynamic curves of nanocomposite Ni/Al_2O_3 coatings at pH 3

The 2 curves of nanocomposite coatings containing alumina particles are almost overlapped: the passivity zone is stable and both specimens present the same passive range.

The electrochemical parameters of the polarization curves in acidic

environment are summarized in the following table where the corrosion current density values are extrapolated by the Tafel approximation.

Table 7. 1 Electrochemical parameters at pH3

PARAMETER	Ni		Ni/SiC		Ni-Al_2O_3	
	DC+US	DC+US	1Hz+US	1Hz+US	DC+US	1HZ+US
E_{corr} [v]	-0.20	-0.13	-0.15	-0.13	-0.13	-0.15
i_{corr} [A/cm²]	$3\cdot10^{-6}$	$4\cdot10^{-6}$	$5\cdot10^{-6}$	$4\cdot10^{-6}$	$1.8\ 10^{-5}$	$1.6\ 10^{-5}$
E_{pp} [v]	-0.12	-0.11	-0.04	-0.09	-0.03	-0.06
i_{cp} [A/cm²]	$2\cdot10^{-5}$	$1.2\cdot10^{-5}$	$3\cdot10^{-5}$	$1.2\cdot10^{-5}$	$9\cdot10^{-5}$	$5\cdot10^{-5}$
E_p [V]	0.27	0.2	0.2	0.18	0.2	0.2
i_p [A/cm²]	$3\cdot10^{-6}$	$7\cdot10^{-7}$	$9\cdot10^{-7}$	$2\cdot10^{-6}$	$3\cdot10^{-6}$	$2\cdot10^{-6}$
E_b [V]	1.0	1.0	1.0	1.0	1.0	1.0

Regarding the electrochemical parameters, the values of the corrosion potential (E_{corr}), the potential of first passivation (E_{pp}) and the breakdown potential (E_b) are very similar for each type of nickel matrix deposits. Some differences are visible only in the current density values: the Ni/Al_2O_3 layers show a higher corrosion current density, while the Ni/SiC deposits show a smaller passive current density. In order to better compare the differences between the different type of coatings in acidic environment the polarization curves of all the samples produced under direct current are plotted in Fig 7.6.

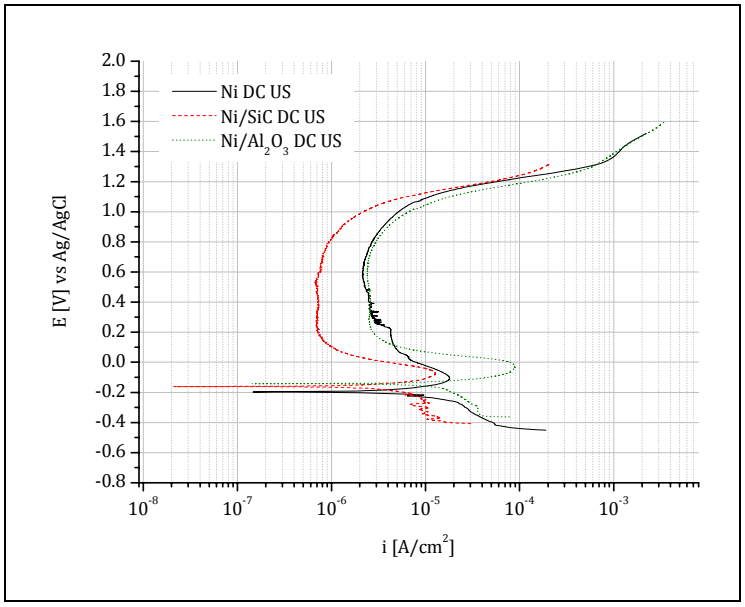

Fig 7.6. Comparison between polarization curves of different coatings deposited under DC and US

From the plot of Fig 7.6 it is quite evident that the passive oxide layer grown on the Ni/SiC surface is more protective since the passive current density is almost one order of magnitude lower, while all the other parameters are comparable to the ones of pure nickel. On the other hand, the polarization curve of the Ni/Al_2O_3 layer is almost overlapped to the one of pure nickel and the only difference is the higher critical current density. Fig 7.7 shows the comparison between the polarization curves of the 3 type of coating produced under pulse current and ultrasonic vibrations. As already pointed out from the comparison of the DC samples, the Ni/SiC nanocomposite coating shows a more protective passive layer with lower passive current density, while the critical current density is higher if compared to pure nickel film and similar to the one of Ni/Al_2O_3.

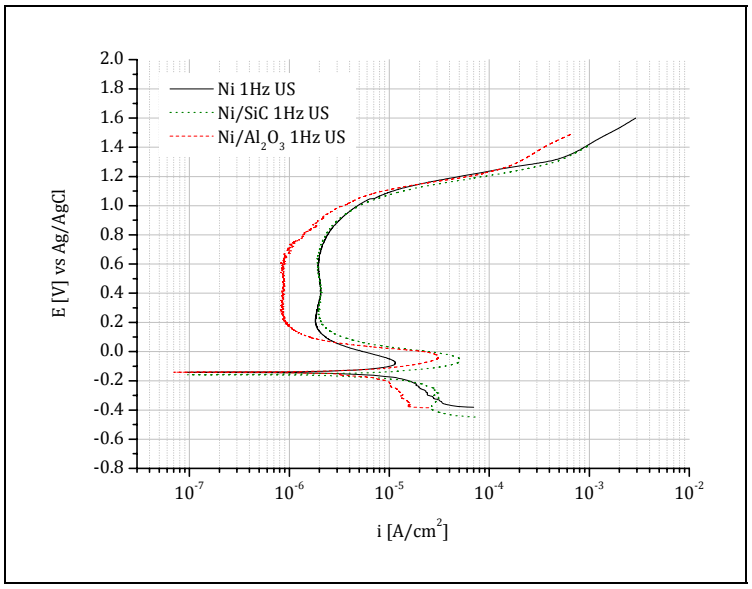

Fig 7.7. Comparison between polarization curves of different coatings deposited under PC and US

The codeposition of SiC nanopowder and the changes induced in the metal matrix microstructure make the surface on Ni/SiC codeposits more resistant to uniform corrosion and lead to the formation of a more stable oxide.

Since nickel is a passive metal, it is very important to evaluate also the resistance to localized corrosion, therefore the polarization curves have been performed in an electrolyte containing chloride ions at neutral pH. The electrolyte used was a 3.5% in weight NaCl. The specimens have been immersed in the electrolyte for 10 minutes in order to stabilize the open circuit potential before the test and the potential scanning was performed from -250mV vs. OCP up to the pitting potential. The scanning rate was maintained at 0.2 mV/s.

In the Fig 7.8 the polarization curves of the pure nickel films deposited with the ultrasonic treatment under DC and PC are plotted. The 2 samples have

similar behaviour, only the pitting potential is slightly improved. by the application of the pulse current.

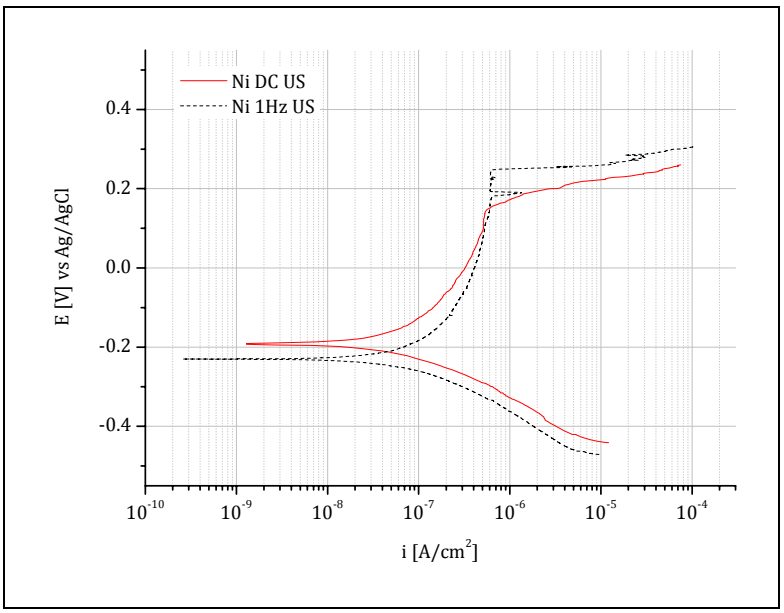

Fig 7.8. Polarization curves of pure nickel in 3.5%w NaCl

The Fig 7.9 shows the polarization curves of the Ni/SiC nanocomposites coatings produced with US under both DC and PC.

The polarization curves of the Ni/SiC nanocomposites are almost overlapped, no differences are visible in the electrochemical behaviour. The Fig 7.10 shows the polarization curves of the Ni/Al_2O_3 nanocomposites coatings deposited under the same conditions.

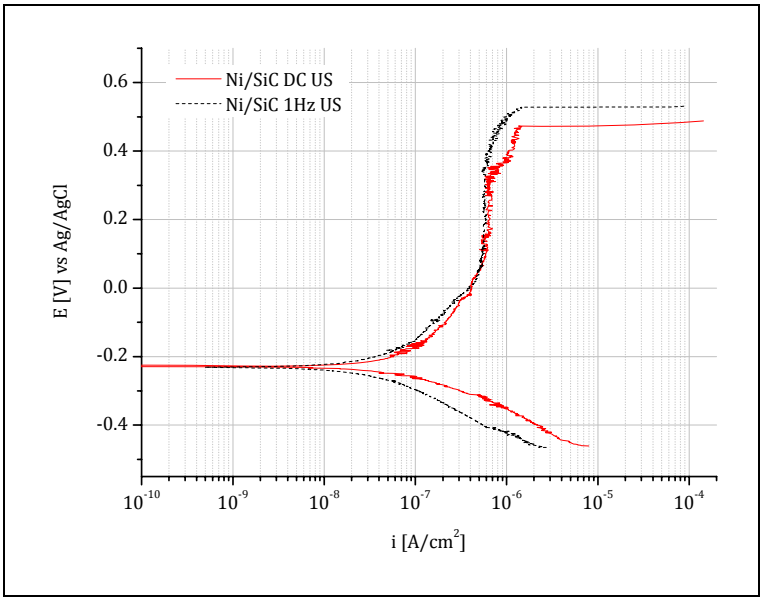

Fig 7.9. Polarization curves of Ni/SiC in 3.5%w NaCl

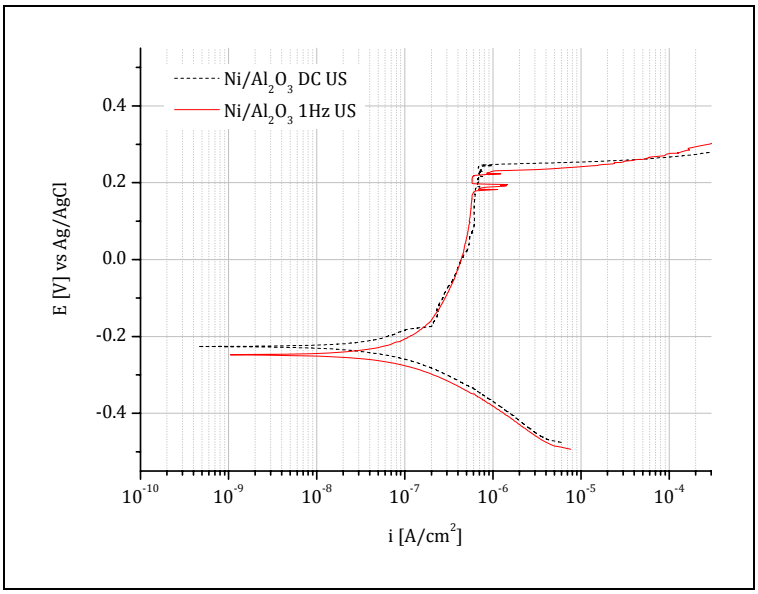

Fig 7.10.Polarization curves of Ni/Al_2O_3 in 3.5%w NaCl

As well as in the previous cases, no big differences are visible in the behaviour of the two Ni/Al_2O_3 nanocomposite coatings.

According to the results presented by other researchers in the literature on the composite electrodeposits[129], the application of the pulse current should improve substantially the corrosion resistance of the coatings. The improvement is mainly correlated to the microstructural changes induced by the pulse current and the consequent decrease of punctual defects. In this study all the specimens have been deposited under ultrasonic vibrations and, as already pointed out in the chapter 4, the microstructure of all the films has been refined, the defects avoided and in these conditions the differences between pulse current and direct current is not as remarkable as under silent conditions. The ultrasonic vibrations seem to enhance the protective properties not only removing the porosity but also thanks to the microstructural changes induced on the coating surfaces.

In the Table 7. 2 the electrochemical parameters of all kind of samples are summarized.

Table 7. 2 Electrochemical parameters in 3.5%w NaCl aqueous solution

PARAMETER	Ni		Ni-Al_2O_3		Ni-SiC	
	DC+US	1Hz+US	DC+US	1HZ+US	DC+US	1HZ+US
E_{corr} [v]	-0.19	-0.22	-0.22	-0.25	-0.22	-0.22
i_{corr} [A/cm²]	$4\cdot10^{-8}$	$5\cdot10^{-8}$	$5\cdot10^{-8}$	$6\cdot10^{-8}$	$4\cdot10^{-8}$	$3\cdot10^{-8}$
i_p [A/cm²]	$6\cdot10^{-7}$	$5\cdot10^{-7}$	$6\cdot10^{-7}$	$5\cdot10^{-7}$	$6\cdot10^{-7}$	$6\cdot10^{-7}$
E_p[V]	0.18	0.23	0.25	0.23	0.43	0.51

[129] M. Lekka, "Design, production and performances of metal matrix micro/nano composite electrodeposites", Ph.D. thesys, University of Trento, 2008- , p. 117-125

To better compare the differences between the pure nickel and the nanocomposites layers the polarization curves of films deposited under direct current are plotted in Fig 7.11 while the curves of layers deposited under pulse current at 1Hz are presented in Fig 7.12.

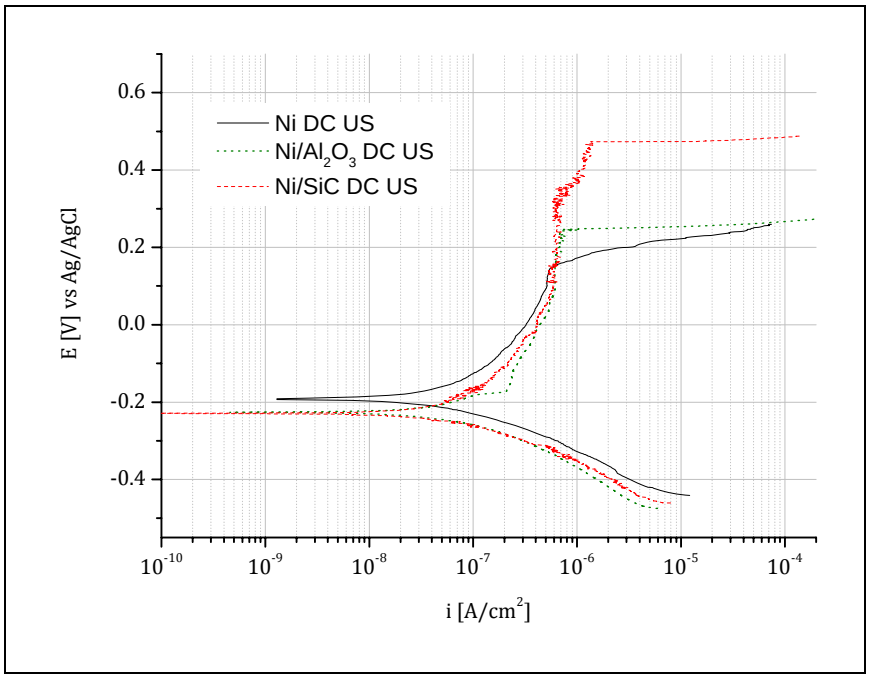

Fig 7.11.Comparison between polarization curves in 3.5%w NaCl of different coatings deposited under direct current and ultrasounds

In chloride-containing environment, all nickel layers present a passive behaviour and similar corrosion potentials. The anodic range of the curves is almost overlapped in the first part, with similar passive corrosion densities. A big difference is visible in the pitting potential: the pure nickel layer presents the lower pitting potential, while the Ni/SiC film has a 300 mV higher pitting potential compared to pure nickel.

The Ni/Al_2O_3 deposit has a pitting potential slightly higher than pure nickel, but substantially lower than the Ni/SiC film. This parameter indicates the resistance to pitting and therefore to localized corrosion in chloride environments. The same behaviour is shown by the curves of the samples deposited under pulse current presented in Fig 7.12.

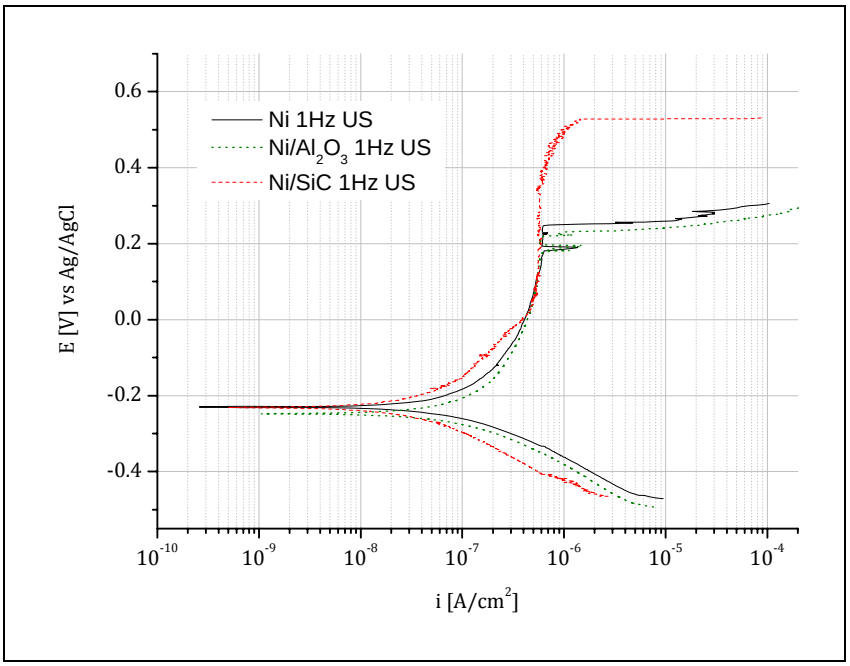

Fig 7.12.Comparison between polarization curves in 3.5%w NaCl of different coatings deposited under pulse current at 1Hz and ultrasound

From these curves it can be deduced that in environments containing chlorides, the presence of the nanoparticles does not affect the corrosion rate , neither the passive current density, but the silicon carbide particles enhances the resistance to pitting corrosion. This is due not to the type of particles, but rather to the dispersion degree of the particles in the metal matrix. As well as in the case of mechanical properties discussed in chapter 6, the silicon carbide

particles are more effective than alumina particles in enhancing the final performance of the coating, since they are better dispersed in the metal matrix and lead to deep changes in the metal properties.

EIS and salt spray exposure

The exposure to the salt spray is a method widely used in order to roughly evaluate the pitting corrosion resistance of coatings. From an industrial point of view, the time of the appearance of the first pit that reaches the substrate, i.e. the appearance of the red rust in the case of steel substrates, is meant to be the best parameter to express the resistance to pitting corrosion of the coating. Five specimens of 5x5cm of each type (pure nickel, nanocomposite Ni/SiC and nano-composite Ni/Al_2O_3 produced either under direct current or under pulse current at the frequency of 1Hz, only under ultrasonic vibrations in order to produce pore-free coatings) have been exposed to the salt spray according to the ASTM B117 standard (test solution: 5% wt. NaCl, chamber temperature: 35°C, Relative humidity: 100%).

The time for the first red pit appearance of the all kind of sample was evaluated by visual inspection and the average results are summarized in the Table 7. 3.

Table 7. 3 Time of first red pit appearance during salt spray exposure

	pure Ni	nanocomposite Ni/SiC	nanocomposite Ni/A_2O_3
DC	18±3 days	>25±3 days	19±3 days
PC	18±3 days	>25±3 days	21±3 days

The results demonstrate that the samples covered by the Ni/SiC nanocomposite resist better to localized corrosion in salt spray, while the Ni/Al_2O_3 samples do not show improvement regarding the time of first pit appearance. The presence of the nanopowder does not improve the corrosion resistance of the samples by itself but these results confirm that it is very important how the particles are embedded and dispersed in the metal matrix. Moreover the application of the pulse current does not affect the resistance to pitting corrosion. As discussed before, the microstructure of the deposit is affected by the pulse current only under silent condition, while under ultrasonic vibration the application of the pulse current leads to too small changes to be significant since the microstructure is already very refined. These results provide an idea of the corrosion protection offered by the coatings but do not characterize their electrochemical resistance.

For the purpose of this thesis therefore the salt spray cabinet has been used mainly to age the samples. The environment of the salt spray cabinet is very aggressive since it contains a high concentration of chlorides at 37°C and 100% of humidity. The corrosion process in this environment is accelerated and localized corrosion is promoted. In order to assess the corrosion resistance of the coatings the evaluation of the time of red rust appearance in not enough, while the EIS monitoring can detect the changes in the surface

properties and in the electrochemical process. The ageing of samples by the exposure to salt spray have been monitored by EIS: in this way the different corrosion resistance of similar coating could be outlined in short time. Three specimens for each type were controlled every 3 days.

A neutral 0.5M Na_2SO_4 solution was used as electrolyte for the EIS measurements in order to evaluate the damage caused by the exposure to the salt spray and not to further corrode the specimens. A 3 electrode system was used over a frequency range from 10 mHz to 100 kHz and an applied AC potential of ±5 mV vs. OCP.

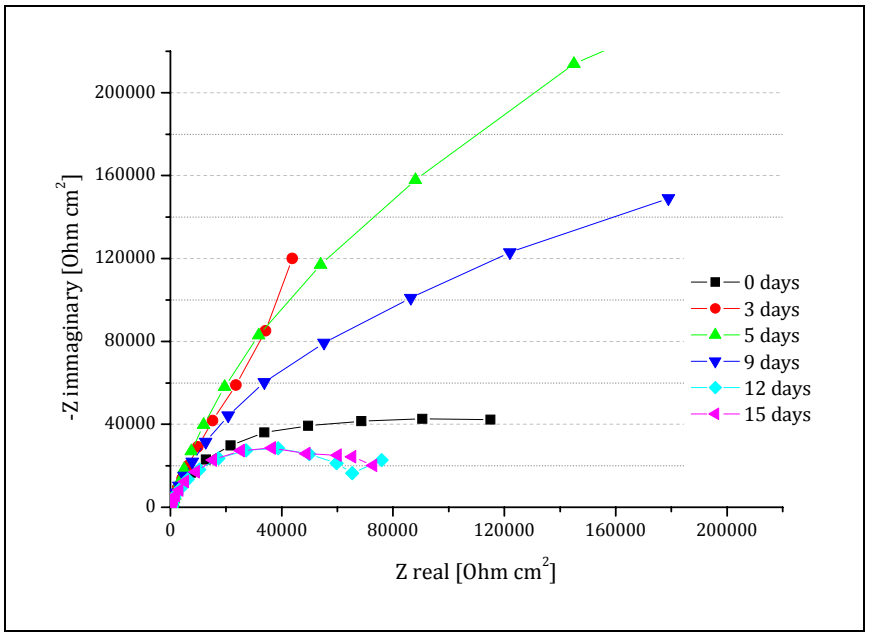

Fig 7.13.Nyquist plot of pure nickel deposited under direct current at different days of exposure

Representative EIS data of pure nickel coatings produced under direct current are presented as Nyquist plot in Fig 7.13 and Bode plots in Fig 7.14.

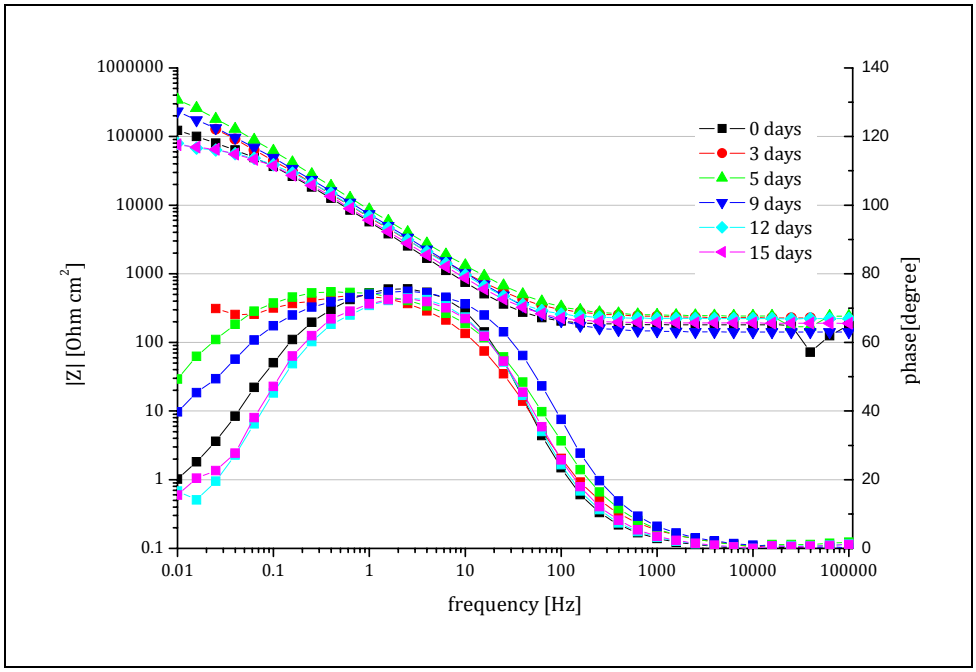

Fig 7.14. Bode plots of pure nickel deposited under direct current at different days of exposure

Before the exposure to the salt spray a measurement was performed and is presented by the black plot. After 3 day of exposure, the EIS spectrum changes completely, the semi-circle of the Nyquist plot is wider, the modulus of the impedance increases and the phase plot is broadened. These changes are related to the formation of a different oxide layer on the surface of the metal due to the exposure to a very oxidant environment at high humidity containing chlorides and very rich in oxygen. The spectra remain almost overlapped during the next days.

A slight decrease after 9 days is visible, but on the 12th day of exposure there is a substantial decrease of the impedance and the phase loop becomes narrower. After 15 days of exposure also a red pit became visible by eye

inspection and the EIS monitoring was interrupted.

The same behaviour is visible in the EIS spectra of the pulse plated pure nickel layer plotted in Fig 7.15 and Fig 7.16.

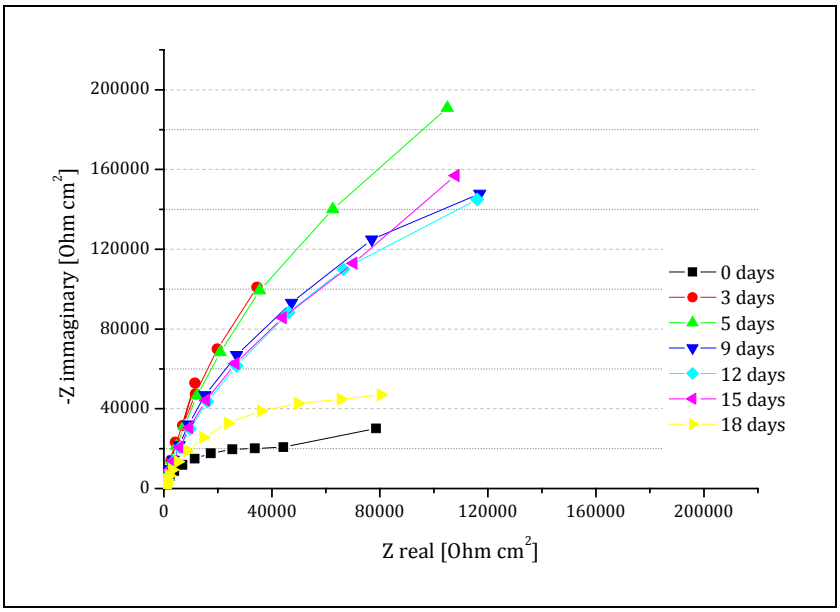

Fig 7.15.Nyquist plot of pure nickel deposited under pulse current at different days of exposure

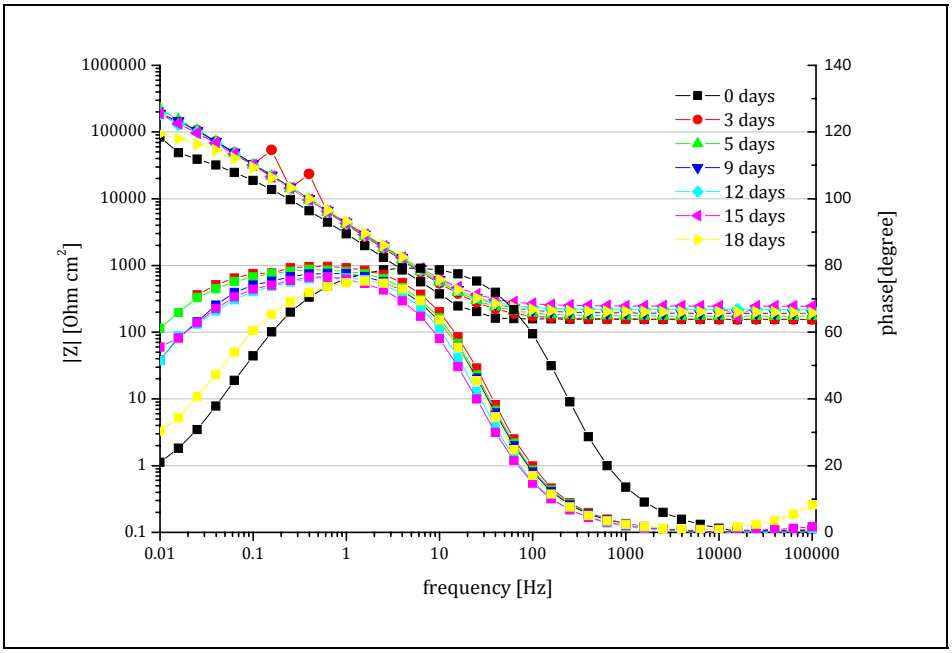

Fig 7.16.Bode plots of pure nickel deposited under pulse current at different days of exposure

In this example the Nyquist plot shows an initial slight decrease after 9 days of exposure and a substantial decrease after 18 days of exposure to salt spray cabinet. The same changes are visible in the phase plot where the phase shift at lower frequency decreases slightly after 9 days and presents a substantial decrease after 18 days when the phase peak becomes narrower.

In order to have an idea of the behaviour of all the 6 samples monitored by EIS (Ni1-Ni3 deposited under direct current and Ni4-Ni6 under pulse current) the results of all samples are plotted in the same graphs at different time of exposure in figures from Fig 7.17 to Fig 7.22.

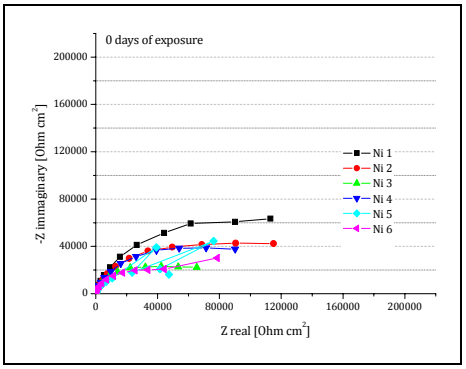

Fig 7.17.Nyquist plots after 0 days

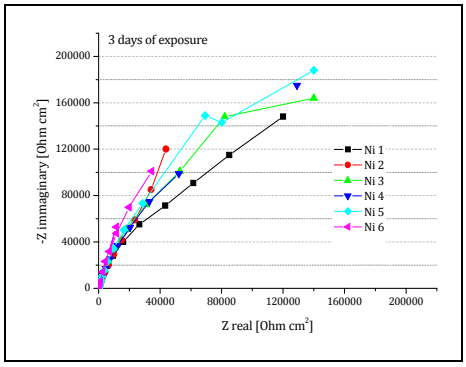

Fig 7.18.Nyquist plots after 3 days

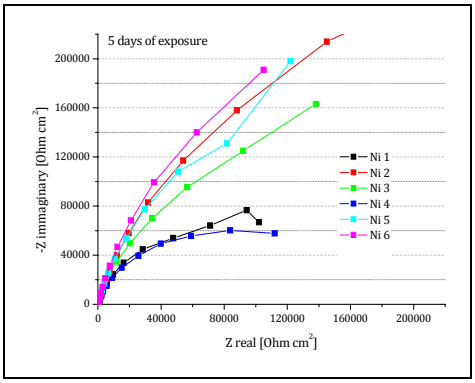

Fig 7.19.Nyquist plots after 5 days

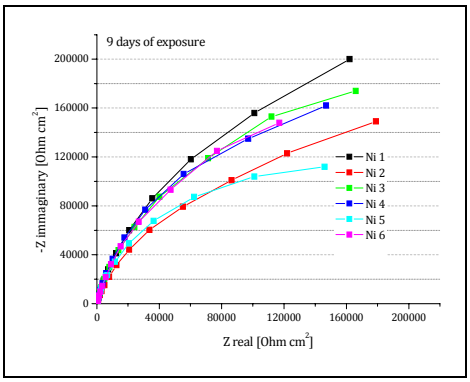

Fig 7.20.Nyquist plots after 9 days

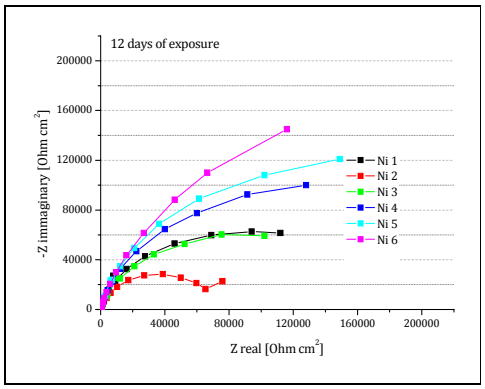

Fig 7.21.Nyquist plots after 12 days

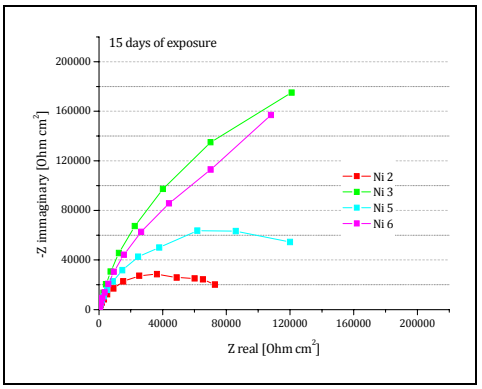

Fig 7.22.Nyquist plots after 15 days

From these graphs the initial increase of the impedance due to the exposure to salt spray cabinet is evident. Two of the samples, Ni1 and Ni4, start to show a decrease in the impedance after 5 days of exposure, but from a simple visual inspection no corrosion attack is visible. Moreover those sample at the next measurements, after 9 days, show again a higher impedance. Nevertheless those samples are the first that show an eyes visible red rust pit after 15 days. After 12 days also samples Ni2 and Ni3 present a decrease in the impedance and show a pit that reaches the substrate after 18 days. The summary of the time of red pit appearance and the first decrease in the impedance spectra are presented in the Table 7. 4.

Table 7. 4 Time of exposure before corrosion attack

sample	decrease in the impedance	first eye visible pit
Ni1 (DC US)	5 days	15 days
Ni2 (DC US)	12 days	18 days
Ni3 (DC US)	12 days	18 days
Ni4 (PC US)	5 days	15 days
Ni5 (PC US)	15 days	18 days
Ni6 (PC US)	18 days	18 days

The decrease of the impedance does not mean that a pit reached the substrate leading the steel substrate to corrode and forming a red small point eye visible, but simply that a pit was formed on the nickel surface and the metal started locally to corrode.

The Ni/SiC nanocomposite layers are the most protective, since they resist for more time to salt spray before the red rust appearance. Nevertheless, the EIS monitoring could evidence in a more detailed way the properties of Ni/SiC surfaces and analyze if the higher resistance is related to some of those surface properties.

The impedance spectra of one representative sample at different time of exposure are plotted in Fig 7.23 and Fig 7.24.

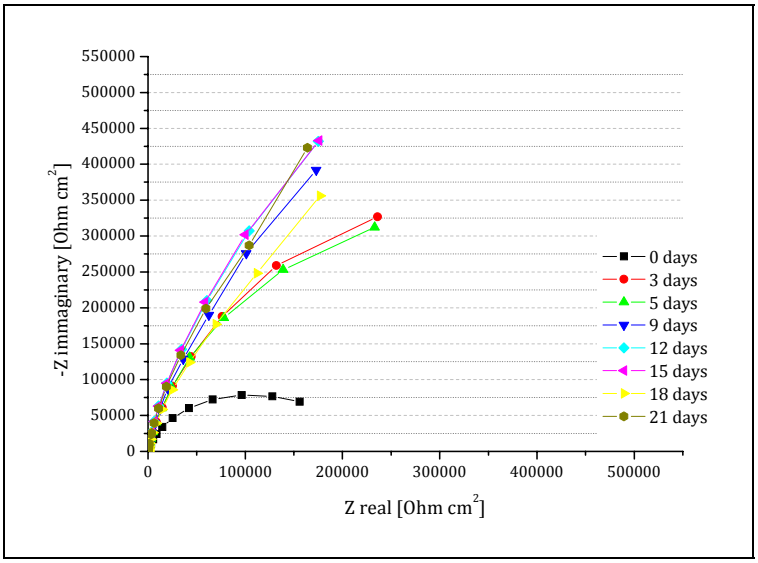

Fig 7.23.Nyquist plot of nanocomposite Ni/SiC at different time of exposure

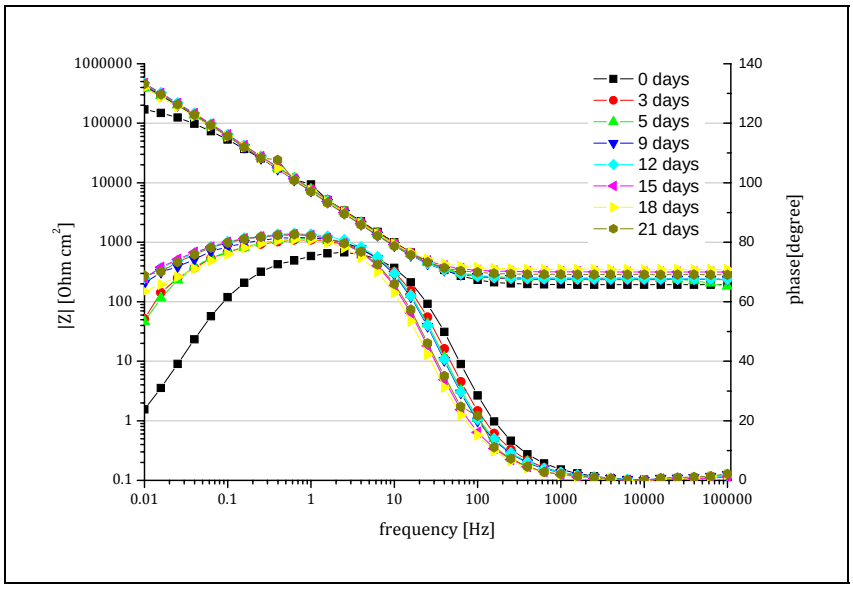

Fig 7.24.Bode plots of nanocomposite Ni/SiC at different time of exposure

Like for pure nickel the impedance increases substantially after the first exposure to the salt spray because of the changes in the oxide layer due to the exposure to the salt spray. In the graphs this is visible by the enlarge of the semicircle in the Nyquist plot, the increase of the modulus at low frequencies and the broadening of the phase peak that becomes asymmetric and could be the result of the superimposition of two different peaks.

The behaviour of all the 6 samples monitored by EIS (Ni/SiC1-3 deposited under DC and Ni/SiC4-6 under PC) are plotted at different time of exposure in Fig 7.25- Fig 7.32.

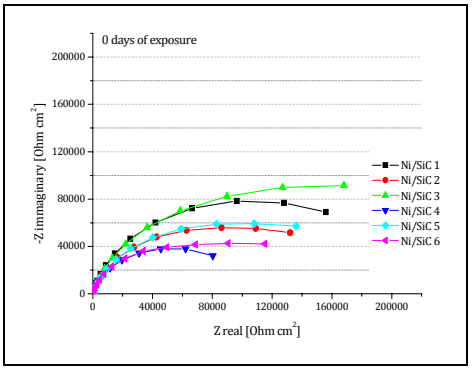

Fig 7.25.Nyquist plots after 0 days

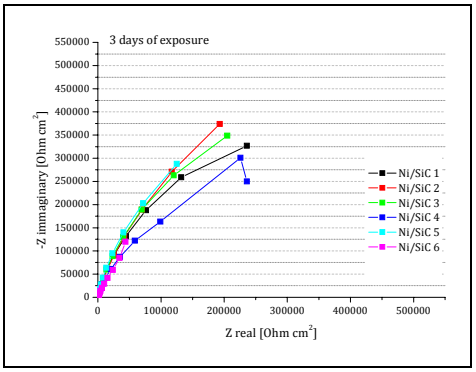

Fig 7.26.Nyquist plots after 3 days

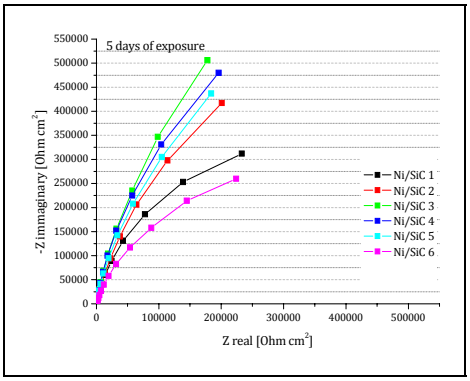

Fig 7.27.Nyquist plots after 5 days

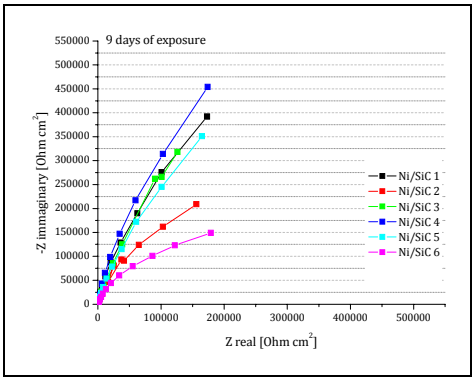

Fig 7.28.Nyquist plots after 9 days

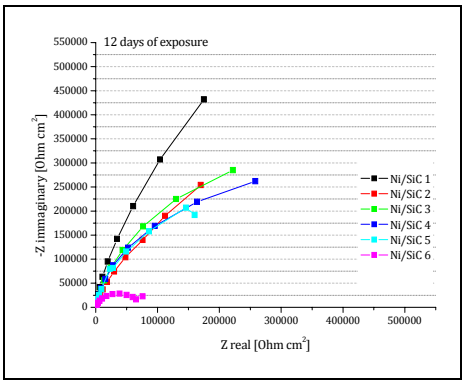

Fig 7.29.Nyquist plots after 12 days

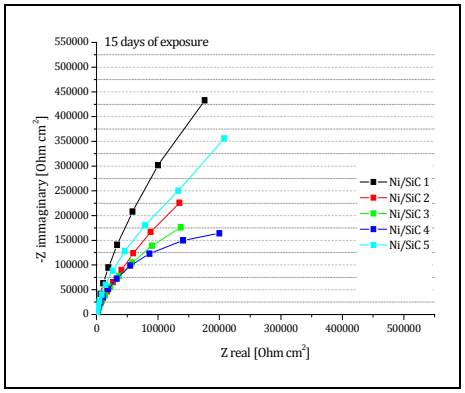

Fig 7.30.Nyquist plots after 15 days

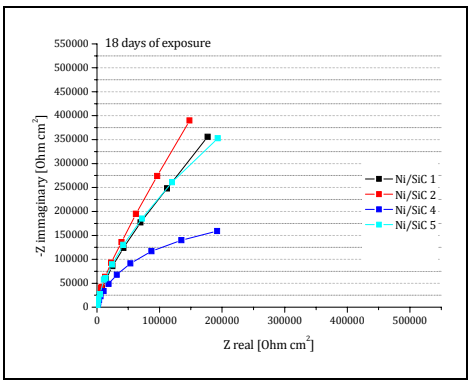

Fig 7.31.Nyquist plots after 18 days

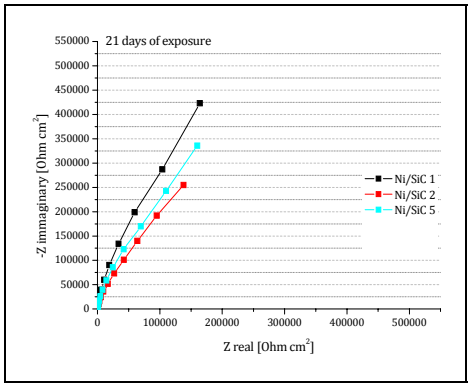

Fig 7.32.Nyquist plots after21 days

These graphs show the same increase of the impedance noted in pure nickel, but in the case on Ni/SiC the impedance increases much more and for longer time of exposure. The enlargement of the Nyquist plot is even more evident after 5 days. After 9 days of exposure the samples Ni/SiC6 present the first decrease in the impedance, much more evident after 12 days, but no eye visible corrosion attack is visible until 15 days of exposure. The samples Ni/SiC3 and Ni/SiC4 show a first shrinkage of the Nyquist plot after 15 days and then the substrate corrosion products are visible after 18 and 21 days respectively. Specimens Ni/SiC1, Ni/SiC2 and Ni/SiC5 do not show substantial changes in the plots and no visible pits for all the exposure time of 25 days.

The resistance of the 6 samples monitored by EIS are reported in Table 7. 5 and compared to the visual inspection.

Table 7. 5 Time of exposure before corrosion attack of Ni/SiC

sample	decrease in the impedance	first eye visible pit
Ni1 (DC US)	>21 days	>25 days
Ni2 (DC US)	partially after 9 days	>25 days
Ni3 (DC US)	15 days	18 days
Ni4 (PC US)	15 days	21 days
Ni5 (PC US)	>21 days	>25 days
Ni6 (PC US)	9 days	15 days

The resistance to pitting corrosion is substantially higher for the Ni/SiC nanocomposite films compared to the others in term of time of the first corrosion attack on the substrate and also in term of first decrease in the EIS data. No differences are noted between film deposited under direct and pulse current as already pointed out by the potentiodynamic curves.

Regarding the nanocomposite Ni/Al_2O_3 coating an example of the impedance as a function of the time of exposure is shown by Nyquist plot in Fig 7.33 and Bode plots in Fig 7.34.

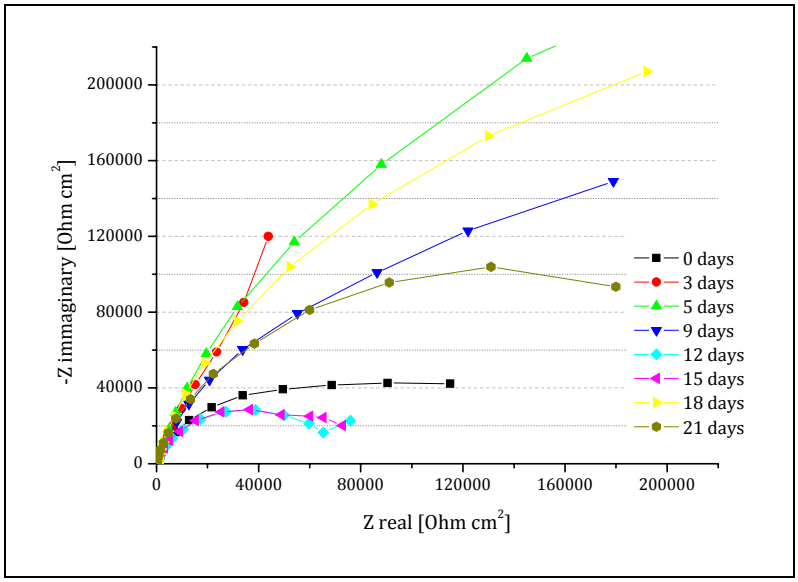

Fig 7.33.Nyquist plot of nanocomposite Ni/Al_2O_3 at different time of exposure

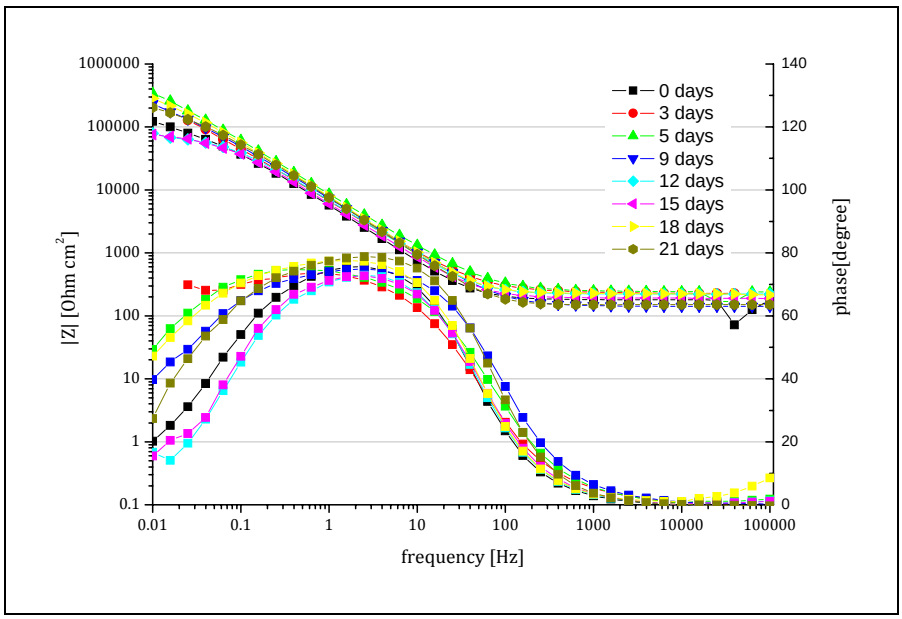

Fig 7.34.Bode plots of nanocomposite Ni/Al_2O_3 at different time of exposure

Again the impedance increases substantially after the first exposure to the salt spray because of the formation of a different and probably ticker oxide layer. A slight decrease of the impedance is represented by the shrinkage of the semicircle in the Nyquist plot after 9 days, but the relevant decrease in the impedance is visible after 12 days. Since no red pit is visible on the surface the exposure to salt spray goes on and at 18 and 21 days the impedance increases again. The increase after some days is probably due to presence of the corrosion products that fill the pit.

In the Bode plots in the Fig 7.34 the decrease of the impedance is expressed by the shrinkage of the phase diagram indicating that the electrochemical process has changed.

The behaviour of all the 6 samples monitored by EIS (3 deposited under direct current and 3 under pulse current) are plotted in the same graphs at different time of exposure in Fig 7.35- Fig 7.40.

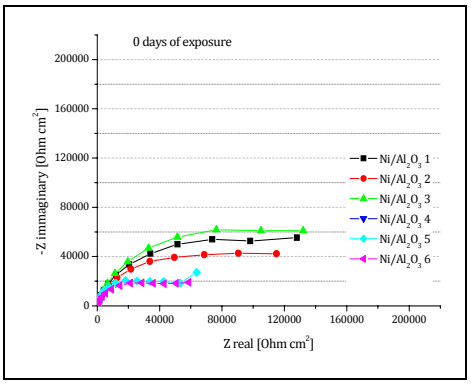

Fig 7.35. Nyquist plots after 0 days

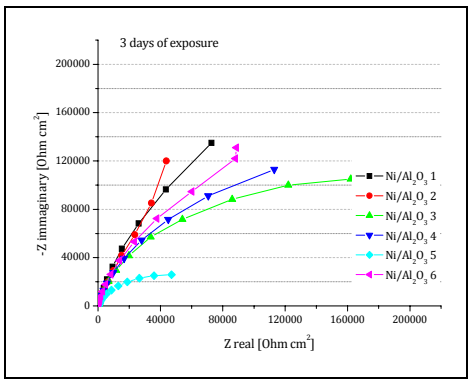

Fig 7.36. Nyquist plots after 3 days

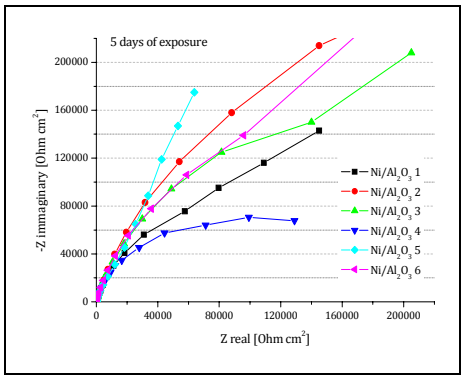

Fig 7.37.Nyquist plots after 5 days

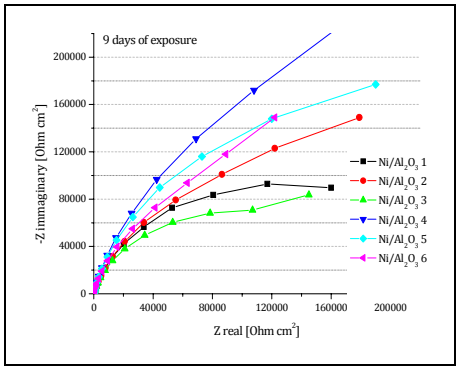

Fig 7.38.Nyquist plots after 9 days

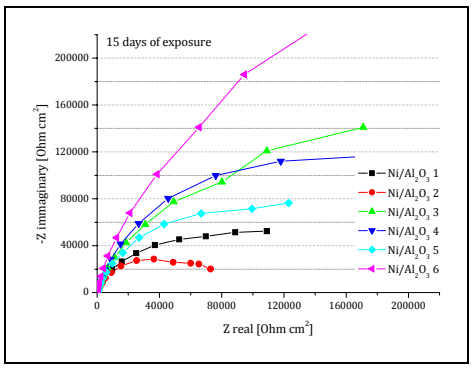

Fig 7.39.Nyquist plots after 5 days

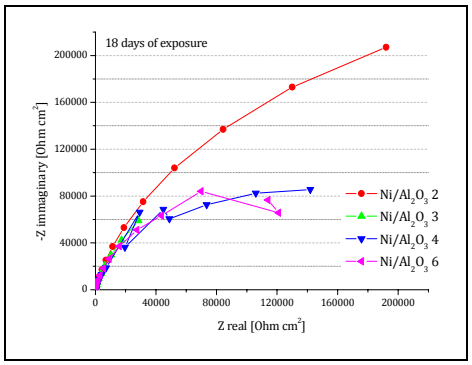

Fig 7.40.Nyquist plots after 18 days

The comparison between the results of the evaluation of the corrosion process by visual inspection and EIS is reported in the Table 7. 6: the pitting formation detected by EIS defines the start of the nickel corrosion and some day after the pit reaches the substrate and also the steel starts to corrode producing the visible red rust.

Table 7. 6 Time of exposure before corrosion attack of Ni/Al_2O_3

sample	decrease in the impedance	first eye visible pit
Ni1 (DC US)	12 days	18 days
Ni2 (DC US)	12 days	18 days
Ni3 (DC US)	9 days	18 days
Ni4 (PC US)	5 days	15 days
Ni5 (PC US)	15 days	21 days
Ni6 (PC US)	18 days	21 days

The resistance to pitting corrosion is slightly higher for the Ni/Al_2O_3 nanocomposite films compared to pure nickel layers in term of time of the first corrosion attack, but much worse than Ni/SiC films. No differences are noted between film deposited under direct and pulse current as already pointed out.

The time to the first red pit appearance and the time of the first decrease in the impedance values is generally increased by the presence of the nanoparticles, but the resistance to the pitting corrosion though is not simply related to the presence of the nanopowder. The improvement due to Al_2O_3 powder is much less relevant compared to the improvement due to the SiC powder. As already pointed out in the microstructure analyses and in the mechanical properties, the silicon carbide powder is better dispersed in the metal matrix and induces a finer electrocrystallization of the coating and therefore is more effective in the improvement of the final properties of the layer.

Moreover the impedance spectra during the exposure confirm that the

presence of well dispersed SiC nanoparticles improves the corrosion resistance changing the electrochemical properties of the coating surface. Comparing the impedance spectra of three kind of samples after 5 days of exposure the semicircle of the Nyquist plot (Fig 7.41) is substantially enlarged and the impedance modulus (Fig 7.42) is higher.

The same comparison at time 0 is very difficult since the differences between the spectra of samples of the same type are comparable to the ones between different kind of deposits. The exposure to salt spray leads to more uniform electrochemical behaviour of similar coatings and enlarges the impedance thus leading to more evident differences between different type of coating.

It can be conclude that the higher corrosion resistance to localized corrosion of the Ni/SiC nanocomposites is related to some surface changes detected by the higher impedance just after the exposure to salt spray.

The fitting of the EIS data is very difficult since the presence of the passive oxide layer make difficult to find the right equivalent circuit. The phase diagrams indicate that 2 different overlapped loops are present and therefore an electrical circuit with 2 time of relaxation is needed.

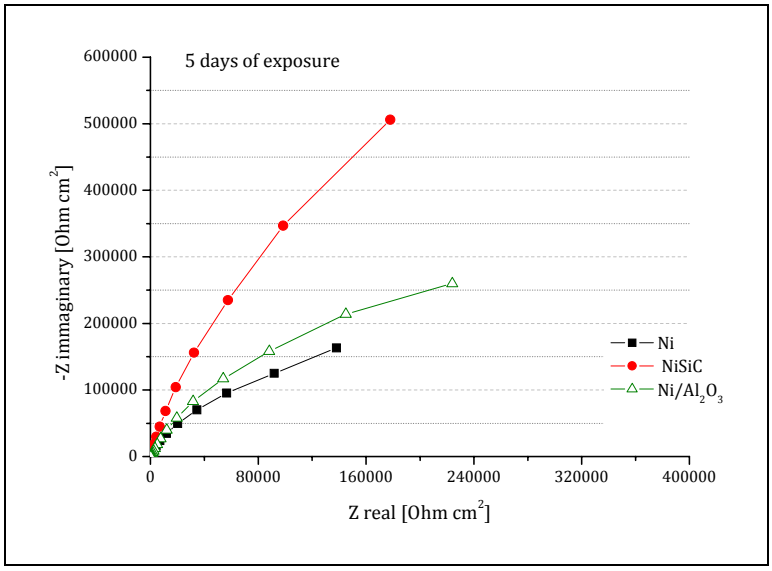

Fig 7.41.Comparison of the Nyquist plot after 5 days of type of samples

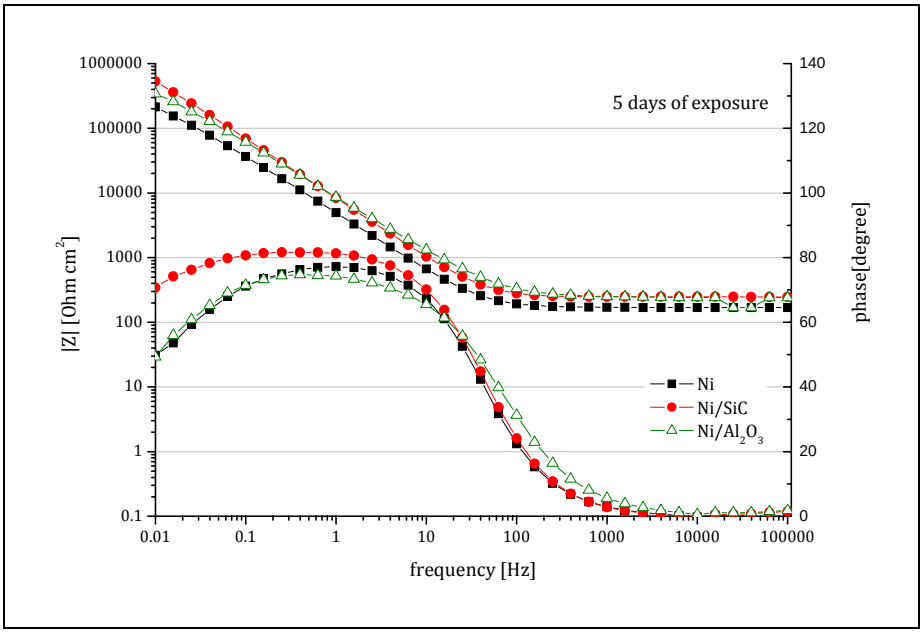

Fig 7.42.Comparison of the Bode plot after 5 days of type of sample

The most part of the studies on the corrosion properties of nickel electrodeposits and especially on composites[130], present EIS spectra with 2 well defined peaks in the phase diagram that are modelled and well fitted by the equivalent circuit of Fig 7.43 where the first RQ corresponds to the electrochemical properties of the nickel coating and its passive layer and the second RQ refers to the faradic process of the corroding substrate. In the case of this study no porosity is present in the nickel coatings and thus no substrate is exposed to the environment. Therefore this model can not be apply.

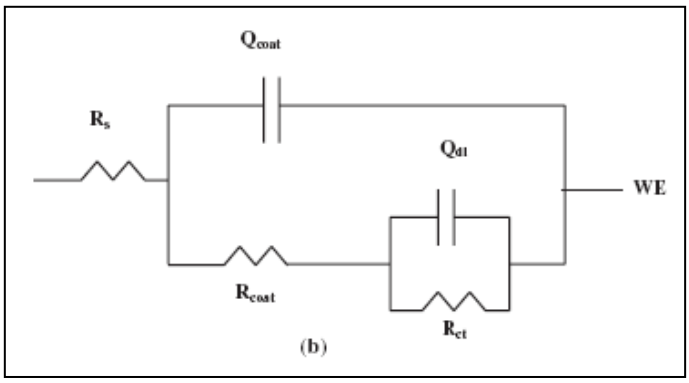

Fig 7.43.Equivalent circuit of ref 4

A big effort have been done in order to improve the deposition process and to produce pore-free coatings and thanks to the application of the ultrasounds it has been possible. Only the layers deposited under ultrasonic vibration were characterized regarding their corrosion resistance and therefore a different fitting approach needs to be used. Some EIS studies present in the literature[131] on corrosion of nickel electrodeposits suggest to use the 2 time constant

[130] B. Szczygieł, M. Kołodziej, Electrochimica Acta 50 (2005) 4188–4195
[131] S.T. Aruna, C.N. Bindu, V. Ezhil Selvi, V.K. William Grips, K.S. Rajam, Surf. Coat. Tech.,200, (2006), 6871

equivalent circuit in order to model the asymmetrical phase peak, where one RC correspond to the properties of the oxide layer and the other to the nickel faradic process. Others[132] suggest to consider the diffusion process and add a Warburg element in the equivalent circuit. In this study the 2 time constant equivalent circuit of the Fig 7.44 was used in order to fit the impedance data.

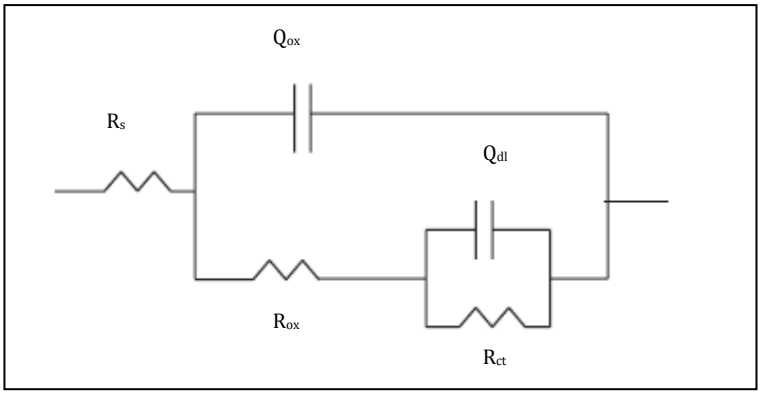

Fig 7.44. Equivalent circuit applied to the experimental data

Where: R_s is the resistance of the electrolyte;

R_{ox} is the resistance of the oxide;

Q_{ox} represents the capacity of the oxide;

R_{ct} is the charge transfer resistance;

Q_{dl} represents the capacity of the oxide.

As an example, the evolution of the equivalent electrical parameters of a representative sample per type is considered. The most interesting parameters are the 2 resistances since they represent the barrier property of the oxide and the dissolution process of the nickel plotted in Fig 7.45 and Fig 7.46.

[132]W, A. Badawy, , K.M. Ismail, A.M. Fathi, J. All. Comp., 484, (2009), 365

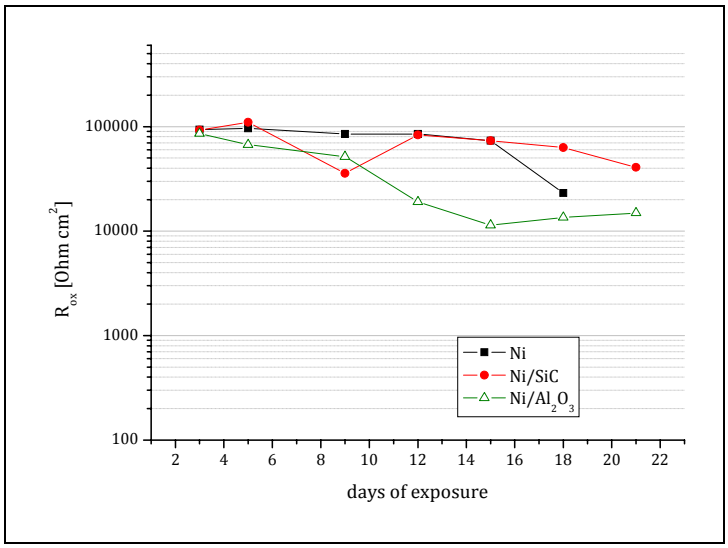

Fig 7.45.Modeled values of the oxide resistances as a function of time of exposure

The oxide resistances of different layers have more or less the same value in the first days of exposure. The Ni/Al_2O_3 value shows a decrease after 12 and 15 days corresponding to the shrinkage of the semicircle in the Nyquist plot reported in the plots Fig 7.33; the Ni oxide resistance shows a decrease after 18 days, while the Ni/SiC oxide resistance maintains a higher values for the whole exposure period.

Regarding the charge transfer resistance a decrease could correspond to the activation of nickel and therefore to the formation of a pit. The Ni/SiC shows a much higher resistance than pure Ni and Ni/ Al_2O_3 after first days of exposure and the R_{ct} remains high during the exposure and no corrosion is visible; on the contrary pure nickel shows a pit formation at the 18th day of exposure, followed by the first eye visible pit after 21 days. The Ni/Al_2O_3 has a decrease

of the R_{ct} at the 12th day corresponding to the formation of a pit that probably is closed by the corrosion product or repassivate since the R_{ct} increases again at the 18th day.

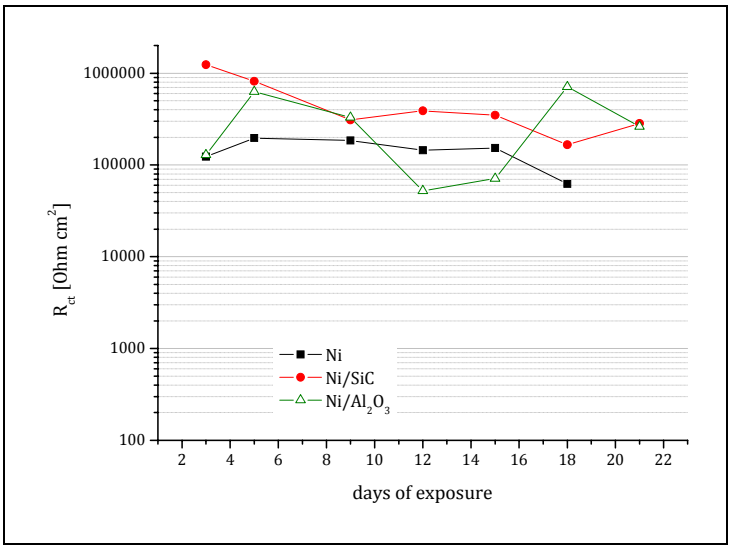

Fig 7.46.Modeled values of the charge transfer resistances as a function of time of exposure

The values of all the fitting equivalent circuit elements are reported in Table 7. 7:

Table 7. 7 Equivalent circuit parameters values

days	R_{ox}	Q_{ox}	n_{ox}	R_{ct}	Q_{dl}	n_{dl}
Ni						
3	9.35E+04	2.29E-05	7.97E-01	1.23E+05	2.40E-04	9.60E-01
5	9.64E+04	6.23E-05	8.55E-01	1.96E+05	1.73E-04	1.00E+00
9	8.48E+04	2.96E-05	8.81E-01	1.85E+05	1.23E-04	1.00E+00
12	8.50E+04	2.64E-05	9.14E-01	1.45E+05	1.12E-05	7.59E-01
15	7.33E+04	2.17E-05	9.37E-01	1.53E+05	4.57E-05	7.64E-01
18	2.32E+04	2.69E-05	9.20E-01	6.22E+04	6.29E-05	7.83E-01
Ni/SiC						
3	9.28E+04	2.06E-05	9.52E-01	1.24E+06	3.90E-06	5.92E-01
5	1.10E+05	2.21E-05	9.51E-01	8.16E+05	4.49E-06	6.63E-01
9	3.58E+04	8.99E-05	9.48E-01	3.10E+05	2.37E-05	6.37E-01
12	8.32E+04	1.33E-04	9.49E-01	3.90E+05	2.45E-05	6.23E-01
15	7.35E+04	1.32E-04	9.52E-01	3.49E+05	2.70E-05	6.86E-01
18	6.31E+04	1.37E-04	9.44E-01	1.66E+05	7.85E-05	8.82E-01
21	4.09E+04	1.26E-04	9.71E-01	2.83E+05	4.65E-05	8.44E-01
Ni/Al_2O_3						
3	8.59E+04	1.43E-04	8.44E-01	1.29E+05	5.47E-05	1.00E+00
5	6.73E+04	2.34E-05	8.52E-01	6.27E+05	6.84E-06	1.00E+00
9	5.15E+04	2.48E-05	8.93E-01	3.29E+05	7.86E-06	6.06E-01
12	1.90E+04	2.37E-05	9.26E-01	5.23E+04	1.13E-05	7.32E-01
15	1.14E+04	1.15E-03	9.38E-01	7.10E+04	3.12E-05	8.90E-01
18	1.35E+04	2.00E-05	9.47E-01	7.12E+05	7.47E-06	5.74E-01
21	1.49E+04	1.94E-05	9.67E-01	2.63E+05	9.72E-06	6.50E-01

These values show that the higher resistance of Ni/SiC is related to the higher impedance and correspond to a higher R_{ct} at the first stages of ageing. Moreover considering the parameters regarding the oxide the n_{ox} of Ni/SiC is higher and therefore the behaviour of the Q element is more similar to a pure

capacity, while is lower for Ni /Al_2O_3 and pure Ni. This trend could represent a different oxide that is more protective in the case of Ni/SiC and more heterogeneous in case of pure Ni and Ni/Al_2O_3.

It seems to be possible to evaluate the effectiveness of the codeposition of a nanopowder in enhancing the properties, just by monitoring the EIS after a short time of aggressive ageing. Since the improvement of the corrosion resistance is related to the dispersion of the nanoparticles[133],the EIS could indirectly verify the agglomeration degree of the codeposited fraction through the electrochemical response.

Comments

The corrosion properties have been measured by both polarization tests and EIS during the ageing by the exposure to salt spray. On one side the properties have been evaluated by imposing an overpotential to the samples and monitoring the current response. On the other side the sample have been exposed to a very aggressive environment containing chlorides and monitoring both the electrochemical impedance and the formation of localized corrosion attacks during the exposure. The usual application of the salt spray cabinet and the relative standards require only a visual check of presence of some corroded points on the surface and as for nickel coated steel this means the appearance of red rust spot on the surface. The red rust is the corrosion product of the steel substrate and therefore indicates the corrosion of the substrate, while the main objective of this work is to evaluate the

[133] Th. Lampke, B. Wielage, D. Dietrich, A. Leopold, Appl. Surf. Sci. (2006)

electrochemical behaviour of the coatings. Therefore the EIS was necessary in order to evaluate of the electrochemical behaviour of the nickel coating, the attacks by chlorides, the breakdown of the passivity layer, the formation of pits by local activation of nickel and the evolution of the corrosion process.

In order to evaluate the real properties of the coatings and do not be affected by the substrate it was very important to deposit pore-free coatings and it was demonstrated that the ultrasounds are a very successful application that allows to produce high quality and protective coatings.

The results of the polarization tests pointed out that Ni/SiC can form a more stable passive oxide that resists more to pitting corrosion. The exposure to the salt spray demonstrate that the resistance to localized corrosion is much higher in term of time of exposure before the first corrosion attack. The EIS measurements reveal that the pit starts some days before to become eye visible, since it needs some time to corrode the whole film thickness and to reach the substrate. Moreover the EIS shows that not only the Ni/SiC last more days in a very aggressive environment but also that the impedance of the Ni/SiC layer is much higher than the ones of pure nickel and Ni/Al_2O_3. The codeposition of a well dispersed ceramic powder, like in the case of SiC in nickel matrix under ultrasonic vibrations, induces a completely different electrocrystallization that changes the electrochemical behaviour and improves the corrosion resistance.

EIS revealed to be a powerful technique to detect the changes induced by a non-agglomerated nanopowder and therefore the successful outcome of the codeposition process.

As for the mechanical properties the simple presence of the ceramic phase leads to an improvement further enhanced by the good dispersion of the

particles. Regarding the corrosion, on the contrary, the presence of the nanopowder is not enough to improve the resistance: the dispersion of the powder is essential.

In the case of Al_2O_3 nanopowder the mechanical properties are affected by the presence of a harder phase but not the corrosion resistance that is similar to the one of pure nickel, since the particles agglomeration is not completely avoided even if deposited under ultrasonic vibration. The SiC particles, on the contrary, can be better dispersed thus leading to improved both mechanical and protective properties.

8. Conclusions

Discussion

The development of enhanced nickel matrix nanocomposite coatings and the optimization of the codeposition parameters were the main objectives of this Ph.D. research work. Two different nanopowder, i.e. silicon carbide and alumina, were added to a Watts type galvanic bath after being characterized mainly by means of DLS and ζ-potential measurements. These tests are usually performed in a KCl electrolyte, but it was demonstrated that the presence of metallic cations and furthermore the high ionic strength change completely the suspension stability and also the ζ-potential values. Powders that are usually very stable and well dispersed as alumina can be completely destabilized and flocculate if suspended in a galvanic bath. Therefore despite alumina and silicon carbide are very different in the as-received state, their behaviour and characteristic are almost equal in the galvanic bath. Moreover the study of the suspensions stability confirmed that the presence of SDS as pitting control agent induce a change in the ζ-potential values and inhibits the codeposition of the powder despite it increases the stability of the suspensions. The absence of the pitting control agent make necessary to find

an alternative to avoid pores and voids produced on the substrate surface by the hydrogen evolution, otherwise the deposited metallic layer would not be protective and therefore useless.

The ultrasonic treatment was considered a good alternative to the surfactants in order to eliminate the porosity left on the cathode by the hydrogen evolution. Therefore an ultrasonic horn was inserted in the deposition cell and ultrasonic vibrations were applied during the whole deposition process and not only for the suspension preparation.

The optimization of the process parameters took into account a large number of parameters (current density, pulse current frequency, powder loading) whose influence has been estimated by creating a parameter map that correlate the amount of codeposited particles to the process parameters in a wide range of values. These experiments permitted to understand that for high powder load or high current density the codeposition system is not affected by the other parameters, and on the contrary for low powder loads and low current densities any small changes of the other parameters strongly affects the codeposition rate. The maximum of the codeposition rate is obtained for "medium" values of the tested parameter range, where also small changes in the process parameters only slightly influence the codeposition efficiency.

The study of the process parameters allowed to define the better parameter combination for the process set-up and continue the work on less variables and to characterize only the optimized coatings.

The microstructures of the deposited layers have been analyzed both on the top view and on the cross-section after etching. The pure nickel and Ni/Al_2O_3 layers deposited under silent conditions showed a field-oriented columnar

microstructure, while the SiC codeposition led to a complete different microstructure. The grains were much refined by the presence of the nanoparticles and the synergic effect of the application of the pulse current and the ultrasounds induced a microstructural change that led to very fine microstructure with a flat and homogeneous surface.

The application of the pulse current and the ultrasounds interrupted the growth of the fibres and in the case of Ni/Al_2O_3 films led to the formation of unoriented equiaxial grains. The ultrasounds were very effective also in improving the particle dispersion when the powder tend to agglomerate as alumina did. Despite silicon carbide tended to agglomerate more in the galvanic bath compared to alumina, in the metal layer the embedded SiC particles were very well dispersed, the agglomerate were formed by 20 particles under silent conditions and 3-5 particles under ultrasonic vibrations. The smaller the embedded aggregates the higher was their influence on the crystallization process and therefore on the microstructural refinement.

Regarding the embedded ceramic fraction, alumina resulted to be easier codeposited, but silicon carbide was better dispersed and therefore more effective in changing the final properties. Moreover the application of the ultrasounds had a beneficial influence also on the codeposition rate, increasing both alumina and silicon carbide in the metal layers when codeposited under ultrasonic treatment.

Since these coating were developed in order to obtained reinforced surfaces the mechanical properties has been evaluated by means of hardness and abrasion resistance tests.

The microhardness of all samples produced under ultrasonic vibrations was higher due to the microstructure modification induced by the ultrasounds

The hardening effect of codeposits depended on both the presence of a second ceramic phase and on the capability of the particles to interact with the electrocrystallization process.

The SiC powder was more effective in hardening: not only the Ni/SiC layers were harder than Ni/Al_2O_3 layers for the same content of ceramic particles, but also the rate of the hardness increase by increasing the ceramic content was higher.

However, the Ni/Al_2O_3 coatings were noticeably improved by the application of the ultrasonic vibrations during the depositions that promote a higher codeposition rate and the dispersion of the powder inside the metal and led to the deposition of a harder and more resistance coating.

In order to evaluate the real protection properties of the layers and do not be affected by the substrate it was very important to deposit pore-free coatings and it has been proved that the ultrasounds are a very successful alternative to surfactants in pitting control and allow to produce high quality and protective coatings. The results of the polarization tests pointed out that Ni/SiC can form a more stable passive oxide that resists more to pitting corrosion. The exposure to the salt spray demonstrated that the resistance to localized corrosion was much higher in term of time of exposure before the first corrosion attack. The EIS measurements revealed that the pit started some days before to become eye visible, since it needs some time to corrode the whole film thickness and to reach the substrate. Moreover the EIS showed that not only the Ni/SiC lasted more days in a very aggressive environment but also that the impedance of the Ni/SiC layer was much higher than the ones of pure nickel and Ni/Al_2O_3. The codeposition of a well dispersed ceramic powder, like in the case of SiC in nickel matrix under ultrasonic vibrations,

induced a completely different electrocrystallization that changed the electrochemical behaviour and improved the corrosion resistance.

Unlike the mechanical hardening, the corrosion was not affected by the simple presence of the nanopowder: to improve the resistance the dispersion of the powder was essential.

Moreover from the experimental results it seemed to be possible to evaluate the effectiveness of the codeposition of a nanopowder in enhancing the properties, just by monitoring the EIS after a short time of aggressive ageing. Since the improvement of the corrosion resistance was related to the dispersion of the nanoparticles ,the EIS could indirectly verify the agglomeration degree of the codeposited fraction through the electrochemical response.

Concluding, Ni/Al_2O_3 nanopowder codeposition leds to hardening effect, but did not affect the corrosion resistance because the particles agglomeration was not completely avoided even if deposited under ultrasonic vibrations. The SiC particles, on the contrary, could be better dispersed thus leading to improved both mechanical and protective properties. Ultrasounds revealed to be a powerful tool in order to substitute pitting control agent, to produce pore-free protective coatings, to disperse the embedded nanoparticles and to increase the nanoparticles codeposition rate.

Future work

The future development of this work should take in consideration the use of different particles and study which powder tends to agglomerate and which ones are easier dispersed. Moreover the SiC particles demonstrated to be the more promising powder to be well dispersed in the metal matrix and other matrixes should be tested as for example nickel alloys or nickel multilayers.
The nanopowder properties and dispersion capability depend strongly on the production process and often the commercial ones can not always provide constant characteristics. Therefore a pre-treatment of the powder should be investigated and developed.